

Aus der Klinik für Strahlentherapie und Radioonkologie
der Medizinischen Fakultät Mannheim
(Direktor: Prof. Dr. med. Frank A. Giordano)

Inverse Treatment Planning of Nasopharyngeal Carcinoma in Gamma Knife Radiotherapy

Inauguraldissertation
zur Erlangung des Doctor scientiarum humanarum (Dr. sc. hum.)
der
Medizinischen Fakultät Mannheim
der Ruprecht-Karls-Universität
zu
Heidelberg

vorgelegt von
Manon Spaniol

aus
Saarbrücken
2023

Dekan: Prof. Dr. med. Sergij Goerd

Referent: Prof. Dr. med. Frank A. Giordano

TABLE OF CONTENTS

	Page
TABLE OF CONTENTS	I
LIST OF ABBREVIATIONS	IV
1 INTRODUCTION	1
1.1 Radiation therapy	2
1.2 Leksell Gamma Knife	2
1.3 Radiation therapy for nasopharyngeal carcinoma	5
1.4 Research objective	6
2 MATERIALS AND METHODS	8
2.1 Inverse planning with Leksell GK Lightning	8
2.1.1 Patient population and planning strategy	10
2.1.2 Statistical analysis of the collected data	13
2.2 Homogenous GK planning	14
2.2.1 Patient selection and treatment planning for GK and LINAC	14
2.2.2 Data acquisition and statistical analysis	17
2.3 Homogenous Leksell GK Lightning for treatment planning of NPC	18
2.3.1 Preliminary patient selection and GK reachability	18
2.3.2 Planning strategy for LINAC and GK boost plans and final patient selection	19

2.3.3	Plan comparison and data analysis	22
3	RESULTS	23
3.1	Inverse planning with Leksell GK Lightning	23
3.1.1	Plan quality and efficiency	23
3.1.2	Inter operator variability	29
3.2	Homogenous Leksell GK Lightning	32
3.2.1	Plan quality and efficiency – medical conditions and total patient cohort 32	
3.2.2	Plan quality and efficiency – exemplary cases	37
3.3	Homogenous Leksell GK Lightning for treatment planning of NPC	39
3.3.1	Patient population: imaging and dose distribution.....	39
3.3.2	Individual dose volume histograms and dose values.....	41
3.3.3	Mean dose volume histograms and dose values	62
4	DISCUSSION	67
4.1	Inverse planning with Leksell GK Lightning: Advantages and limitations	67
4.1.1	Plan quality: metastases	68
4.1.2	Plan quality: acoustic neuromas and meningiomas.....	68
4.1.3	Plan efficiency, inter-operator-variability and additional findings	69
4.2	Homogenous Leksell GK Lightning: OAR dose sparing and homogeneity..	71
4.2.1	Target dose homogeneity	71
4.2.2	Plan quality and efficiency	72
4.3	Homogenous Leksell GK Lightning for treatment planning of NPC	73
4.3.1	Anatomical changes and dose distribution	73

4.3.2	Benefit of OAR sparing	76
4.3.3	SRT for NPC.....	79
4.3.4	Limitations and future challenges	80
5	SUMMARY	83
6	BIBLIOGRAPHY.....	86
7	CURRICULUM VITAE	97
8	OWN PUBLICATIONS.....	99
9	AKNOWLEDGMENT	100

LIST OF ABBREVIATIONS

AN	Acoustic neuroma
ART	Adaptive radiotherapy
BOT	Beam-on-time
CBCT	Cone beam computed tomography
cc	Cubic centimeter
cov	coverage
CRT	Conformal radiotherapy
CT	Computed tomography
dB	Decibel
DICOM	Digital imaging and communications in medicine
DVH	Dose-volume histogram
EBRT	External beam radiotherapy
fc	Full coverage
FFF	Flattening filter free
forw	Forward
FSRT	Fractionated stereotactic radiotherapy
GK	Gamma Knife
GI	Gradient index
GTV	Gross tumor volume
Gy	Gray
HNC	Head and neck cancer
IDL	Isodose line
IMRT	Intensity modulated radiotherapy
inv	Inverse
IOV	Inter-operator-variability
LC	Local control
LGP	Leksell GammaPlan
LINAC	Linear accelerator
MEN	Meningioma
MET	Metastasis
MLC	Multi-leaf collimator

MRI	Magnetic resonance imaging
MTRA	Medical technical radiology assistant
NPC	Nasopharyngeal carcinoma
NTCP	Normal tissue complication probability
OAR	Organ at risk
OCD	Obsessive-compulsive disorder
PA	Pituitary adenoma
PD	Prescription dose
PET	Positron emission tomography
PTV	Planning target volume
QoL	Quality of life
ROI	Region of interest
RION	Radiation-induced optic neuropathy
RT	Radiotherapy
SBRT	Stereotactic body radiotherapy
SCC	Squamous cell carcinoma
SIB	Simultaneous integrated boost
SNHL	Sensori-neural hearing loss
SRS	Stereotactic radiosurgery
SRT	Stereotactic radiotherapy
TCP	Tumor control probability
TMJ	Temporomandibular joint
TPS	Treatment planning system
VMAT	Volumetric intensity modulated arc therapy

1 INTRODUCTION

In 2018 around 498 000 German citizens were newly diagnosed with cancer and the numbers are rising ¹. With nearly 10 million deceased in 2020, it is one of the leading causes of death worldwide ² where an estimate of 277.597 are due to head and neck cancer (HNC) ³. Almost 90% of HNC are laryngeal, pharyngeal or oral squamous cell carcinoma (SCC) ⁴. Although the incidence of Nasopharyngeal Carcinoma (NPC) which arises from the epithelium of the nasopharynx is globally low and most prevalent in Eastern countries with 20 cases per 100.000 people, its treatment requires special attention due to its radioresistance and recurrence ⁵. Risk factors include Epstein–Barr virus (EBV), gender, geographic area and genetic disposition ^{6, 7}. Histologically, two main types can be differentiated: squamous cell carcinoma (SCC) and undifferentiated carcinoma and their prevalence was often linked to the geographic area. While SCC is more common in Europe and USA, undifferentiated carcinoma—which was also associated with EBV—is more frequent in Eastern countries ⁵. Although various treatment options for HNC and cancer in general depending on different factors (e. g. cancer type and stage, potential side effects, patient’s general condition) exist, NPC typically arises in practically inaccessible location, making it challenging for surgery ^{5, 8}. Hence, surgery which—together with radiation therapy and chemotherapy—is one of the most common options that aims at eliminating the cancer while not compromising the function of the nearby tissues and nerves is not suitable ^{4, 9}. NPC can generally be classified in three main settings using the international TNM staging system (tumor-node-metastasis) ¹⁰: early stage (T1–N0M0), locally advanced (T2–N0 until T4–N3M0) and recurrent or metastatic disease ⁵. Typically, early stage and some locally advanced tumors can be managed with radiotherapy alone while the remaining might require combined radio-chemotherapy ⁵. While the prognosis for early and locally advanced NPC managed with intensity-modulated radiotherapy (IMRT) alone or combined with chemotherapy is good (five year survival rate of 80–86% ¹¹), patients with recurrent/metastatic disease have a 5-year overall survival (OS) rate of approximately 28.8% ¹² and median survival time of 33 months. Recurrent diseases are developed by an estimate of 10% of the NPC patients after upfront radiotherapy using IMRT technique ¹³.

1.1 Radiation therapy

Radiation therapy (RT) aims at destroying malignant cancer cells while sparing the surrounding normal tissues. This is achieved by damaging the cancer cell's DNA using ionizing radiation. Due to faster repair mechanism of normal cells compared to cancer cells, the delivery of the radiation dose over multiple fractions can reduce normal tissue side effects without compromising the lethal effects on the cancer cells ^{4, 14, 15}.

External beam radiotherapy (EBRT) with linear accelerators (LINACs) uses high-energy photons or electrons generated outside the patient to deposit the dose in the depth of the tumor location inside the patient. Due to the fact that LINACs are built on gantries that can rotate around the patient, radiation can be delivered under a great amount of beam angles whose dose contributions focus inside the target volume ^{4, 15}. With therapy techniques such as IMRT and volumetric modulated arc radiotherapy (VMAT), conformal dose distribution of irregular-shaped cancer and improved sparing of nearby organs at risk (OAR) can be achieved ¹⁶⁻¹⁸. For some cancer types (e.g. liver, lung, brain) stereotactic radiosurgery (SRS) or stereotactic body radiotherapy (SBRT) using small photon fields with high doses, multileaf collimators (MLC) and flattening filter free (FFF) radiation beams are used to enhance the local tumor control probability (TCP) while reducing the treatment time and the OAR doses ¹⁹⁻²¹. Apart from LINACs, other stereotactic machines such as the Leksell Gamma Knife® (GK, Elekta AB, Sweden) or CyberKnife® (CK, Accuray, USA) enable fractionated or single fraction treatments of intracranial (GK, CK) and extracranial (CK) tumors.

1.2 Leksell Gamma Knife

The first GK prototype using cobalt-60 was installed in 1968 and was continuously improved ²². Today, the GK Perfexion™ and Icon™ are the latest models of the SRS device. While the former can only be used for single fraction treatment using a stereotactic head frame, the latter enables fractionated treatment with thermoplastic mask, cone beam computed tomography (CBCT) for positioning verification and infrared camera for motion tracking during treatment.

The GK units Perfexion and Icon consist of 192 cobalt-60 sources equally distributed in eight sectors around the patient head. The radiation from each source converges at the radiation focal point (RFP) which coincides with the mechanical isocenter of the

machine. The high dose volume around the isocenter originated from the convergence of radiation is called a shot that is characterized by its weighting, collimator setting (blocked, 4 mm, 8 mm or 16 mm) and position in stereotactic space. Using the aforementioned shot information together with the prescription (prescription dose and iso-dose line) and GK specific calibration and attenuation values, LGP calculates the required beam-on-time (BOT) for each shot and delivers the dose to the target by moving the patient treatment couch accordingly to the shot position in stereotactic space ²³. Because of dose rates between 1.4–3.2 Gy/min depending on the source age, GK treatments last typically longer than LINAC treatments ^{24, 25}. Due to the great number of non-coplanar, highly focused beams, the GK provides a dose fall-off outside the target and low dose to the healthy brain and OAR ^{24, 26-28}. Another advantage of the device is the high system positioning accuracy compared to conventional C-arm LINAC which allows to reduce the gross tumor volume (GTV) to planning target volume (PTV) setup margin when using mask treatment ²⁹⁻³¹. For stereotactic frame treatment, usually no margins are applied so that treatment planning is done directly on the GTV ³¹. Three dimensional treatment planning for GK SRS and fractionated stereotactic RT (FSRT) is done in Leksell GammaPlan® (LGP, Elekta AB, Sweden) Treatment Planning System (TPS) and was exclusively based on manual forward planning until 2021. For each patient, computed tomography (CT) or magnetic resonance imaging (MRI) techniques with specialized stereotactic protocols are used as a fundament for the delineation of targets and OAR, the creation of unique and highly accurate treatment plans and positioning verification ³². LGP allows for treatment planning with two dose calculation algorithms. While the tissue-maximum-ratio based algorithm (TMR10) models the head as a homogenous water volume, the convolution algorithm accounts for heterogeneities such as bone and air by using the electron density information extracted from CT data ²³. Because of the convolution algorithm needing additional CT imaging and the fact that the current GK clinical knowledge results from TMR experience, the use of the convolution algorithm in clinical practice has only been modestly adopted even though differences have been shown ³³⁻³⁷. Hence, when using the TMR10 dose calculation algorithm, treatment plans can be created after target delineation on the MR dataset. For frame based treatments, a CT scan on the treatment day is required as stereotactic reference and co-registered with the planning MR dataset to account for slight setup differences. For mask treatments, the on-board CBCT is used and co-registered with the MR dataset for the same purpose. In our institution,

the planning MRI is done in other departments or institutions resulting in different and unknown image distortions for each patient. To account for these distortion insecurities, CT imaging is routinely done for each patient independent of the fixation configuration. Consequently, for each of our patients, electron density information is available and the convolution algorithm could be used.

During the planning process, treatment shots are manually defined to achieve optimal target coverage, conformity (given by the selectivity metric or the Paddick Conformity Index “PCI”), Gradient Index (GI) and BOT. In addition to the enumerated plan metrics which are directly given by the TPS, dose values of Regions Of Interest (ROI) can be read from the Dose-Volume-Histogram (DVH). As mentioned previously, until 2021 the standard planning process in LGP was based exclusively on manual forward planning but can be assisted using the fill functionality and automated shot optimization³⁸. The former tool automatically positions shots inside the lesion in accordance to the prescription isodose line (IDL). The second optimizes the collimator configuration, weight and position of shots according to an objective function that is defined by the operator. This objective function works by using the operator’s relative importance settings (sliders) for the metrics coverage, selectivity, gradient index and BOT. This optimization does not change the number of shots inside the target nor does it allow for input of dose or dose-volume constraints, which is one of the key features of inverse planning^{38, 39}.

In 2021, Leksell Gamma Knife® Lightning (Elekta AB, Sweden) was introduced as the new inverse planning optimizer and integrated into LGP. Using the inverse optimization, the operator defines inverse planning constraints and the optimizer chooses the solution including shot number, position, weight, collimation and prescription (hereinafter also called planning) IDL with optimal merit.

Because of its geometry, GK treatment is commonly reduced to the brain and upper cervical regions. Typical medical conditions include small to medium sized benign and malignant brain tumors and metastases, arteriovenous malformations but also neurological conditions as trigeminal neuralgia, epilepsy or in some cases obsessive-compulsive disorder (OCD). In our institution, most patients treated at the GK present single or multiple metastases (MET), meningiomas (MEN), acoustic neuromas (AN) and pituitary adenomas (PA).

1.3 Radiation therapy for nasopharyngeal carcinoma

Radiation therapy is the main treatment option for NPC. In many cases, positive regional lymph nodes have to be treated in addition to the primary tumor as NPC has a high likelihood of developing nodal metastases^{40, 41}. With today's advances in MRI and Positron Emission Tomography (PET), affected regions can accurately be identified and delineated with the help of guidelines⁴². With imaging, the primary nasopharyngeal tumor and, if applicable, positive regional lymph nodes can be identified (GTV) and low- and high-risk clinical target volumes (CTV) need to be determined by the radiation oncologist. The optimal expansion margins to apply to these CTVs and whether they have to be considered high- or low-risk varies depending on the stage of the disease, guidelines and also institutional practices⁴⁰. Additionally, if the GTV is infiltrating critical structures, a tighter GTV to CTV margin can be applied. In this scenario, however, the TCP to normal tissue complication probability (NTCP) ratio needs to be rigorously evaluated⁴⁰. Although international CTV delineation guidelines as presented by Lee et al.⁴² advise to symmetrically include structures with risk of developing microscopic spread—regardless of the primary tumor location (e. g. central or lateral)—, research on sparing the contralateral structures for patients with unilateral tumors is going on⁴⁰.

Similarly to target delineation, radiation therapist usually adhere to international guidelines for dose prescription. Commonly, a simultaneous integrated boost (SIB) technique with IMRT is used to deliver 70 Gray (Gy) to the high risk volumes and lower doses of 50–60 Gy to low and intermediate risk volumes⁴⁰. IMRT has been reported to enable conformal dose delivery to the GTV while at the same time lowering the OAR doses which consequently improves LC and reduces adverse events⁴³⁻⁴⁶. Compared to the previously performed 2-dimensional conformal RT (2D CRT) and 3-dimensional conformal RT (3D CRT), the 5-year survival rates for T1–T4 NPC rose from 59–76% to 80–86% with modern IMRT^{11, 47}. Despite the advances in imaging, dose calculation and delivery techniques, the radio-therapeutic treatment of NPC remains challenging with, among other things, poor Local Control (LC) especially for larger tumors, little success of reirradiation and a high rate of late complications^{44, 48, 49}. In fact, most failures were found likely to be linked to radio-resistance and recurrences are often located in the high dose zones⁵⁰⁻⁵². With this knowledge, dose escalation strategies have been adopted to increase LC rates, however, the close proximity of radiosensitive

structures represents a challenge of local dose intensification⁵²⁻⁵⁴. Especially for recurrent diseases where the OAR already received doses close to the recommended limit, reirradiation has to be cautiously undertaken. In order to reduce the OAR doses and the radiation side effects, recent research has been focusing on identifying functionally active or radio-resistant areas for dose intensification. This way, dose escalation is performed on a smaller volume instead of the whole tumor⁴⁰.

1.4 Research objective

The aim of this research work was to investigate the feasibility of combining LINAC base and GK boost treatment for NPC. For this purpose, intermediate steps had to be taken.

The first step consisted in analyzing the advantages of the novel inverse planning module of GK TPS called Leksell Gamma Knife Lightning. Prior to Lightning, GK planning was based on manual forward planning which is known to be time consuming and the resulting plan quality and efficiency dependent on operator's experience. During the manual forward planning process, a multitude of shots in which the radiation from the cobalt sources focus have to be manually chosen. With the possibility of setting each sector to four different collimations and adjusting the shot weights and positions in three spatial directions in submillimeter steps, the potential of plan variations especially for novice operators is huge. With inverse planning using Lightning, the operator can choose maximum doses to the target and OAR and determine the relative importance of reaching low dose outside of the target and the BOT. Based on this input, the optimizer automatically achieves a treatment plan with optimal merit. Here, the benefits of the inverse optimizer in terms of plan quality and efficiency compared to manual forward planning were analyzed for different medical conditions extracted retrospectively from our clinical patient data base. Additionally, the inter operator variability of the plans was assessed.

Second, to pave the way to HNC treatment using the GK, the degree of inhomogeneity of Lightning plans had to be reduced in order to minimize normal tissue effects inside the target resulting from high point doses. As the clinical Lightning version does not allow for a maximum target dose below 133% of the prescription dose (PD) resulting in hotspots inside the target $\geq 1.33 \cdot PD$, a prototype version enabling higher homogeneity was provided by Elekta Instrument AB for research purposes only. When treating

cerebral cases like acoustic neuromas (AN), OAR as the cochlea and/or acoustic and facial nerves tend to be located inside the target volume and are very responsive to radiation. Similarly, for NPC, the mucous membranes inside and close to the target volume are particularly radiosensitive. In these cases, it is desirable to achieve a more homogenous dose distribution inside the target volume⁵⁵⁻⁵⁷. To analyze the potential of this prototype version, different medical conditions with OAR involvement requesting more homogenous plans were retrospectively selected from our database, treatment plans were generated and homogeneity and OAR sparing ranges compared to clinical LINAC and GK plans were defined.

Finally, the prototype version was used to generate treatment plans of selected NPC cases that have received in-house LINAC treatments. The aim was to investigate the feasibility and potential dosimetric advantage of delivering the last 10 Gy to the primary tumor (boost treatment) using the GK instead of the LINAC, to take advantage of the steep GK dose gradients. After the determination of a suitable patient cohort, boost plans for LINAC and GK were generated in order to compare the resulting plan quality. The homogenous prototype version was used for the GK plans since, as mentioned previously, radiosensitive structures are involved in NPC treatment and their protection requires higher homogeneity than is possible with inverse planning of the clinical version. A search of the available literature showed that this feasibility study is the first of its kind combining primary LINAC IMRT and fractionated GK Boost using inverse planning for NPC.

2 MATERIALS AND METHODS

In order to enable GK treatment planning for HNC and in this work especially for HNC of the NPX, more homogenous and automated treatment planning had to be utilized. First, the benefits of Leksell Gamma Knife Lightning, the novel inverse planning module integrated into Leksell Gamma Plan (LGP), were analyzed using retrospective clinical cases (chapter 2.1). Second, a more homogenous prototype version of Lightning was used retrospectively on clinical cases with OAR involvement to investigate the level of homogeneity and OAR sparing that can be achieved (chapter 2.2). Lastly, this homogenous prototype version was used to retrospectively generate boost plans of clinical NPC cases which are compared to the LINAC plans in order to analyze the feasibility and possible benefits of boosting NPC tumors using the GK (chapter 2.3).

2.1 Inverse planning with Leksell GK Lightning

While inverse planning for LINACs has been available for more than two decades and was shown to result in higher quality and less user dependent plans, it has only been introduced recently for GK SRS and FSRT ^{39, 58-60}. Until then, treatment planning had to be done exclusively with manual forward planning. With Leksell Gamma Knife Lightning, Elekta has launched their first inverse treatment optimizer for GK SRS and FSRT in 2021. The optimizer enables inverse planning for single or multiple targets using objectives like prescription, maximum dose to the target and OAR as well as BOT and low dose penalization (figure 2.1). Additionally, by activating the full coverage option (“fc” box, “cov” box in the released version) in the optimization dialog, the optimizer is forced to cover the entire target with the PD resulting in the highest possible target coverage.

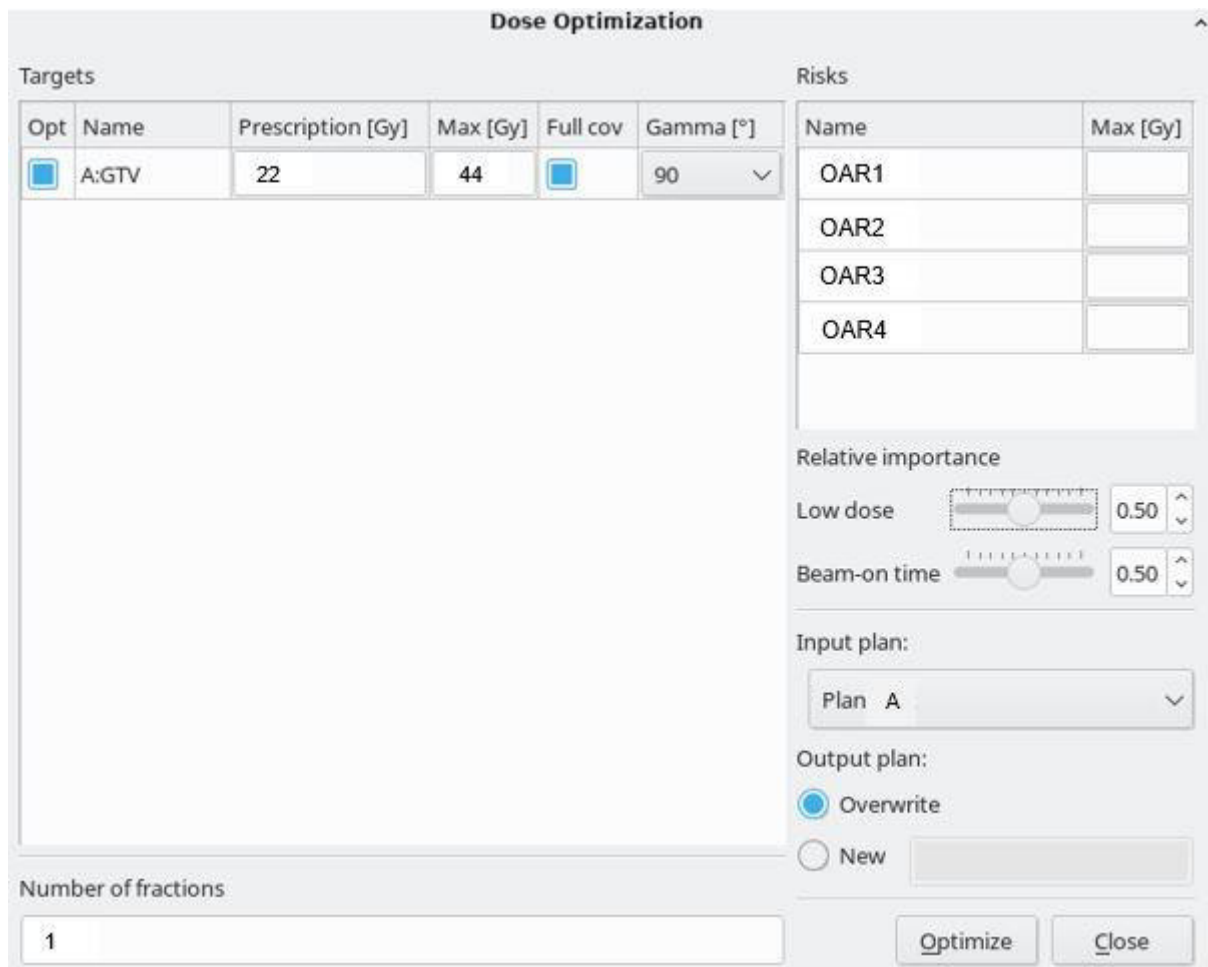


Figure 2.1: Dose optimization window with the pre-release version of Leksell Gamma Knife Lightning. GTV=gross tumor volume, OAR=organ at risk, full cov=full coverage.

The above figure 2.1 shows the optimization window which allows the user to determine the prescription dose and maximum dose to the target for the previously defined target (“A:GTV”). For structures defined as OAR, maximum doses can be set and the relative importance of the low dose and BOT using sliders can be fixed. The user can choose whether an existing plan should be overwritten or a new plan created. According to the fixed objectives, the optimizer finds the best solution in three phases: isocenter placement, optimization and sequencing⁶¹. During the first phase, isocenter positions are chosen which remain unchanged during the following phases, this way elaborating the search area of the optimization process. The more isocenter are set, the higher the degree of freedom to create a high quality plan but the longer the time needed to solve the optimization problem. In the second phase consisting of sector-duration-optimization, linear programming is used which is an approach that differs from early and traditional attempts⁶¹⁻⁶³. Knowing that multiple, possibly conflicting objectives can be set, their exact priority can be elaborated by the user and the optimizer will demonstrate

the possible concessions. The only physical hard constraint in the optimization is that times must be non-negative, meaning that this is a requirement that the solution must fulfill. For the remaining constraints, if each can be represented by a cost function, forming their weighted sum results in a single cost function where the weights represent the importance of each part of the function. When taken together, the different parts of the optimization problem can be described as a linear programming problem. The last phase consists in converting irradiation times to shots with collimator and sector configuration for each isocenter position ⁶¹.

This chapter focusses on determining the advantages of inverse planning using Lightning's inverse treatment optimizer in terms of plan quality and efficiency as well as inter-operator-variability (IOV).

2.1.1 Patient population and planning strategy

Patients with selected medical conditions and treated in-house with GK Icon between 2015 and 2020 were randomly chosen and their data sets retrospectively analyzed following IRB approval 2015–621 N-MA. The considered medical conditions were acoustic neuroma (AN, n=11), single and multiple metastases (MET, n=15) and meningioma (MEN= 12). Information about the study population is shown in table 2.1.

Table 2.1: Retrospective study population characteristics (AN = acoustic neuroma, MEN = meningioma, MET = metastases, Gy=Gray).

	AN	MEN	MET
Number of patients	11	12	10
Targets per patient (n=number of patients)	1 (n=11)	1 (n=12)	1(n=8), 2 (n=1), 5 (n=1)
Target volume (cc), median (range)	1.56 (0.24–5.77)	6.48 (0.27–15.96)	0.66 (0.04–7.02)
Prescription dose (Gy), median (range)	12 (11–50)	25 (12–52.2)	22 (8–22)
Prescription isodose line (%), median (range)	65 (50–80)	50 (45–80)	50
Number of fractions, median (range)	1 (1–27)	5 (1–26)	1 (1–2)

Patients were immobilized for stereotactic imaging and treatment with either the stereotactic G-Frame (single fraction SRS) or thermoplastic masks (single or multiple fractions). Each patient data set comprised the diagnostic MRI images used for initial treatment planning, CT images and, for mask treatments, CBCT images. Stereotactic CT and CBCT images were acquired following the same clinical in-house GK protocol for all patients. The diagnostic MRI images, however, originated from different departments whose imaging protocols might slightly differ. In the considered period, contouring and matching of the images from different modalities and the clinical treatment plan for each patient were realized by different physicians and physicists, respectively.

First, for each patient the clinical GK treatment plan with image, dose and structure data was exported from LGP v11.1, anonymized and imported into LGK Lightning (pre-release version with the complete inverse planning functionality of the released version) which was installed on a research laptop (research agreement). This way, by copying the delivered clinical plan (hereinafter referred to as forward plan), the dose rate was updated to the one of the deposited ^{60}Co sources to establish a baseline for comparison. As mentioned before, these clinical plans were generated by different op-

erators each of them having their own planning strategy. Hence, the complete functionality of LGP including the fill functionality and automated shot optimization might have been used. For targets with nearby OAR, the target coverage was compromised in order to meet the OAR dose constraints defined by the clinicians.

The next step consisted in calculating the inverse plans using the dose optimization dialog. Here, at least equal plan quality with the clinical forward plans was aimed. Due to the high number of planning metrics and the nature of the studied medical conditions, different strategies were adopted for the malign MET, the benign MEN and the AN. For MET, equal target coverage between forward and inverse plans was aimed which was likely to be achieved due to the typically round and even shape of metastases. For the remaining metrics, no equality with the forward plans was sought. For MEN and AN, the equality of the metrics coverage, selectivity and D_{\max} OAR between forward and inverse plans was pursued. Since these medical conditions have OAR involvement, according to the clinical practice the OAR sparing was prioritized in cases of conflict between target coverage and OAR doses exceeding clinical thresholds. In these benign situations, the main objective was to analyze how GK Lightning manages the conflict between OAR sparing and target coverage and the resulting impact on the plan efficiency described by the BOT.

Using these strategies for the corresponding medical conditions, two inverse plans per patient with (fc) and without (inv) the use of the full coverage box were created by a single operator. During the optimization process, D_{\max} OAR and D_{\max} target were restricted according to constraints set by the physician. D_{\max} target was restricted as it is the only way to influence the optimizer's choice of the planning IDL, which is usually part of clinicians' dose prescription. In light of this, for MET, two additional plans (inv and fc) were created without limiting D_{\max} target during the optimization process. The purpose of this was to let the optimizer freely choose the planning IDL that best fits the optimization constraints and compare the results to the plans with maximum dose limitation. Here it has to be emphasized, that in order to create a new plan the TPS requires the input of the PD, number of fraction and the prescription IDL. The IDL, however, is not maintained during the optimization process as the optimizer will chose the planning IDL that best fits the planning constraints.

To assess the effect different operators have on the optimization, one medical condition per group was planned by two additional operators with different planning experience. One operator had prior LGK Lightning and long forward planning experience with

LGP, the other LGP forward planning experience only. The planning objectives of this IOV analysis for the different groups were the same as mentioned above. All three operators were asked to create forward, inv and fc in adherence to clinician's constraints.

2.1.2 Statistical analysis of the collected data

The following plan quality and efficiency characteristics were extracted for all forward and inverse plans:

- Planning IDL (%)
- Number of shots
- Coverage
- Selectivity
- Gradient Index
- Beam-on-time (sec)
- D_{\max} target (Gy)
- $V_{12\text{Gy}}$ skull (cc)
- D_{\max} OAR (Gy) for AN and MEN

Rstudio® (PBC, USA) was used for statistical analysis of each group separately. As mentioned before, MET plans were calculated with and without maximum dose limitation to the target resulting in two groups: MET and MET_no_ D_{\max} .

The data was represented as boxplots and median, mean and interquartile range (IQR) were reported. The significance of the results was assessed using a paired samples Wilcoxon test (significance < 0.05) between forward and inverse plans. Additionally, for the metastases, the significance analysis was performed between the inverse plans of the MET and MET_no_ D_{\max} groups to evaluate the importance of limiting the maximum dose to the target.

For the IOV analysis, the absolute standard deviation of the operator dependent plans was calculated and graphically represented.

2.2 Homogenous GK planning

As mentioned previously, for some medical conditions with OAR respectively nerves crossing or abutting the target, a higher plan homogeneity is required to avoid normal tissue side effects. In the current clinical version of LGK Lightning, the maximum dose to the target cannot be set below $1.33 \cdot PD$. Elekta AB provided a prototype version of LGK Lightning, that allows for D_{max} target input inferior to that threshold (about $1.15 \cdot PD$). In this chapter, the range of homogeneity and OAR sparing that can be achieved using a more homogenous prototype version of LGK Lightning is presented. The results are set in proportion to the plan quality and efficiency that can be achieved with treatment plans of LINAC and the clinical GK TPS.

2.2.1 Patient selection and treatment planning for GK and LINAC

The in-house clinical database of patients treated between 2015 and 2022 with LINAC (Elekta Versa™ or Synergy™) or LGK Icon™ was searched for acoustic neuromas (AN, $n=10$), pituitary adenomas (PA, $n=10$) and meningiomas (MEN, $n=10$). Among these patients, cases requiring special plan homogeneity resulting from close OAR involvement were selected. The considered OAR for each patient was either in close proximity, abutting or crossing the target. The OAR (one per patient) were the cochlea, optic tract or pituitary stalk for AN, MEN and PA, respectively. For two patients, one AN and one PA, the considered OAR was located entirely inside of the target volume resulting in these two OAR to be analyzed separately from the other OAR of the groups. Figure 2.2 shows one example of target volume and considered OAR for each medical condition and table 2.2 gives an overview of the patient population together with the OAR constraints used for planning.

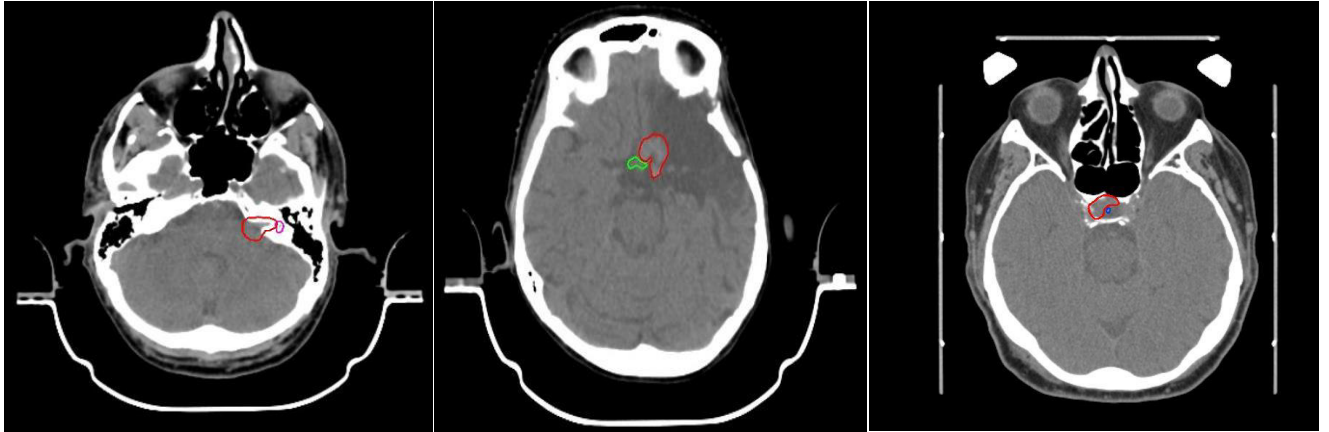


Figure 2.1: Example of studied acoustic neuroma (left), pituitary adenoma (middle) and meningioma (right). The target volume is represented in red and the organs at risk in pink, green and blue.

As can be seen from figure 2.2, the clinical treatments were done on the GK either with thermoplastic mask or stereotactic G-frame resulting in differences in target volume delineation. Additionally, PTV margins for mask treatments are usually chosen smaller when using modern frameless SRS systems⁶⁴⁻⁶⁶ compared to conventional LINACs. Hence, the LINAC PTV margin was chosen for treatment planning to create comparable conditions between the two devices.

Table 2.2: Characteristics of the retrospective study population and organs at risk dose constraints used for planning, OAR = Organ at risk, AN = acoustic neuroma, PA = pituitary adenoma, MEN = meningioma.

	AN	PA	MEN
Number of patients and OAR	10 (OAR n=9)	10 (OAR n=9)	10 (OAR n=10)
Considered OAR and dose constraint	cochlea ($D_{\text{mean}} < 45 \text{ Gy}$)	pituitary stalk ($D_{2\%} < 50 \text{ Gy}$)	chiasma ($D_{2\%} < 50 \text{ Gy}$)
Median distance OAR–target (mm): median axial sagittal coronal (range)	0.4 0.6 0.2 (0–1.1 0–1.6 0–2)	2.5 4.6 2.6 (0–6.2 0–10.9 0–6.8)	7.7 3.3 3.3 (0.8–19 0.6–12.1 0.6–13.5)

The Digital Imaging and Communications in Medicine (DICOM) image and structure data was extracted from the clinical database, anonymized and imported into Monaco TPS (Elekta AB, Sweden) version 6.1.1.0 and into the homogenous LGK Lightning

prototype version featuring the complete functionality of the clinical version but additionally enabling D_{\max} target $< 133\%$ of PD. For each clinical case, one LINAC (Monaco TPS) and three GK plans (prototype LGK Lightning TPS) were created with a PD of 54 Gy given in 30 fractions. To allow for easier analysis, this identical prescription was chosen throughout the whole patient population even though depending on the medical condition and the tumor stage prescriptions differ.

In Monaco, LINAC plans were calculated using VMAT technique for an Elekta Versa HD™ LINAC and a grid spacing of 0.1 cm. For each VMAT plan, two arcs were used: one full arc and one short, partial arc with couch rotation of 90° . The latter was used to ensure target coverage while at the same time preventing the radiation beam the eyes and optic pathways.

In the Lightning prototype version, three plans were generated for each patient: “LGK”, “LGK Hom” and “LGK OAR”. All three plans (hereinafter together referred to as “*Lightning plans*”) were optimized to meet the OAR dose constraints. The dose fall-off in the DVH was used as plan homogeneity indicator for plan selection and was defined as the difference between $D_{2\%}$ and $D_{99\%}$. LGK plans were optimized according to the lowest D_{\max} target value possible in the current clinical version ($1.33 \cdot PD$) and give the best achievable homogeneity. The plans entitled LGK Hom give the best achievable homogeneity ($< 1.33 \cdot PD$) while limiting the OAR dose to the LINAC plan value. LGK OAR plans aim at achieving similar or equal OAR dose values compared to the LGK plans while setting D_{\max} target $< 1.33 \cdot PD$. In case of OAR dose equality between LGK OAR plans, the plan with the best homogeneity was chosen. For all Lightning plans, the BOT which is a plan efficiency indicator, was not allowed to exceed 15 min per fraction which is in our experience a well-tolerated time for patients treated in 30 fractions. The LINAC and GK plans were calculated considering tissue inhomogeneities. This means, that in opposition to the common practice in the GK world where the TMR10 algorithm assumes the head as water, the convolution algorithm was used for calculation to account for tissue inhomogeneities cause by air and bone. Pantelis et al. recently published a study, where excellent agreement between convolution dose calculations, GafChromic EBT3 measurements and Monte-Carlo simulations was found ³⁶. With Monaco TPS, Monte Carlo algorithm was used.

2.2.2 Data acquisition and statistical analysis

After plan calculation all Lightning plans including dose, image and structure data were imported into Monaco TPS to start from a common baseline for the following statistical analysis. In Monaco, each patient contained four treatment plans (three GK plan, one LINAC plan) for which the cumulative DVHs of the considered structures were exported as text file (bin width = 1.0 cGy, resolution = 0.1 cm, volume units = %). Afterwards, the DVH text files were imported in RStudio® (PBC, USA) to normalize each plan to $D_{95\%}$ of the target volume. In Rstudio, mean DVHs for each structure, plan type and medical condition as well as for the total patient population generated and dosimetry characteristics as $D_{2\%}$ and D_{mean} for the target volume and considered OAR and the BOT per fraction were extracted. As an additional step in Rstudio®, a paired samples Wilcoxon test with a significance level of 0.05 was performed between the Lightning and LINAC plans.

For the last step of the analysis, Velocity™ (Varian Medical Systems Inc., USA) was used. The LINAC and Lightning plans were normalized to $D_{95\%}$ of the target volume and structures to define the plan quality metrics Gradient Index (GI), Paddick Conformity Index (PCI) and Homogeneity Index (HI) were created. The metrics are defined as:

$$GI = \frac{PV_{50\%}}{PIV} \quad (1)$$

$$PCI = \frac{TV_{PIV^2}}{TV \cdot PIV} \quad (2)$$

$$HI = \frac{D_{2\%} \text{ target}}{PD} \quad (3)$$

where PD is the prescription dose, TV the tumor volume, $PV_{50\%}$ the patient volume covered by 50% of the prescription IDL, PIV the prescription isodose volume and TV_{PIV} the target volume enclosed by the prescription IDL ^{24, 27}. The aforementioned metrics and the BOT were represented for each medical condition and for the total patient cohort as boxplots using Rstudio®.

2.3 Homogenous Leksell GK Lightning for treatment planning of NPC

In this chapter the previously acquired knowledge is used to retrospectively assess the feasibility and the extent of the dosimetric advantage of GK boost treatment of NPC compared to LINAC boost. This region was chosen because it was first estimated to be geometrically accessible for GK treatment and second, only the gross tumor is typically boosted in the last treatment fractions ^{40, 67}.

2.3.1 Preliminary patient selection and GK reachability

Because of the GK's static geometry, the anatomical reachability is limited and commonly restricted to the brain. However, in the past, some working groups explored treatment of the jaw and cervical regions pushing the assumed GK limits ⁶⁸⁻⁷⁰.

The in-house clinical database was searched for patients that were treated for NPC with LINAC between 2015 and 2023 in order to retrospectively use the DICOM images, plan, dose and structure files following IRB approval 2021–841 N-MA. Patients were immediately excluded if the tumor was assessed inaccessible due to anatomical reasons (short neck length) and large tumor size (long GK BOT). The remaining NPC patient DICOM data were anonymized and transferred from Monaco TPS to the homogenous Lightning prototype version which was also used in chapter 2.2. In GK TPS, the planning CT was visualized and patient positioning assessed with the assistance of a highly experienced Medical-Technical Radiology Assistant (MTRA) for GK. Since the planning CT was performed for LINAC treatment, patient positioning during the CT included LINAC specific patient positioning aids that differ from the GK aids. To retrospectively simulate the treatment at the GK without the specific positioning aids and hence assess the reachability of the target volume, the experienced MTRA performed the patient positioning based on the patient CT images and GK head rest for mask fixation in all three dimensions (figure 2.3). As for the anterior/posterior positioning of the head in the head rest, the thinnest but still tolerable head cushion was assumed which would reduce possible collisions ⁷¹. In craniocaudal direction, positioning was done according to the visible shoulder positions in the CT scan although, in a clinical setting, the shoulders are sometimes moved in caudal direction to increase the reachability if necessary. Based on this positioning, the inverse optimization console (chap-

ter 2.1) was used to quickly generate a first draft of a treatment plan in order to immediately exclude patients with a high number of colliding shots. Patient treatment plans that showed no or only a few collisions in the order of ≤ 10 shots for an average total shot number of 150 shots remained in the patient population.

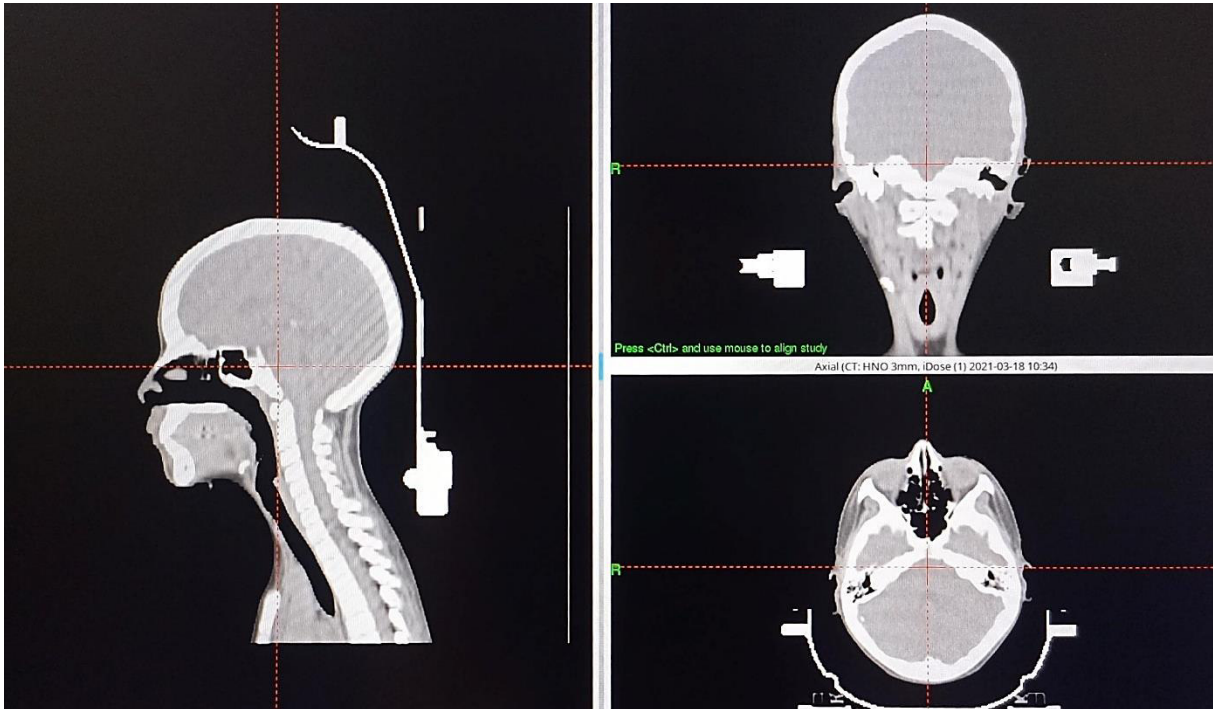


Figure 2.2: Patient positioning of the planning CT for LINAC treatment in Leksell GammaPlan. The patient head rest in the Gamma Knife head frame according to the anatomical patient properties.

2.3.2 Planning strategy for LINAC and GK boost plans and final patient selection

In Monaco TPS (Monte Carlo algorithm), the already delivered LINAC patient treatment plans were anonymized and transferred to a Monaco research platform to separate them from the clinical platform. Most patient folders comprised two plans: one base plan where the PTV includes the primary tumor and the lymph nodes (60 Gy, 2 Gy/fraction) and one boost plan to give additional dose (10 Gy, 2 Gy/fraction) to the gross tumor with a 5 mm margin (clinicians' definition) to increase tumor control. This procedure was chosen as common concept for the analysis. Hence, for patients with only one plan up to 70 Gy, the plan was recalculated with 60 Gy covering the previously mentioned PTV of the primary tumor and the lymph nodes ("PTV60") with the planning constraints adapted to a 60 Gy prescription. Afterwards, for all patients, a new volume

was generated as boost volume for the primary tumor. This volume was chosen to be the primary GTV + 3 mm margin which is a smaller margin than in our clinical practice for LINAC treatment. The reason for this is the higher total system accuracy of GK enabling smaller margins for mask treatment compared to conventional LINACs ^{29, 30}. A boost plan of 10 Gy with 2 Gy/fraction was calculated for this volume. During the optimization process, dose constraint for the considered OAR were tried to not be exceeded (table 2.3).

Table 2.3: Considered organs at risk and dose constraints ⁷².

Organs at risk	Considered dose constraints
Brainstem	0.035 cc < 60 Gy
Spinal cord	0.035 cc < 52.8 Gy
Parotids (each)	0.035 cc < 32 Gy
Parotids (each)	Mean < 26 Gy
Cochlea	0.035 cc < 40 Gy
Pituitary gland	0.035 cc < 50 Gy
Optic chiasm	0.035 cc < 52 Gy
Temporomandibular joint (TMJ)	0.035 cc < 65 Gy

In GK TPS (convolution algorithm), the newly generated PTV for each patient was uploaded from Monaco TPS and boost plans were calculated. As GK BOT are commonly significantly longer than LINAC BOT for large volumes, a maximum BOT of 60 min/fraction was set as planning constraint: plans exceeding this limit were discarded. Additionally, hot spots inside the target volume and especially in the mucous membranes, jaw bones and cranial/facial nerves were tried to be kept as low as achievable. At the end of the optimization process, the clearance window was used to check for collisions between the patient and the GK. In case of potential collisions of a few millimeters (marked as “i” or “!” in GK system), the shots in question were moved while ensuring target coverage. In case of unreachable and clearly colliding shots (marked as “x”) the patient was excluded from the patient population. Here, as for the LINAC plans, the constraints in table 2.3 were used as a guideline for OAR dose limitation. It has to be emphasized that the primary and nodal PTV (PTV60) can intersect with OAR resulting in already high OAR doses with the primary plan. Especially the parotids, one or both, are often partially or completely involving PTV60.

The final patient population using the first prototype version of homogenous Leksell Gamma Knife Lightning consisted of the patients listed in table 2.4. As it can be seen from the table, all patients had nodal involvement and different boost volume sizes. Four out of five tumors were central tumors whereas one tumor (patient P4) was more left-sided. Figure 2.3 shows an axial and sagittal slice of two studied patient CT scans: P1 with the largest (106.3 cc) and P5 with the smallest (26.8 cc) tumor volume.

Table 2.4: Considered organs at risk and dose constraint

Patients (NPC)	Tumor stage	Boost planning target volume (cc)	Intermediate imaging
P1	T2N2M0	106.3	No
P2	T3N1M0	58.8	No
P3	T2N3M0	65.5	No
P4	T2–3N0M0	57.0	No
P5	T4N2M0	26.8	Yes

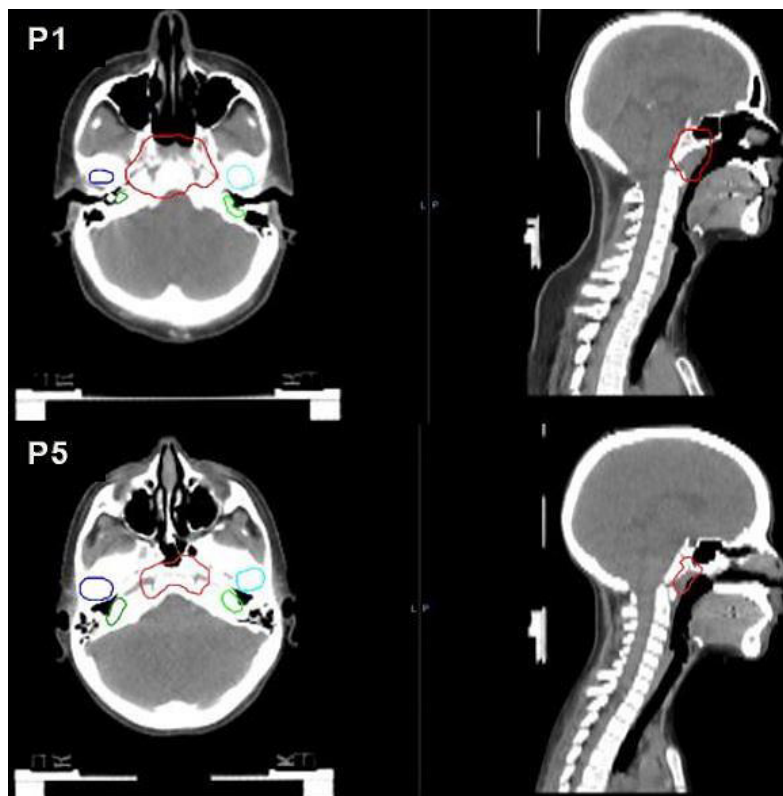


Figure 2.3: Axial and sagittal view of one CT scan slice of patient P1 (A) and P5 (B). The planning target volume is represented in red, the temporomandibular joints in dark (right) and light (left) blue and the cochleae in dark (right) and light (left) green.

2.3.3 Plan comparison and data analysis

For plan visualization and plan summation purposes, both LINAC and GK boost plans were transferred to Velocity and a normalization to $D_{90\%}$ of the target volume was done for each plan and a sum of boost and base plan was done. An experienced radiation therapist specialized in HNC treatment evaluated the dose distribution and plans were recalculated if needed. Once satisfying plans were obtained, the dose values of the sum plans were reported, GI and PCI were calculated for the boost plans (equations (1) and (2) chapter 2.2.2) and the not normalized GK boost plans were transferred from GK TPS to Monaco. In Monaco TPS, the cumulative DVHs for LINAC and GK boost plans were exported as text files for further analysis in Rstudio. The DVHs were exported twice, once with the volume units in % and once in cc to allow for further extraction of dose volume constraints. The remaining DVH settings were: bin width = 1.0 cGy and resolution = 0.1 cm. The transfer to Monaco was necessary because Velocity does not allow for cumulative DVH export.

Similar to Velocity, RStudio was first used for normalization of the plans to $D_{90\%}$ of the target volume. This was necessary because it is technically not possible to normalize GK plans in Monaco, nor is it possible to transfer the normalized dose files from Velocity. Second, the DVHs for LINAC and GK boost were represented together in one DVH for each patient and structure and as a mean over all patient. Finally, the dose values of the normalized boost for the different structures were reported.

3 RESULTS

3.1 Inverse planning with Leksell GK Lightning

3.1.1 Plan quality and efficiency

The plan quality (cov, sel, GI, D_{\max} OAR) and efficiency (BOT) characteristics for each plan and medical condition are represented in figure 3.1. The fc plans stand out from the forward and inverse plans with coverage > 0.99 and improved GI (lower values). The selectivity and OAR doses, however, are inferior compared to the other plan types. This reflects the fundamental idea behind the full coverage setting which, before anything else, aims at achieving maximum coverage of the target volume at the expense of other metrics. The selectivity of the inverse plans is enhanced or maintained compared to forward plans while higher coverage is achieved for AN and MEN. Additionally, despite the increased coverage, the OAR doses for MEN and AN are reduced compared to the forward plans. For MET, the coverage of forward plans is already high as these tumors are generally of round and even shape which facilitates forward planning. Hence, except for one outlier due to an uncommon target shape, the coverage of the inverse plans is equal or slightly worse compared to forward plans. Inverse and full coverage plans are also characterized by lower GI except for MEN and inverse plans. Finally, the BOT are reduced in both, inverse and full coverage plans.

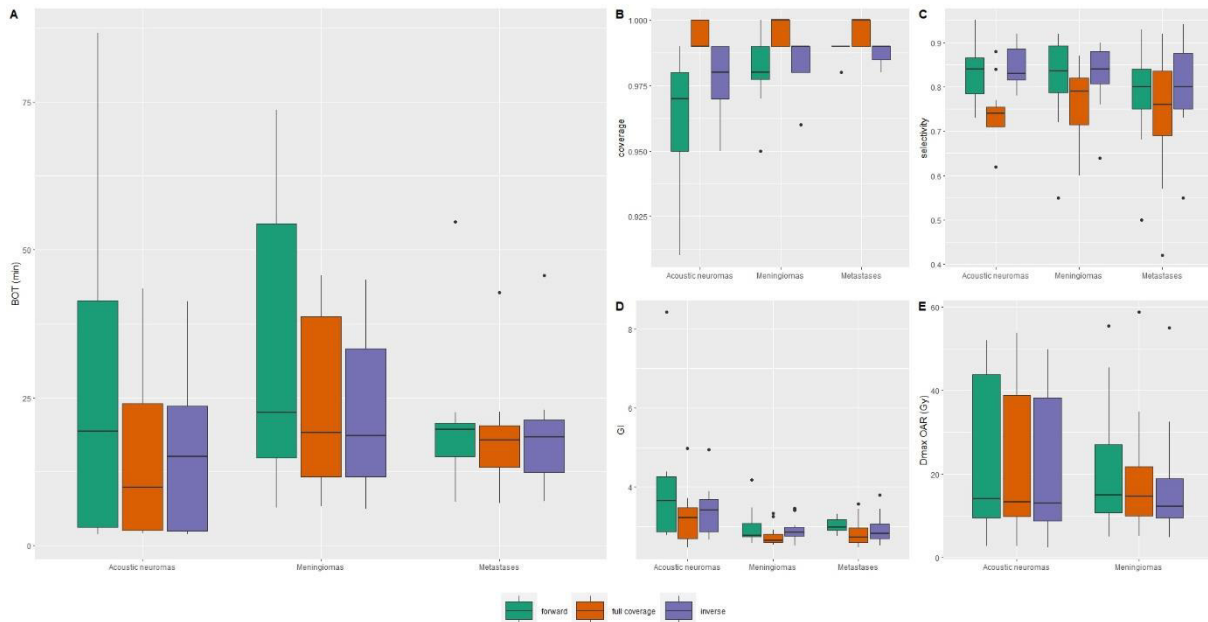


Figure 3.1: Beam-on-time (BOT) (A), coverage (B), selectivity (C), Gradient Index (GI) (D) and D_{max} OAR (E) for forward (green), full coverage (orange) and inverse (purple) plans and the medical conditions acoustic neuromas, meningiomas and metastases. The organs at risk doses are only shown for acoustic neuromas and meningiomas since for the metastases no organs at risk were analyzed.

Table 3.1–3.4 give the detailed plan statistics for the studied metrics per medical condition together with the p-values. From these tables, the significance of the changes between forward and inv/fc plans depicted in figure 3.1 can be assessed. The improvement in coverage is significant for all medical conditions and fc plans (AN: $p=0.006$; MEN: $p = 0.005$; MET: $p = 0.006$; MET_no_Dmax: $p = 0.01$) as well as for AN inv plans ($p = 0.042$). Similarly, GI is significantly improved for all fc plans (AN: $p = 0.001$; MEN: $p = 0.01$; MET: $p = 0.024$; MET_no_Dmax: $p = 0.012$) and for AN inv plans ($p = 0.005$). The selectivity is significantly decreased in all fc plans (AN: $p = 0.008$; MEN: $p = 0.028$; MET: $p=0.035$; MET_no_Dmax: $p=0.046$) and improved in MET inv plans ($p = 0.049$). The difference in planning IDL between forward and Lightning inv plans is significant for MEN ($p = 0.007$) and MET ($p = 0.007$), where the optimizer chose higher IDL in both cases. As mentioned previously, the change in IDL results in a change of D_{max} target which is significant for MEN inv ($p = 0.001$) and fc ($p = 0.038$) plans and MET inv plans ($p = 0.021$). In the benign groups, the reduction in D_{max} OAR is significant for inv plans in both medical conditions (AN: $p = 0.007$; MEN: $p = 0.002$) and the BOT is significantly shortened (AN: fc $p = 0.01$, inv $p = 0.008$; MEN: fc $p = 0.017$, inv $p = 0.007$). For metastases, V_{12Gy} skull is significantly reduced for the inverse plans for MET and MET_no_Dmax (MET: $p = 0.025$; MET_no_Dmax: $p = 0.049$).

The significance analysis between the MET and MET_no_Dmax groups shows significant changes for the planning IDL, GI and D_{max} target. Without maximum dose limitation to the target and for fc plans, GI ($p = 0.032$) and the planning IDL ($p = 0.021$) are decreased and Dmax target ($p = 0.022$) increased.

Table 3.1: Plan quality and efficiency metrics with statistics (median, inter quartile range, mean) for acoustic neuroma (AN). cov = coverage, sel = selectivity, GI = Gradient Index, BOT = beam-on-time, forw = forward, fc = full coverage, inv = inverse.

AN	Planning IDL (%)			Number of shots			Cov		
	median	IQR	mean	median	IQR	mean	median	IQR	Mean
forw	65	30	66.36	13	30	17.65	0.97	0.03	0.959
fc	67	11	65	11	11	17.9	0.99	0.01	0.994
p-value	0.755			0.964			0.006		
inv	74	11.5	68.45	13	4.5	17.73	0.98	0.02	0.977
p-value	0.285			0.929			0.042		
	sel			GI			D _{max} target (Gy)		
	median	IQR	mean	median	IQR	mean	median	IQR	Mean
forw	0.84	0.08	0.83	3.65	1.38	3.934	24	37.8	38.36
fc	0.74	0.045	0.743	3.22	0.795	3.227	21.4	47.6	40.38
p-value	0.008			0.001			0.365		
inv	0.83	0.07	0.845	3.41	0.82	3.375	23.1	46.6	38.86
p-value	0.247			0.005			0.656		
	V _{12Gy} skull (cc)			D _{max} OAR (Gy)			BOT (min)		
	median	IQR	mean	median	IQR	mean	median	IQR	Mean
forw	6.606	15.9	11.225	14.1	34.3	23.58	19.3	38.2	28.19
fc	7.527	14.3	11.157	13.35	28.9	23.61	9.8	21.4	14.23
p-value	0.278			0.985			0.01		
inv	6.875	13.7	9.797	12.95	29.5	22.52	15	21.2	14.71
p-value	0.067			0.007			0.008		

Table 3.2: Plan quality and efficiency metrics with statistics (median, inter quartile range, mean) for meningioma (MEN). cov = coverage, sel = selectivity, GI = Gradient Index, BOT = beam-on-time, forw = forward, fc = full coverage, inv = inverse.

MEN	Planning IDL (%)			Number of shots			Cov		
	median	IQR	mean	median	IQR	mean	median	IQR	mean
forw	50	0	52.17	25	18.20	28.5	0.98	0.012	0.979
fc	66.5	5.5	66.75	36	20.50	35.83	1	0.01	0.997
p-value	0.322			0.169			0.005		
inv	69.5	5	68.67	34.5	16.50	35.25	0.99	0.001	0.985
p-value	0.007			0.147			0.071		
	sel			GI			D _{max} target (Gy)		
	median	IQR	mean	median	IQR	mean	median	IQR	mean
forw	0.83	0.105	0.818	2.77	0.345	2.982	50	18	43.27
fc	0.79	0.105	0.767	2.64	0.208	2.772	35.2	14	34.85
p-value	0.028			0.01			0.038		
inv	0.84	0.072	0.826	2.85	0.21	2.917	35.45	12.6	33.55
p-value	0.788			0.754			0.001		
	V _{12Gy} skull (cc)			D _{max} OAR (Gy)			BOT (min)		
	median	IQR	mean	median	IQR	mean	median	IQR	mean
forw	15.363	24.7	26.046	14.9	16.2	21.74	22.55	39.6	33.07
fc	17.262	24	25.355	14.4	11.7	19.75	19.05	27.1	24.15
p-value	0.266			0.192			0.017		
inv	15.316	23.4	24.439	12.25	9.4	17.94	18.55	21.7	22.06
p-value	0.97			0.002			0.007		

Table 3.3: Plan quality and efficiency metrics with statistics (median, inter quartile range, mean) for metastases (MET). cov = coverage, sel = selectivity, GI = Gradient Index, BOT = beam-on-time, forw = forward, fc = full coverage, inv = inverse.

MET	Planning IDL (%)			Number of shots			cov			Sel		
	median	IQR	mean	median	IQR	mean	median	IQR	mean	median	IQR	mean
forw	50	0	50	7	5	11.87	0.99	0	0.998	0.8	0.09	0.782
fc	51	6	51.8	9	13.5	13.87	1	0.01	0.995	0.76	0.145	0.754
p-value	0.322			0.255			0.006			0.035		
inv	53	7.5	54.93	11	10	14.2	0.99	0.005	0.987	0.8	0.125	0.805
p-value	0.007			0.115			0.766			0.049		
	GI			D _{max} target (Gy)			V _{12Gy} skull (cc)			BOT (min)		
	median	IQR	mean	median	IQR	mean	median	IQR	mean	median	IQR	mean
forw	2.99	0.09	3.021	40	15	35.73	3.812	3.33	4.557	19.6	5.6	19.74
fc	2.73	0.36	2.835	37.3	14.2	35.23	4.21	2.53	4.598	17.8	7.1	18.17
p-value	0.024			0.906			0.761			0.306		
inv	2.83	0.125	2.922	36.1	12.5	33.35	3.476	2.7	4.294	18.4	8.85	18.36
p-value	0.065			0.021			0.025			0.125		

Table 3.4: Plan quality and efficiency metrics with statistics for metastases (MET) without maximum target limitation (MET no Dmax). cov = coverage, sel = selectivity, GI = Gradient Index, BOT = beam-on-time, forw = forward, fc = full coverage, inv = inverse.

MET no Dmax	Planning IDL (%)			Number of shots			cov			Sel		
	median	IQR	mean	median	IQR	mean	median	IQR	mean	median	IQR	mean
forw	50	0	50	7	5	11.87	0.99	0	0.988	0.8	0.009	0.787
fc	50	7.5	50.27	9	12.5	13.53	0.99	0.01	0.995	0.73	0.15	0.745
p-value	1.00			0.267			0.010			0.046		
inv	53	8.5	53.13	11	14.5	14.6	0.99	0.005	0.987	0.79	0.13	0.803
p-value	0.083			0.100			0.053			0.068		
	GI			D _{max} target (Gy)			V _{12Gy} skull (cc)			BOT (min)		
	median	IQR	mean	median	IQR	mean	median	IQR	mean	median	IQR	mean
forw	2.99	0.27	3.021	40	15	35.73	3.812	3.33	4.557	19.6	5.6	19.74
fc	2.71	0.365	2.801	37.3	13.8	36.86	4.21	2.52	4.557	18.5	7.5	18.58
p-value	0.012			0.553			0.842			0.977		
inv	2.78	0.415	2.896	36.1	12.5	34.22	3.476	3.05	4.365	18.4	7.15	18.57
p-value	0.053			0.147			0.049			0.222		

Figure 3.2–3.4 show the dose distribution in one axial slice for one studied case per medical condition and table 3.5 gives the relevant DVH statistics extracted from the dose evaluation window for each plan type. The planning IDL, cov, PCI (measure for sel), GI, D_{max} target and OAR and the BOT per fraction are represented.

For the benign cases, the exemplary AN was planned with 50 Gy in 25 fractions (figure 3.2) and the MEN with 25 Gy in 5 fractions (figure 3.3). For AN, the responsible clinician prescribed 50 Gy to the 80% target covering IDL. The optimizer, however, chose a slightly lower IDL for the inv (76%) and fc (75%) plans resulting in higher D_{max} target. While the coverage is slightly increased (fc) or equal (inv), the Lightning plans result in reduced GI and OAR doses compared to the manual forward plans but slightly inferior conformity (PCI). For MEN, 25 Gy were prescribed to the 50% target covering IDL (fig. 3.3). In the Lightning plans, the optimizer chose higher planning IDL (fc: 64%; inv: 68%) to meet the optimization constraints resulting in lower D_{max} target compared to the forward plan. In the Lightning plans, the OAR doses are maintained or reduced while the coverage is increased by an important amount (forw: 0.95; fc: 0.99; inv: 0.98). GI is improved for fc and slightly worsened for inv and the PCI is increased for inv. For both benign conditions, BOTs are reduced.

For MET (figure 3.4), 22 Gy in one fraction were prescribed to the 50% target covering IDL resulting in D_{max} target of 44 Gy. For inv and fc plans, the optimizer chose higher IDL (fc: 59%; inv: 61%) resulting in D_{max} target < 44 Gy. The high coverage of 0.99 that is reached in the forward plan is maintained in the Lightning plans. The GI are reduced

and the BOT per fraction increased. Additionally, the conformity of the Lightning plans is increased (forw: 0.84; fc: 0.90; inv: 0.91).

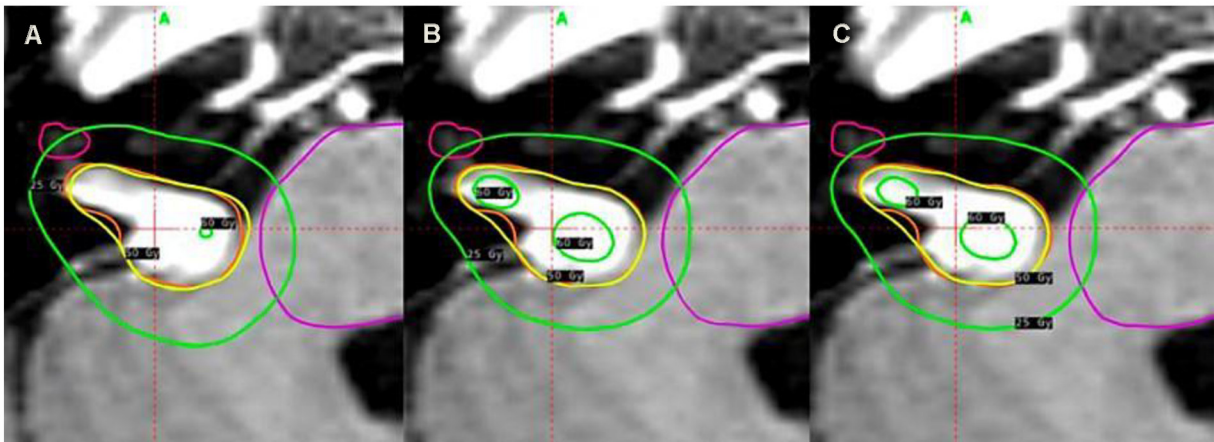


Figure 3.2: Dose distribution in one slice of one studied acoustic neuroma and forward (A), full coverage (B) and inverse (C) plans. The PTV (orange), brainstem (purple), cochlea (pink), planning isodose line (yellow) and isodose lines (green) for 25 Gy and 60 Gy are shown.

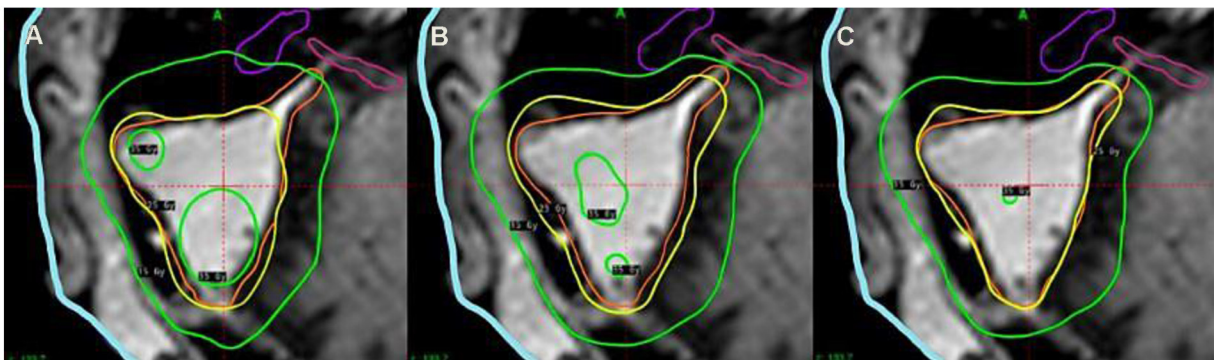


Figure 3.3: Dose distribution in one slice of one studied meningioma and forward (A), full coverage (B) and inverse (C) plans. The PTV (orange), cochlea (purple), acoustic nerve (pink), skull (light blue), planning isodose line (yellow) and isodose lines (green) for 15 Gy and 35 Gy are shown.

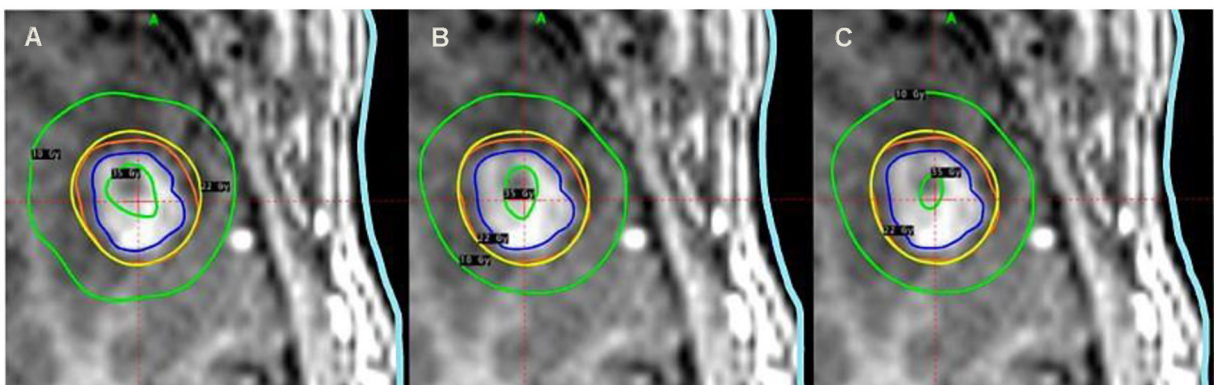


Figure 3.4: Dose distribution in one slice of one studied meningioma and forward (A), full coverage (B) and inverse (C) plans. The PTV (orange), GTV (blue), skull (light blue), planning isodose line (yellow) and isodose lines (green) for 10 Gy and 35 Gy are shown.

Table 3.5: Plan quality and efficiency metrics with statistics for the exemplary cases in figures 3.2–3.4
cov = coverage, *PCI* = Paddick Conformity Index, *GI* = Gradient Index, *BOT* = beam-on-time, *fx* = fraction, *forw* = forward, *fc* = full coverage, *inv* = inverse.

	metric	forw	fc	Inv
AN	Planning IDL (%)	80	75	76
	<i>cov</i>	0.98	0.99	0.98
	<i>PCI</i>	0.87	0.84	0.86
	<i>GI</i>	4.34	3.33	3.46
	D_{\max} target (Gy)	62.5	66.7	65.8
	D_{\max} OAR (Gy)	Brainstem: 46,8 Cochlea: 42.8	Brainstem: 45,2 Cochlea: 36.6	Brainstem: 44.6 Cochlea: 36.1
	<i>BOT</i> / <i>fx</i> (min)	2.7	2.2	2.1
MEN	Planning IDL (%)	50	64	68
	<i>cov</i>	0.95	0.99	0.98
	<i>PCI</i>	0.79	0.70	0.82
	<i>GI</i>	2.75	2.63	2.83
	D_{\max} target (Gy)	50	39.1	36.8
	D_{\max} OAR (Gy)	Acoustic nerve: 13.7 Cochlea: 22.1	Acoustic nerve: 13.7 Cochlea: 21.8	Acoustic nerve: 10.6 Cochlea: 20.1
	<i>BOT</i> / <i>fx</i> (min)	21.9	18.1	18.4
MET	Planning IDL (%)	50	59	61
	<i>cov</i>	0.99	0.99	0.99
	<i>PCI</i>	0.84	0.90	0.91
	<i>GI</i>	2.87	2.48	2.50
	D_{\max} target (Gy)	44	37.3	36.1
	<i>BOT</i> / <i>fx</i> (min)	22.3	25.7	22.6

3.1.2 Inter operator variability

The absolute IOV of the operator dependent plans is represented in figure 3.5. Additionally, the values of the plan quality and efficiency metrics can be found for each plan and operator in table 3.6. The smaller the IOV, the lower the plan variation between the different operators. An IOV of zero stands for equality of the considered metric.

In general, as it can be seen in figure 3.5, the metrics *cov*, *sel*, *GI* as well as the OAR doses are very similar between the operators and for all medical conditions. For the remaining metrics, the most differences are observed for the MEN case.

As mentioned previously, there is a link between planning IDL and D_{\max} target. Hence, for forward planning, these metrics show no variation since the planning IDL stays unchanged during forward planning. For AN, while the IOV is small for the plan quality metrics, high variations are found for the BOT (IOV = 16 min). This is linked to one operator planning with a high amount of blocked sectors which is often observed when using the automated shot optimization. For MEN, the highest IOV is observed for the number of shots (2.3) and V_{12Gy} skull (5.08 cc). For MET, only small deviations occur. The highest variations are observed for the metrics number of shots (1.53) and BOT (1.5 min).

With inverse planning using Lightning, the planning IDL is not maintained during the optimization process. These variations are especially expressed for AN and MEN (AN: fc = 2.65, inv = 4.04; MEN: fc= 3.05, inv = 6.03) and result in differences in D_{\max} target (AN: fc = 0.74, inv = 1.01; MEN: fc= 2.02, inv = 3.43). Although the number of shots differ for all medical conditions, the variability is more expressed for MEN (fc = 7.0, inv = 7.23) which can be linked to generally larger targets compared to AN and MET and also shows in the metric V_{12Gy} skull (fc = 2.21, inv = 1.90). Finally, similar to forward planning, small variations in BOT occur for all medical conditions and mostly in the fc plans (AN: fc = 3.35; MEN: p = 2.37; MET: p = 1.08).

Table 3.6: Plan quality and efficiency metrics for different operators (Op1, Op2, Op3) and one case of each medical condition group. AN = acoustic neuroma, MEN = meningioma, MET = metastases, cov = coverage, sel = selectivity, GI = Gradient Index, BOT = beam-on-time, forw = forward, fc = full coverage, inv = inverse.

		AN				MEN				MET			
		Op1	Op2	Op3	IOV	Op1	Op2	Op3	IOV	Op1	Op2	Op3	IOV
Planning IDL (%)	forw	65	65	65	0	50	50	50	0	50	50	50	0
	fc	69	70	65	2.65	64	60	58	3.05	59	60	60	0.58
	inv	74	74	67	4.04	68	73	61	6.03	61	62	62	0.58
No. of shots	forw	6	6	5	0.58	22	22	26	2.3	7	9	6	1.53
	fc	11	9	14	2.52	40	47	33	7.0	14	10	10	2.31
	inv	15	15	15	0	45	32	33	7.23	12	12	13	0.58
cov	forw	0.91	0.91	0.91	0	0.95	0.94	0.96	0.01	0.99	0.99	0.99	0
	fc	1.0	0.99	1.0	0.01	0.99	0.99	0.99	0	1.0	1.0	0.99	0.01
	inv	0.98	0.97	0.97	0.01	0.98	0.97	0.98	0.01	0.99	0.99	0.99	0
sel	forw	0.81	0.83	0.82	0.01	0.83	0.77	0.84	0.04	0.85	0.87	0.89	0.02
	fc	0.71	0.74	0.72	0.01	0.70	0.68	0.75	0.04	0.88	0.88	0.88	0
	inv	0.83	0.86	0.84	0.01	0.84	0.83	0.82	0.01	0.92	0.92	0.93	0.01
GI	forw	3.65	3.56	3.42	0.12	2.75	3.06	3.06	0.12	2.87	2.84	3.23	0.23
	fc	3.22	3.18	2.99	0.12	2.63	2.54	2.63	0.05	2.47	2.48	2.49	0.01
	inv	3.41	3.6	3.32	0.14	2.83	2.93	2.73	0.10	2.50	2.51	2.50	0.01
D_{max} target (Gy)	forw	18.5	18.5	18.5	0	50.0	50.0	50.0	0	44.0	44.0	44.0	0
	fc	17.4	17.1	18.5	0.74	39.1	41.6	43.1	2.02	37.3	36.7	36.7	0.35
	inv	16.2	16.1	17.9	1.01	36.8	34.2	41.0	3.43	36.1	35.5	35.5	0.35
D_{max} OAR1 (Gy)	forw	10.2	10.7	10.6	0.26	22.1	20.7	21.7	0.72	NN			
	fc	12.6	13.0	12.6	0.23	21.8	23.3	21.5	0.96				
	inv	12.6	11.8	11.4	0.61	20.1	19.7	20.4	0.35				
D_{max} OAR2 (Gy)	forw	5.3	5.5	5.3	0.15	13.7	15.0	14.3	0.65				
	fc	4.8	4.9	5.2	0.21	13.7	14.7	13.0	0.85				
	inv	5.1	4.6	4.8	0.25	10.6	10.6	12.4	1.04				
V_{12Gy} skull (cc)	forw	0.32	0.32	0.32	0	53.11	63.15	59.54	5.08	6.52	6.36	6.99	0.32
	fc	0.42	0.4	0.41	0.01	62.90	63.26	59.26	2.21	5.55	5.57	5.55	0.01
	inv	0.35	0.33	0.33	0.001	55.44	58.62	55.24	1.90	5.33	5.34	5.28	0.03
BOT (min)	forw	39.5	11.9	11.6	16.0	20.2	19.6	20.9	0.51	20.6	22.1	23.6	1.50
	fc	18.2	18.0	23.9	3.35	16.7	21.3	20.0	2.37	21.6	19.9	19.6	1.08
	inv	3.41	3.6	3.32	0.14	17.0	17.2	19.0	1.10	21.3	19.2	19.9	1.07

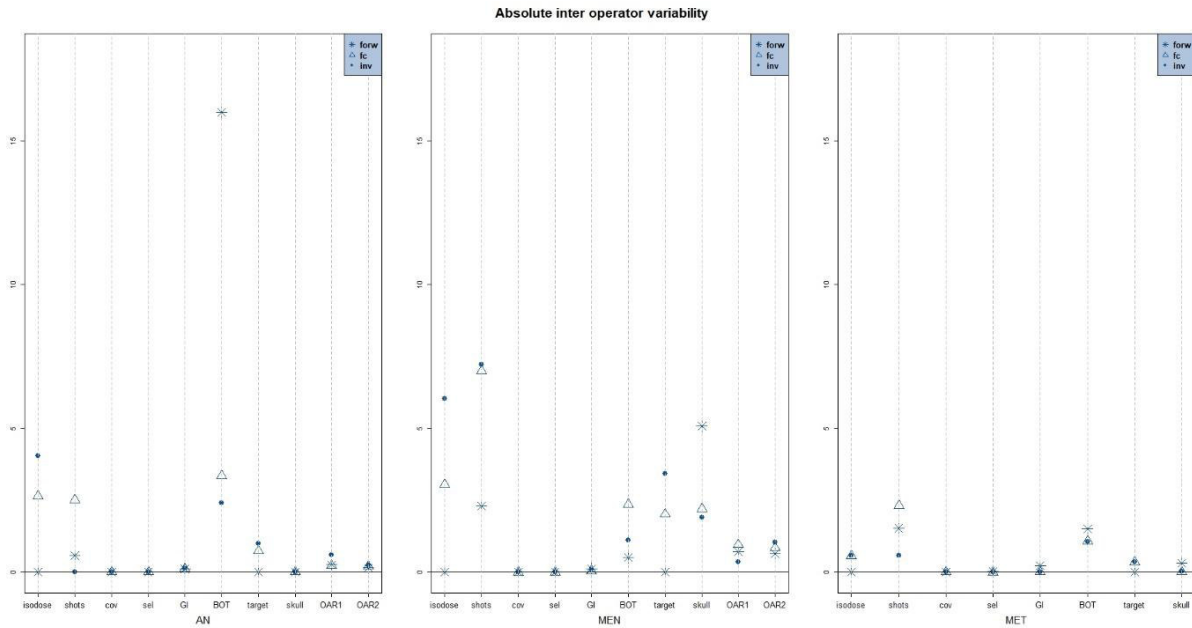


Figure 3.5: Absolute inter operator variability (IOV) for the plans forward (forw), full coverage (fc) and inverse (inv) and the metrics isodose, shots, coverage (cov), selectivity (sel), Gradient Index (GI), beam-on-time (BOT), D_{max} target (target), V_{12Gy} skull (skull) and D_{max} OAR1 and 2 (OAR1, OAR2).

3.2 Homogenous Leksell GK Lightning

3.2.1 Plan quality and efficiency – medical conditions and total patient cohort

Figure 3.6 shows the metrics GI, PCI, HI and BOT for the medical conditions and plan types as boxplots. The statistical values (mean, median, IQR) for the plans can be found in table 3.7 for each medical condition group separately as well as in table 3.8 for the total patient cohort. Table 3.8 also features the results of the paired samples Wilcoxon test.

When comparing the Lightning and the LINAC plans, the GI is significantly improved for the former (LGK Hom: $p < 0.001$ | LGK OAR: $p < 0.001$ | LGK: $p < 0.001$). Especially for AN, median GI for the group is improved from 7.80 (LINAC) to 3.78 (LGK Hom), 3.67 (LGK OAR) and 3.05 (LGK). The PCI is increased for PA (LGK Hom, LGK OAR, LGK) and MEN (LGK OAR, LGK) and decreased for AN in all Lightning plans. Considering the total patient cohort, the change in PCI only reaches significance for LGK compared to LINAC (LGK Hom: $p = 0.0976$ | LGK OAR: $p = 0.859$ | LGK: $p < 0.001$). For all Lightning plans in the total patient population the HI is significantly worse compared to the LINAC plans (LGK Hom: $p < 0.001$ | LGK OAR: $p < 0.001$ | LGK: $p < 0.001$). The LGK plans show

the highest inhomogeneity followed by LGK OAR and LGK Hom. Comparing the IQR for the different medical conditions and plans, the LINAC IQR is small for all medical conditions. All Lightning plans exhibit higher BOT per fraction compared to the LINAC plans (LGK Hom: $p < 0.001$ | LGK OAR: $p < 0.001$ | LGK: $p < 0.001$) but the times remain within the planning constraint limit (BOT < 15 min). The BOTs for the different medical conditions are longest for MEN followed by PA and AN and the IQR is highest for AN and lowest for MEN. For small targets (AN and PA) the increase of homogeneity in the Lightning plans results in comparable or shortened BOTs. For larger targets (MEN), however, the BOTs are increased with higher homogeneity. Although the BOT of the LINAC plans is significantly shorter, it does not include the time needed for the couch rotation (treatment time).

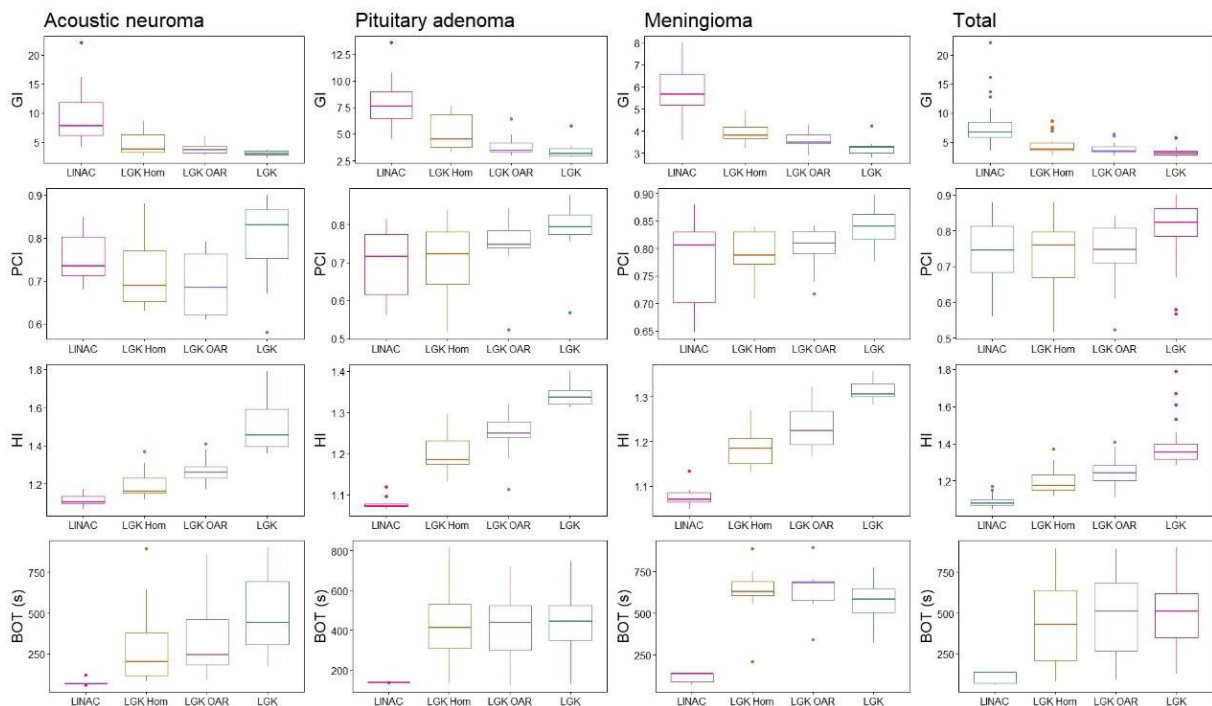


Figure 3.6: Gradient Index (GI), Paddick Conformity Index (PCI), Homogeneity Index (HI) and beam-on-time (BOT) for acoustic neuromas, pituitary adenomas, meningiomas and the plans LINAC (pink), LGK Hom (yellow), LGK OAR (purple) and LGK (green).

Figures 3.7–3.10 show the mean DVHs for the medical conditions, plan types and the structures PTV, skull and the considered OAR (cochlea for AN, pituitary stalk for PA and chiasma for MEN). The DVHs for PTV show that for all medical conditions, the highest homogeneity is given by the LINAC plans. LGK Hom is the second homogenous, LGK OAR the third homogenous and LGK the least homogenous. The difference

in dose drop-off between LGK Hom and LGK OAR is smallest for MEN and similar between AN and PA. For AN, the LGK Hom curve seems to be closer to the LINAC curve than for PA and MEN. When looking at the total patient cohort (figure 3.10) the LGK curve for PTV converges towards higher dose values due to high PTV doses and flat dose drop-off of the LGK plans for AN.

When analyzing the OAR doses for all medical conditions, the highest values can be found in the LINAC plans and the lowest in LGK plans. LGK OAR plans are the second lowest and LGK Hom the third lowest. The significance analysis (table 3.8) shows, that the OAR dose reduction of the Lightning plans compared to the LINAC plans is significant for LGK and LGK OAR (LGK Hom: $p=0.152$ |LGK OAR: $p<0.001$ |LGK: $p<0.001$). For OAR in all three medical conditions, LINAC and LGK Hom have a similar curve progression and partially overlap. The same characteristic can be observed for LGK OAR and LGK plans. For the skull, the Lightning plan curves are very similar and partially overlapping, the LINAC curve, however, shows higher dose values.

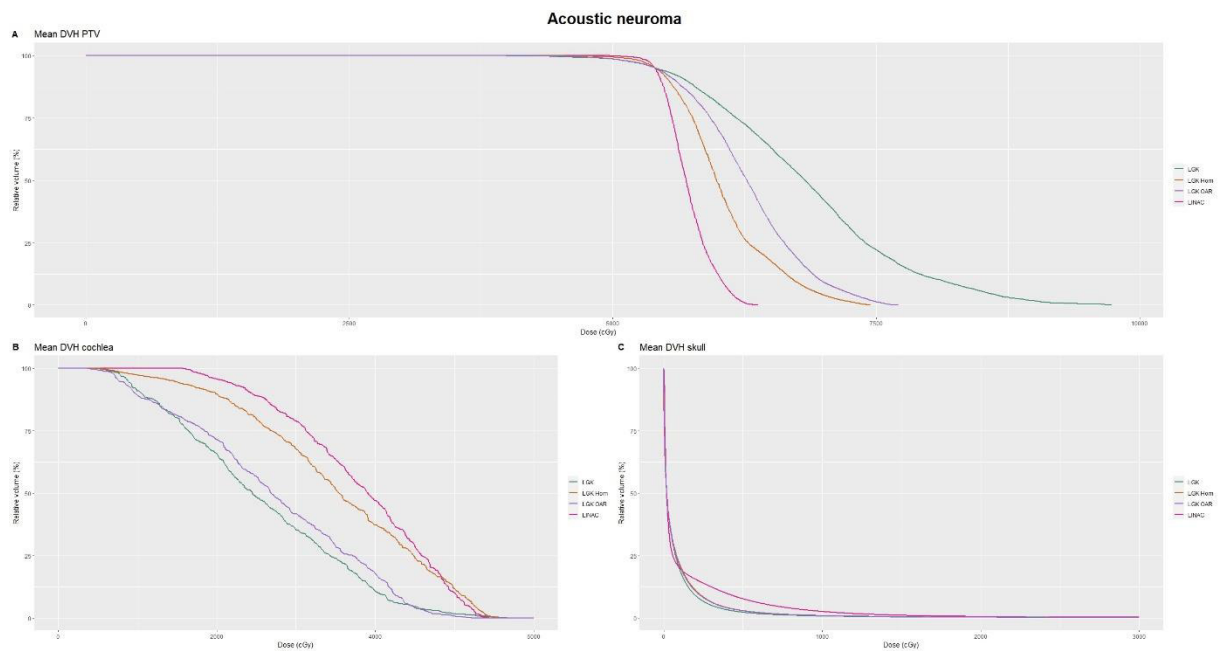


Figure 3.7: Mean DVHs for acoustic neuromas and the structures PTV (A), cochlea (B) and skull (C). The plans are LGK (green), LGK Hom (orange), LGK OAR (purple) and LINAC (pink). DVH=dose-volume-histogram, PTV=planning target volume

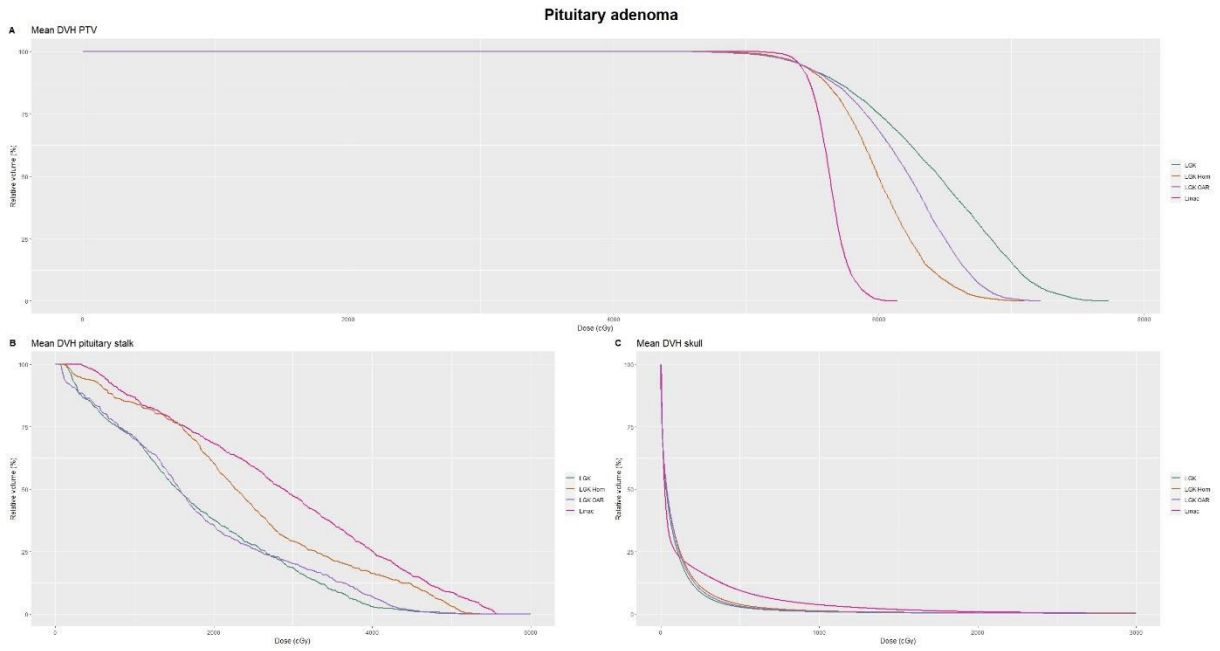


Figure 3.8: Mean DVHs for pituitary adenoma and the structures PTV (A), pituitary stalk (B) and skull (C). The plans are LGK (green), LGK Hom (orange), LGK OAR (purple) and LINAC (pink). DVH=dose-volume-histogram, PTV=planning target volume

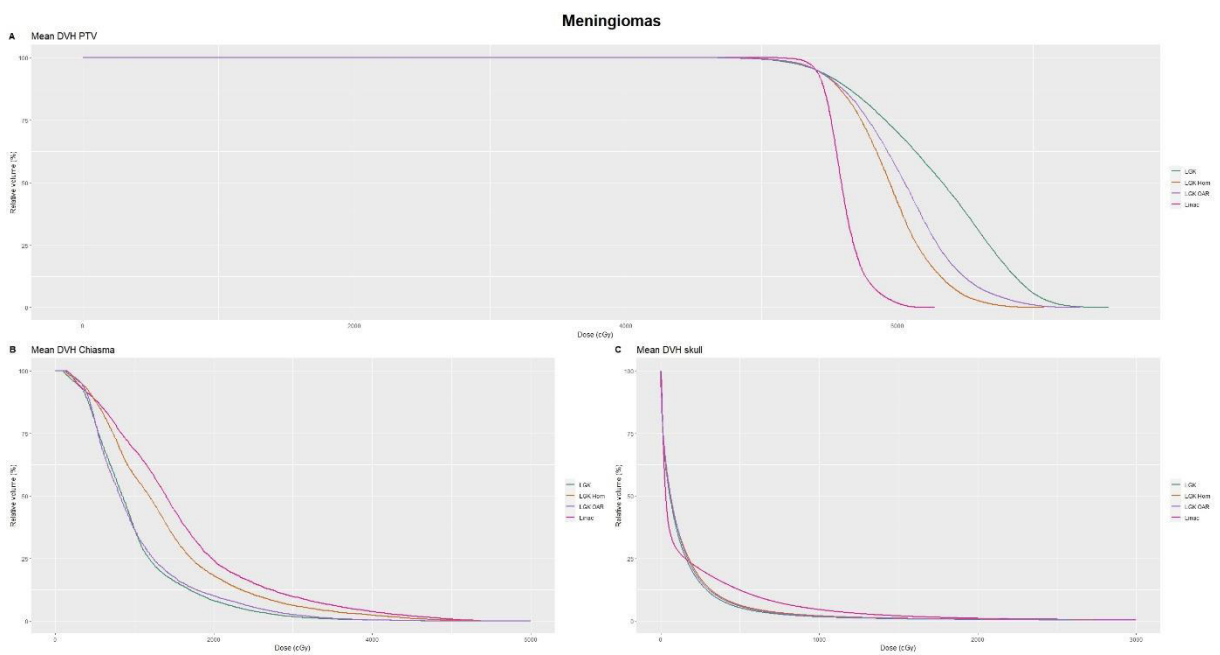


Figure 3.9: Mean DVHs for meningiomas and the structures PTV (A), chiasma (B) and skull (C). The plans are LGK (green), LGK Hom (orange), LGK OAR (purple) and LINAC (pink). DVH=dose-volume-histogram, PTV=planning target volume.

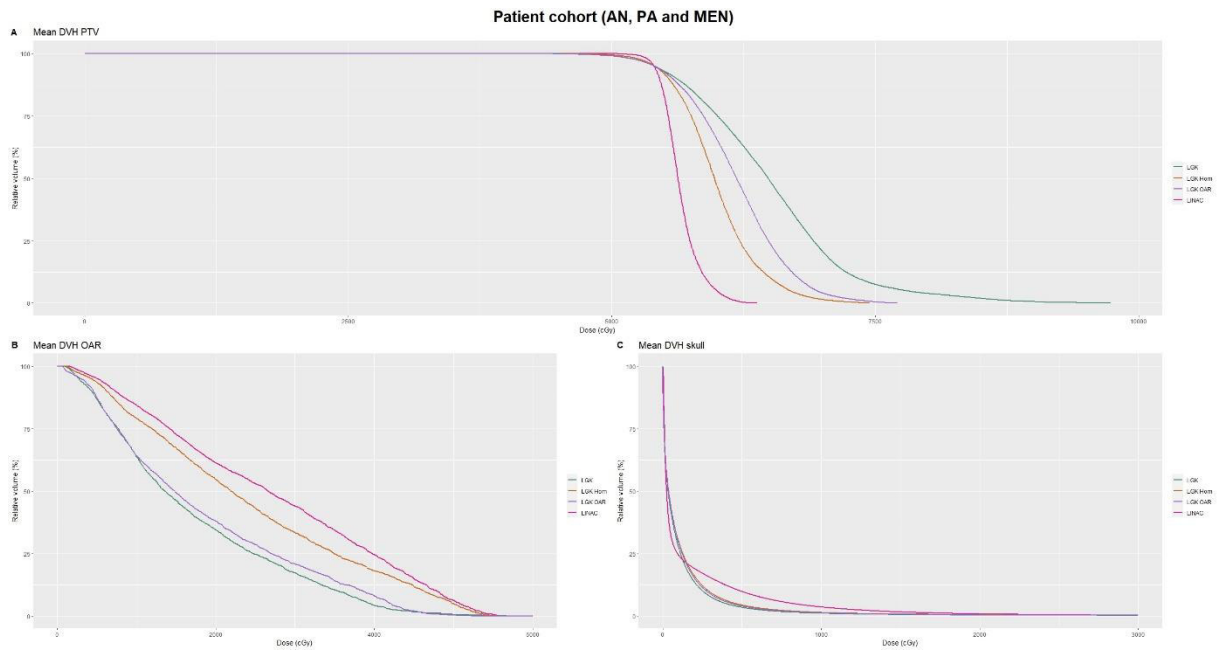


Figure 3.10: Mean DVHs for the total patient cohort (AN, PA and MEN) and the structures PTV (A), OAR (B) and skull (C). The plans are LGK (green), LGK Hom (orange), LGK OAR (purple) and LINAC (pink). DVH=dose-volume-histogram, PTV=planning target volume, AN=acoustic neuroma, PA=pituitary adenoma, MEN=Meningioma.

Table 3.7: median, minimum and maximum values for acoustic neuromas (AN), pituitary adenoma (PA) and meningioma (MEN) and the metrics Gradient Index (GI), Paddick Conformity Index (PCI), Homogeneity Index (HI), OAR dose and beam-on-time (BOT). The OAR doses are D_{mean} cochlea (AN), $D_{2\%}$ pituitary stalk (PA) and $D_{2\%}$ chiasma (MEN).

		AN				PA				MEN			
		LINAC	LGK Hom	LGK OAR	LGK	LINAC	LGK Hom	LGK OAR	LGK	LINAC	LGK Hom	LGK OAR	LGK
GI	Median	7.80	3.78	3.67	3.05	7.59	4.50	3.46	3.15	5.66	3.81	3.50	3.25
	IQR	4.64	2.35	1.05	0.74	2.51	3.07	0.80	0.74	1.41	0.51	0.42	0.33
	Mean	9.71	4.80	3.88	3.13	8.12	5.10	3.92	3.46	5.80	3.92	3.62	3.25
PCI	Median	0.73	0.69	0.68	0.83	0.72	0.72	0.75	0.79	0.81	0.79	0.81	0.84
	IQR	0.07	0.11	0.12	0.10	0.16	0.14	0.05	0.05	0.13	0.06	0.04	0.05
	Mean	0.75	0.72	0.69	0.80	0.69	0.70	0.74	0.79	0.77	0.79	0.80	0.84
HI	Median	1.10	1.16	1.26	1.45	1.07	1.19	1.25	1.34	1.07	1.18	1.22	1.31
	IQR	0.03	0.13	0.11	0.24	0.01	0.06	0.04	0.03	0.02	0.06	0.07	0.03
	Mean	1.11	1.21	1.30	1.56	1.08	1.20	1.24	1.35	1.08	1.19	1.23	1.30
BOT (s)	Median	70	204	246	444	139	378	375	429	138	630	684	576
	IQR	4.0	249	243	453	1	188	258	191	50	83	113	119
	Mean	79	331	376	561	139	378	389	370	118	624	663	498
OAR dose (Gy)	Median	39.68	37.11	26.69	23.41	46.18	38.87	34.08	38.55	28.76	26.32	16.94	16.61
	IQR	10.58	13.73	12.52	9.71	6.68	11.12	19.59	16.50	18.59	19.73	16.34	15.65
	Mean	37.26	32.90	24.71	24.06	45.74	40.42	31.66	32.00	32.07	27.53	20.26	20.58

Table 3.8: Median, inter quartile range (IQR), mean and p-value for all patients and for the metrics Gradient Index (GI), Paddick Conformity Index (PCI), Homogeneity Index (HI), D_{mean} cochlea, $D_{2\%}$ pituitary stalk, $D_{2\%}$ chiasma and beam-on-time (BOT). Median, IQR and mean are given for the different organs at risk (OAR) separately the p-values, however, apply to the total patient cohort (n=30).

		LINAC	LGK Hom	P value	LGK OAR	P value	LGK	P value
GI (n=30)	Median	6.68	3.86	<0.001	3.50	<0.001	3.19	<0.001
	IQR	2.70	1.22		0.84		0.62	
	Mean	7.92	4.63		3.80		3.28	
PCI (n=30)	Median	0.75	0.76	0.976	0.75	0.859	0.82	0.001
	IQR	0.13	0.13		0.09		0.08	
	Mean	0.74	0.74		0.75		0.81	
HI (n=30)	Median	1.08	1.18	<0.001	1.24	<0.001	1.35	<0.001
	IQR	0.03	0.08		0.08		0.08	
	Mean	1.09	1.19		1.25		1.39	
D_{mean} cochlea (Gy) (n=9)	Median	39.68	37.11	0.152	26.69	<0.001	23.41	<0.001
	IQR	10.58	13.73		12.52		9.71	
	Mean	37.26	32.90		24.71		24.06	
$D_{2\%}$ pituitary stalk (Gy) (n=9)	Median	46.18	38.87		34.08		38.55	
	IQR	6.68	11.12		19.59		16.50	
	Mean	45.74	40.42		31.66		32.00	
$D_{2\%}$ chiasma (Gy) (n=10)	Median	28.76	26.32		16.94		16.61	
	IQR	18.59	19.73		16.34		15.65	
	Mean	32.07	27.53		20.26		20.58	
BOT (s) (n=30)	Median	137	432	<0.001	510	<0.001	510	<0.001
	IQR	68	427		473		273	
	Mean	111	454		415		504	

3.2.2 Plan quality and efficiency – exemplary cases

Figure 3.11 gives the dose distribution for one of the studied PA cases. It represents the PTV (green) and the pituitary stalk as OAR (black). For the pituitary stalk the dose constraint $D_{2\%} < 50$ Gy can be approximated by the 50 Gy IDL (orange) which shows that the OAR sparing is best for LGK and LGK OAR. The hot spots in the PTV are greater than 66 Gy ($1.22 \cdot PD$) for the Lightning plans whereas for the LINAC plans no hotspots are visible. Finally, all Lightning plans show higher dose conformity compared to the LINAC plans.

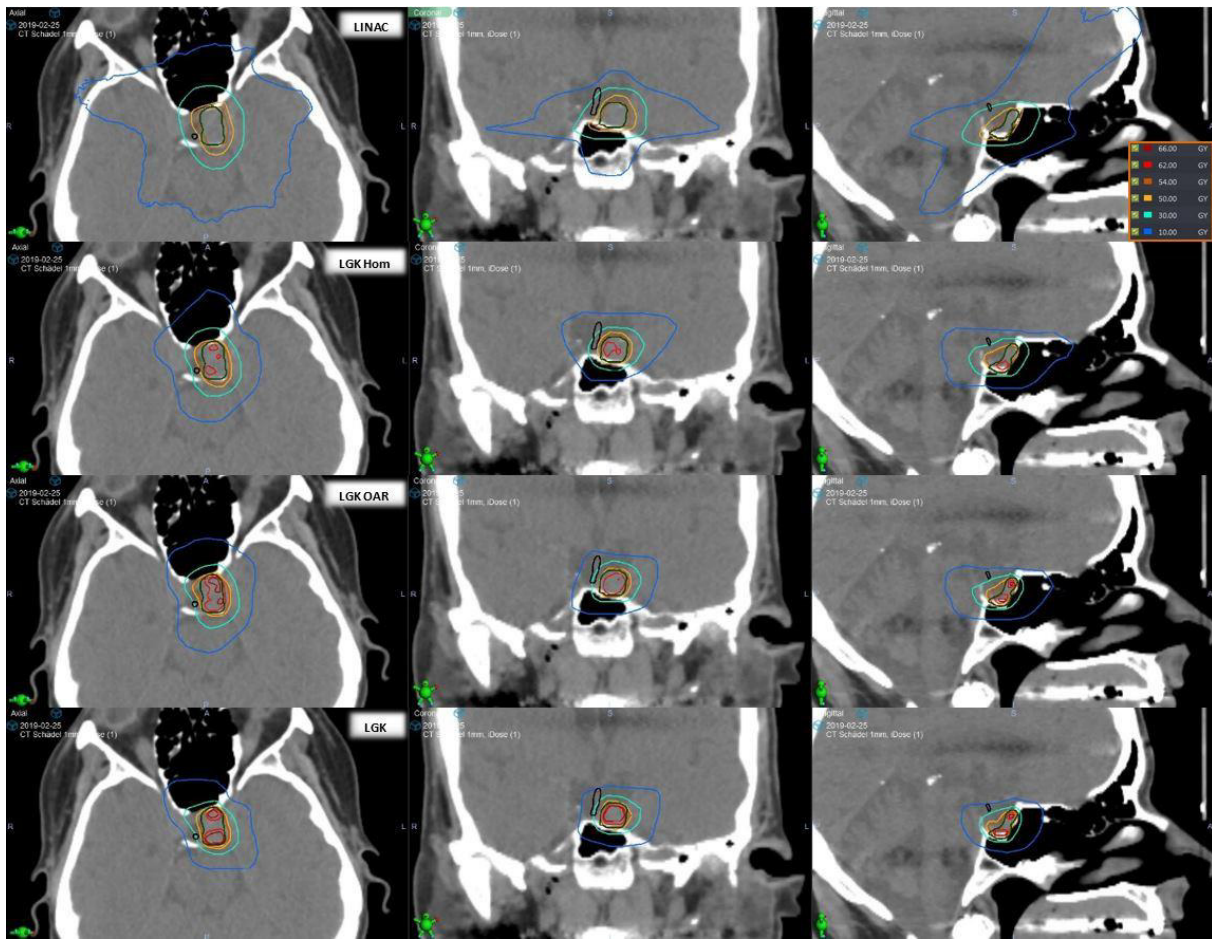


Figure 3.11: Dose distribution in axial, coronal and sagittal view for one pituitary adenoma case and the plans LINAC, LGK Hom, LGK OAR and LGK. The structures are the PTV (green) and the pituitary stalk (black) and the isodose lines 66 Gy (dark red), 62 Gy (red), 54 Gy (orange), 50 Gy (yellow), 30 Gy (light blue) and 10 Gy (blue).

As mentioned previously, two OAR were excluded from the group analysis as they are located entirely inside the target volume. For these two cases (AN and PA) the plan quality and efficiency metrics are listed in table 3.9. Although HI is increased in all Lightning plans, OAR doses are found similar between LINAC and LGK Hom especially for AN. Additionally, GI is considerably reduced in all Lightning plans.

Table 3.9: Plan quality and efficiency metrics for one acoustic neuroma (AN) and one pituitary adenoma (PA) with organ at risk (OAR) situated inside the target volume. For AN, the OAR doses are mean doses (OAR=cochlea) and for PA maximum doses (OAR=pituitary stalk). GI=Gradient Index, PCI=Paddick Conformity Index, HI=Homogeneity Index, BOT=beam-on-time.

Medical condition	LINAC		LGK Hom		LGK OAR		LGK	
	AN	PA	AN	PA	AN	PA	AN	PA
GI	8.45	6.25	3.96	3.72	3.88	3.28	2.76	2.80
PCI	0.73	0.75	0.71	0.81	0.71	0.84	0.82	0.87
HI	1.11	1.07	1.34	1.22	1.55	1.11	2.12	1.35
OAR dose (Gy)	56.89	57.24	56.77	62.14	58.67	60.13	61.57	65.44
BOT (s)	122	138	336	414	378	402	810	432

3.3 Homogenous Leksell GK Lightning for treatment planning of NPC

3.3.1 Patient population: imaging and dose distribution

Due to anatomical and BOT related limitations the retrospective patient population only comprises five patients whose target volume related characteristics can be found in table 2.4 of the methods section. Out of this group, an intermediate CT scan seven days after the first scan was available for one of the patient (P5) due to significant changes in patient positioning. The second CT shows a GTV regression from 77.0 cc to 13.8 cc (figure 3.12). For the remaining patients, only the initial planning CT is available for treatment planning purposes so that no statement about tumor regression during LINAC base plan treatment is available. Hence, for patients P1 to P4 the time needed for optimization using the prototype version was ≥ 30 min. However, for patient P5 with a tumor volume of about 25% of tumor P1, a treatment plan was calculated in less than 10 min. The BOT limitation of 60 min per fraction was almost exhausted by all patient plans with BOTs per fraction ranging from 51 to 58 minutes.

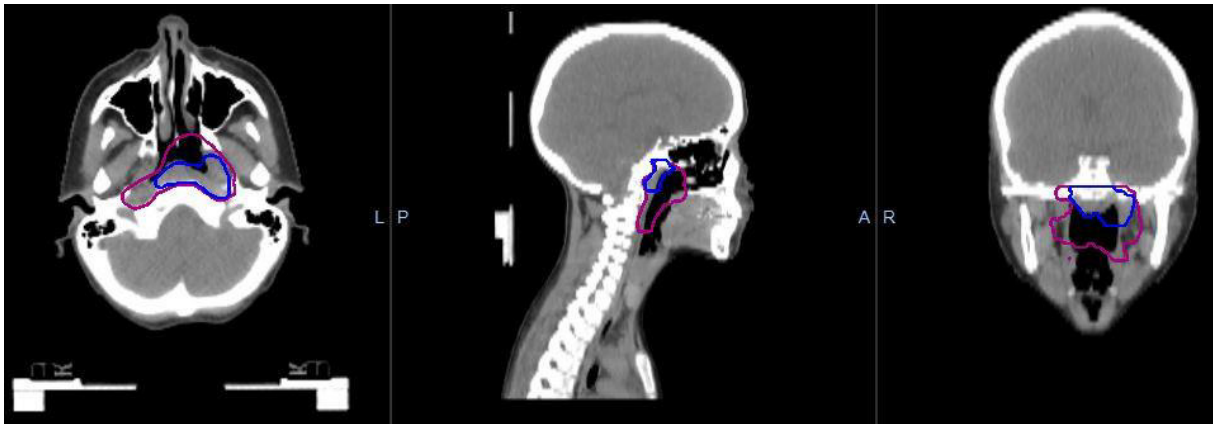


Figure 3.12: Gross tumor volume regression patient P5. The primary gross tumor volume is represented in purple and the gross tumor volume after partial irradiation in blue.

For patients P2 and P4, OAR are intersecting with the PTV (figure 3.13). In these cases it is especially challenging to ensure target coverage. As found previously with cerebral tumors, even though the GK prototype version was shown to be more homogenous than the current clinical version, the degree of inhomogeneity is still significantly higher compared to LINAC homogeneity. Hence, restricting the maximum dose to the intersecting OAR results in an important loss of target coverage and eventually in even higher hotspots inside the target volume after normalization to $D_{90\%}$. Consequently, for these two patient, the dose to the intersecting OAR was tried to be reduced while at the same time not compromising the target coverage.

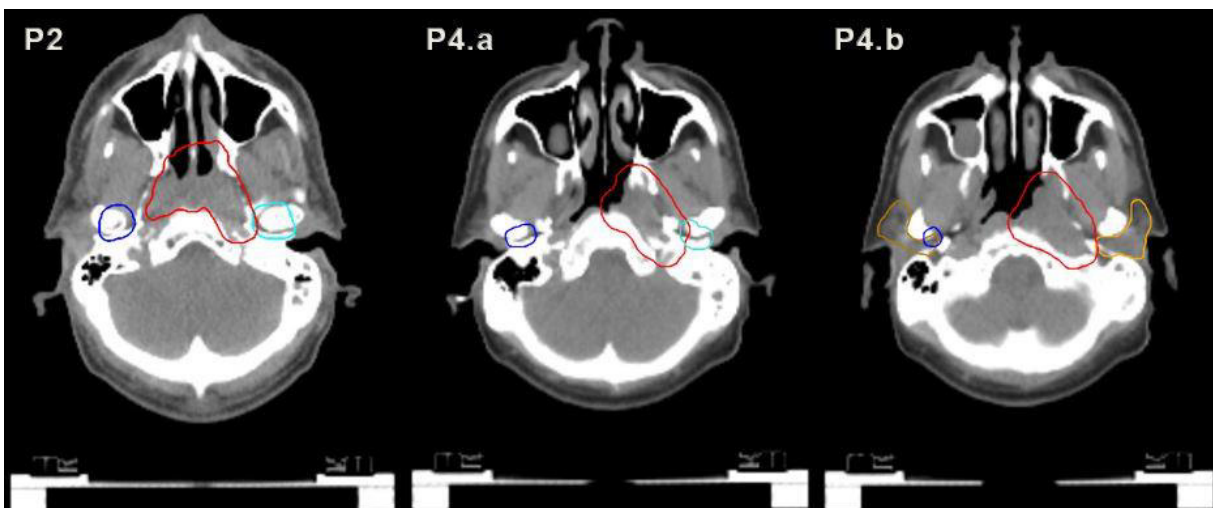


Figure 3.13: Intersection of OAR and PTV for patients P2 and P4. For P2, the PTV (red) intersects with the left temporomandibular joint (light blue). For P4, the PTV (red) intersect with the left temporomandibular joint (light blue, P4.a) and the left parotid (light orange, P4.b). PTV=planning target volume, OAR=organs at risk.

3.3.2 Individual dose volume histograms and dose values

In the following, the dose distribution in one slice, the DVHs and relevant dose values and plan quality metrics are shown for each boost plan and patient individually.

Patient P1

The dose distributions for the boost plans in three axial slices is shown in figure 3.14. Figures 3.15 and 3.16 show the DVHs per structure for LINAC and GK boost plans of patient P1 and table 3.10 gives the dose values for the considered OAR.

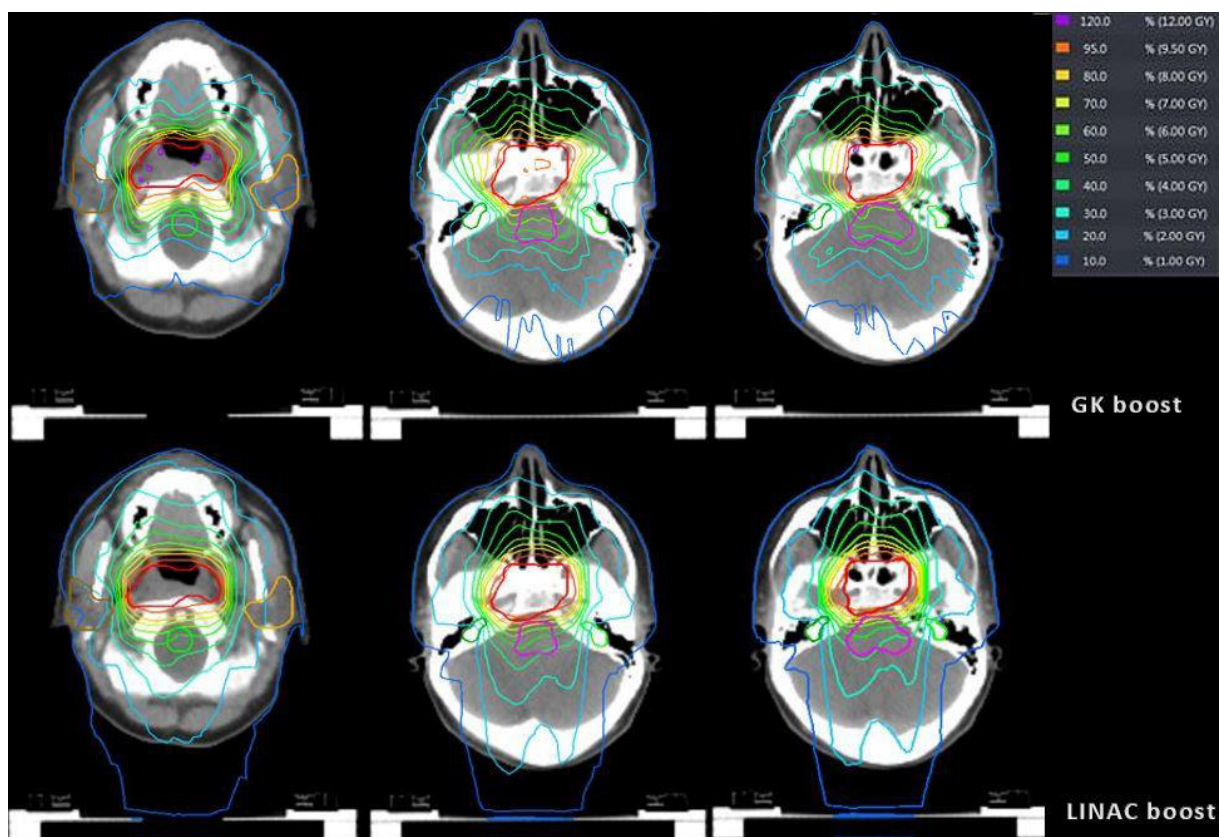


Figure 3.14: Dose distribution for patient P1 and the GK and LINAC boost plans. Planning target volume (red), left parotid (light orange), right parotid (dark orange), spinal cord (neon green), brainstem (pink), left cochlea (light green), right cochlea (dark green). The isodose lines are represented on the right side of the figure. GK = Gamma Knife, LINAC = linear accelerator.

Apart from high doses inside the delineated OAR, hotspots in the boost plans were tried to be kept ≤ 12 Gy in osseous structures comprising sensitive nerves and in mucous membranes. According to our institutional planning aims, the 95% IDL which ideally should comprise the integrity of the boost target volume is represented. When comparing the high dose (120%, purple), it is noticeable that the LINAC boost plan is

more homogenous than the GK plan which was already shown in the previous analysis of the homogenous prototype version. The location of the GK hotspots, however, is out of the aforementioned risk zones so that the boost plan was judged satisfying by the physician. Additionally, the isodose lines show higher dose conformity and that the GK plan spares the OAR better than the LINAC plans. Similarly, the low dose spread in the skull is reduced. Especially the left parotid (light orange) appears to benefit from the GK dose distribution. The comparison of the GK and LINAC dose distribution for the remaining patients can be found in the following section.

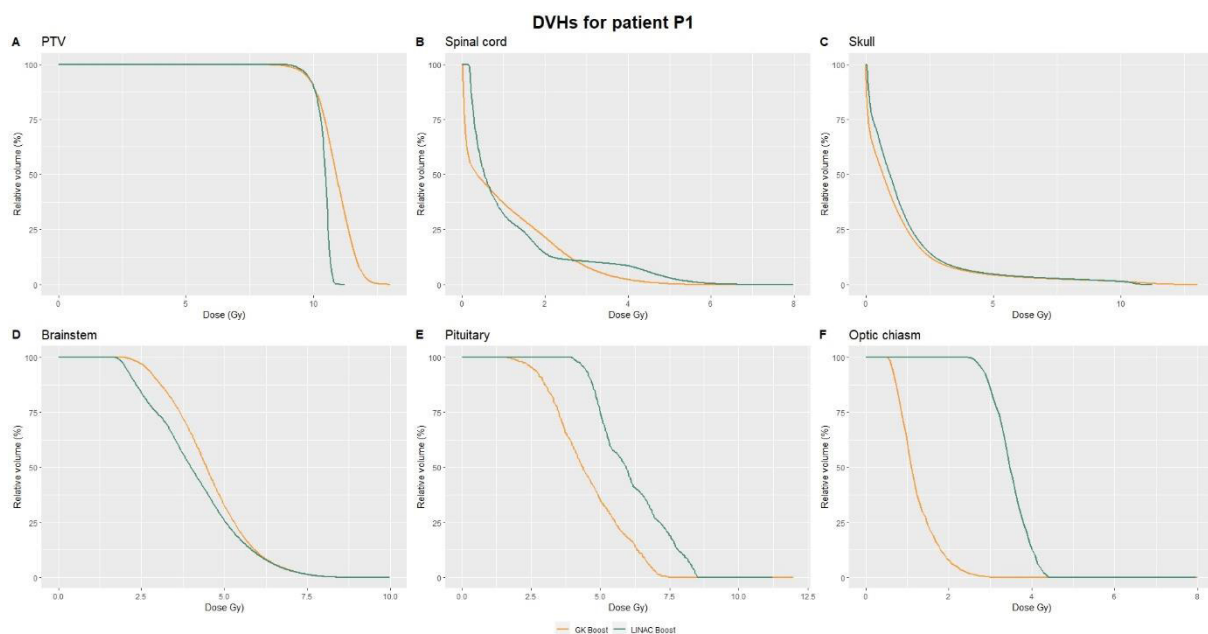


Figure 3.15: DVHs for patient P1, the plans GK Boost (yellow) and LINAC Boost (green) and the structures PTV (A), spinal cord (B), skull (C), brainstem (D), pituitary (E) and optic chiasm (F). DVHs = dose-volume histograms, GK = Gamma Knife, LINAC = linear accelerator, PTV = planning target volume, Gy = Gray.

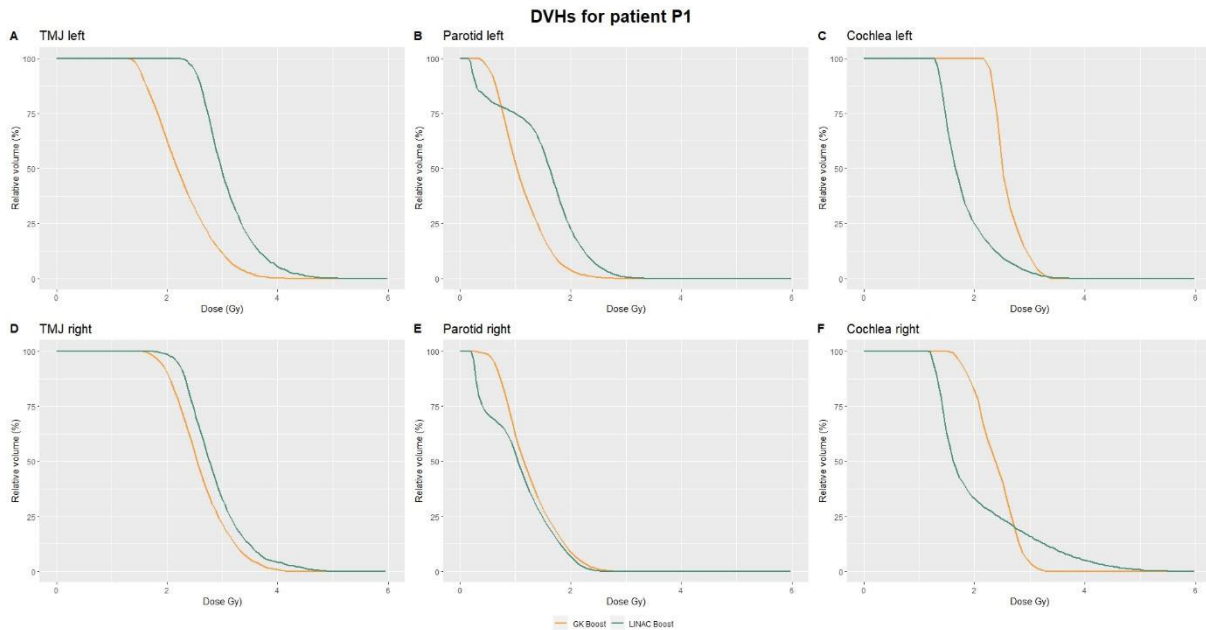


Figure 3.16: DVHs for patient P1, the plans GK Boost (yellow) and LINAC Boost (green) and the structures TMJ left (A), parotid left (B), cochlea left (C), TMJ right (D), parotid right (E) and cochlea right (F). DVHs = dose-volume histograms, GK = Gamma Knife, LINAC = linear accelerator, PTV = planning target volume, TMJ = temporomandibular joint, Gy = Gray.

Table 3.10 gives the boost plan values and the LINAC + boost sum plan values. It has to be emphasized, that for this and all following patients the sum dose values are extracted from the sum plan and are not the results of a sum between the LINAC base plan column and the boost plan column. With the sum plan, the dose distribution of each plan is added voxel-by-voxel which provides a sum dose distribution with spatial relationship between the two plans. Dose values exceeding the planning constraint in table 2.3 are highlighted in red and OAR intersecting or abutting the PTVs are marked with asterisks * (PTV60 one asterisk, PTV boost two asterisks).

Table 3.10: Dose constraints and metrics (GI, PCI) for patient P1 and the LINAC base, LINAC boost, GK boost and the sum plans LINAC+GK boost and LINAC+LINAC boost. The dose values are in the unit Gray (Gy) and the red shaded areas in the sum plan columns represent dose values exceeding the planning constraints. OAR intersecting or abutting PTV60 (base plan) are marked with one asterisk and OAR intersecting or abutting PTV boost with two asterisks. GI = gradient index, PCI = Paddick conformity index, GK = Gamma Knife, LINAC = linear accelerator, TMJ = temporomandibular joint, OAR = organ at risk.

Patient P1	LINAC base	GK boost	LINAC boost	LINAC+ GK boost	LINAC+ LINAC boost	Constraints
Brainstem (D _{0.035cc}) [Gy]	38.1	7.3	7.5	45.1	45.1	< 60
Spinal cord (D _{0.035cc}) [Gy]	29.3	4.6	6.0	32.1	33.7	< 52.8
Parotid left* (D _{0.035cc}) [Gy]	60.5	2.6	3.2	61.8	62.3	< 32
Parotid right* (D _{0.035cc}) [Gy]	62.0	2.7	2.5	64.1	63.8	< 32
Parotid left* (D _{mean}) [Gy]	39.9	1.1	1.5	41.1	41.5	< 26
Parotid right* (D _{mean}) [Gy]	30.4	1.2	1.1	31.5	31.3	< 26
Cochlea left (D _{0.035cc}) [Gy]	32.9	3.2	3.0	36.3	36.3	< 40
Cochlea right (D _{0.035cc}) [Gy]	37.3	3.1	4.4	39.8	41.1	< 40
TMJ left (D _{0.035cc}) [Gy]	42.9	3.6	4.5	44.3	45.2	< 65
TMJ right (D _{0.035cc}) [Gy]	37.9	3.9	4.5	41.0	41.6	< 65
Pituitary gland* (D _{0.035cc}) [Gy]	49.7	6.8	8.3	50.4	52.3	< 50
Optic chiasm (D _{0.035cc}) [Gy]	21.4	2.5	4.2	23.4	24.5	< 52
PTV (D _{0.035cc}) [Gy]	64.2	12.8	11.0	75.0	74.9	-
PTV (D _{mean}) [Gy]	59.4	10.1	10.1	69.5	69.4	-
GI PCI	-	3.19 0.79	3.54 0.80	-	-	-

As it can be seen from table 3.10 and the DVHs above, the GK boost plan shows an advantage over the LINAC boost plan for most OAR. For the brainstem, the advantage is less expressed and can be explained by the close proximity of the OAR to the PTV

in some slices. As for the left cochlea and right parotid, LINAC boost doses are slightly lower than the GK boost doses. This patient suffers from a central and large NPC (table 2.4) with PTV60 partially involving both parotids which explains the already high parotid mean and $D_{0.035 \text{ cc}}$ doses in the LINAC base plan. Additionally, the pituitary gland is abutting the PTV60 resulting in an already high OAR dose in the base plan almost exceeding the constraint (50 Gy). Consequently, the constraint is violated by adding either of the boost plans but, with the GK boost, a dose reduction of 3.6% is reached in the GK sum plan compared to the LINAC sum plan. Similarly, for this patient, the distance between the right cochlea and PTV60 is in the order of 2 mm resulting in a cochlea dose of 37.3 Gy, which is already close to the 40 Gy constraint. With the advantageous GK dose gradient, the constraints was not violated and the dose difference for this OAR with the LINAC boost plan is more than 1 Gy.

The PTV high dose for the GK boost plan is about 1.8 Gy higher which could already be observed in figure 3.14 but the location of the hot spots is judged uncritical. The PTV mean dose is equal between both boost plans and very similar for the sum plans. Regarding the plan quality metrics, the GK boost plan has a better GI (3.19 vs. 3.54) while the conformity of the boost plans given by the PCI is similar (0.79 vs. 0.80).

Patient P2

The dose distributions for the boost plans in three axial slices is shown in figure 3.17. Figures 3.18 and 3.19 show the DVHs per structure for LINAC and GK boost plans of patient P2 and table 3.11 gives the dose values for the considered OAR.

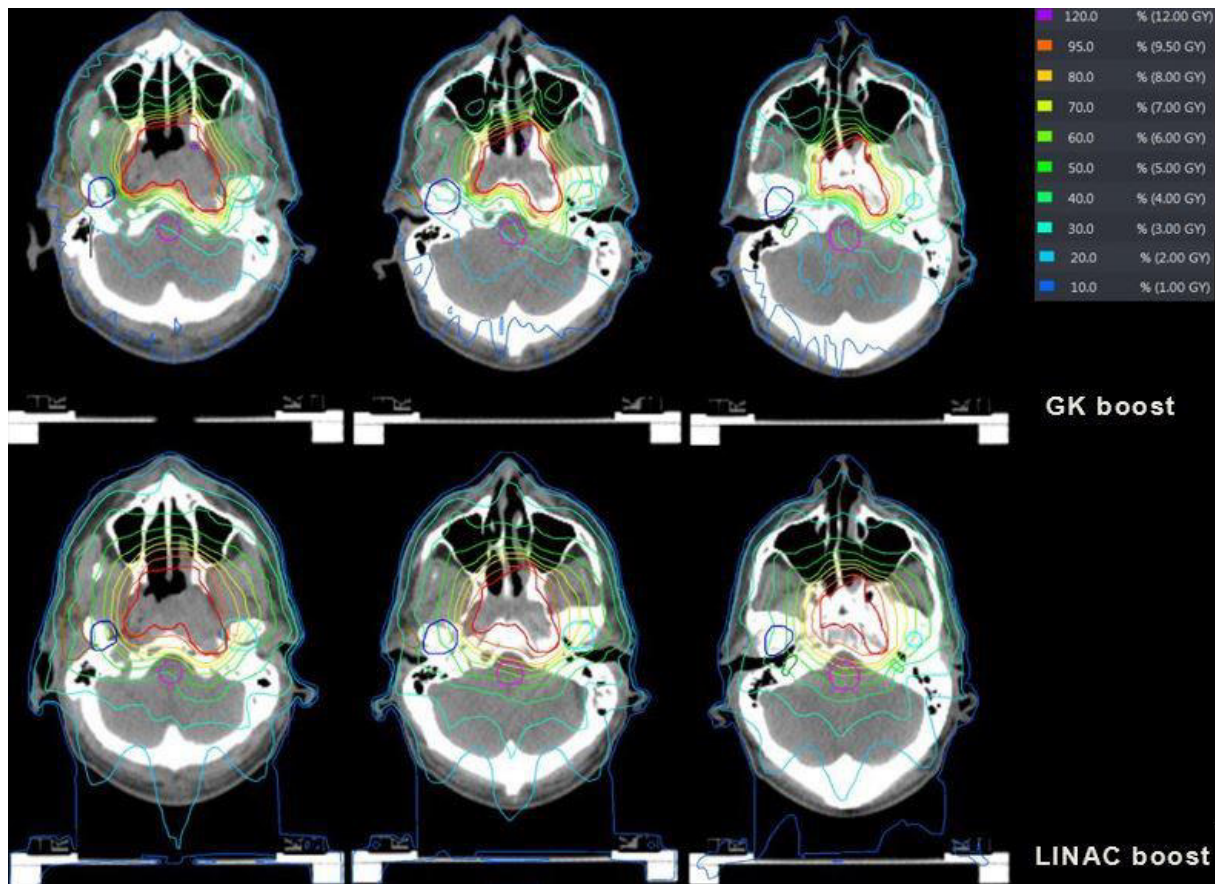


Figure 3.17: Dose distribution for patient P2 and the GK and LINAC boost plans. Planning target volume (red), left temporomandibular joint (light blue), right temporomandibular joint (dark blue), brainstem (pink), left cochlea (light green), right cochlea (dark green). The isodose lines are represented on the right side of the figure. GK = Gamma Knife, LINAC = linear accelerator.

Figure 3.17 gives the dose distribution in three axial slices for the LINAC and GK boost plans and patient P2. It is visible, that the studied patient suffered from a central NPC tumor. While the IDL in the GK plan are more conformal, the LINAC plan has no hotspots $\geq 120\%$. In the first and third axial slice, small cold spots $< 95\%$ adjacent to (slice 1) and inside (slice 3) the osseous structure can be seen in the GK boost plan. For all represented OAR—namely the brainstem (pink), left and right TMJ (light and dark blue), left and right cochlea (light and dark green)—the GK boost appears more advantageous compared to the LINAC boost. TMJ left is crossing the PTV, which explains the small underdosage in the first slice of the GK plan.

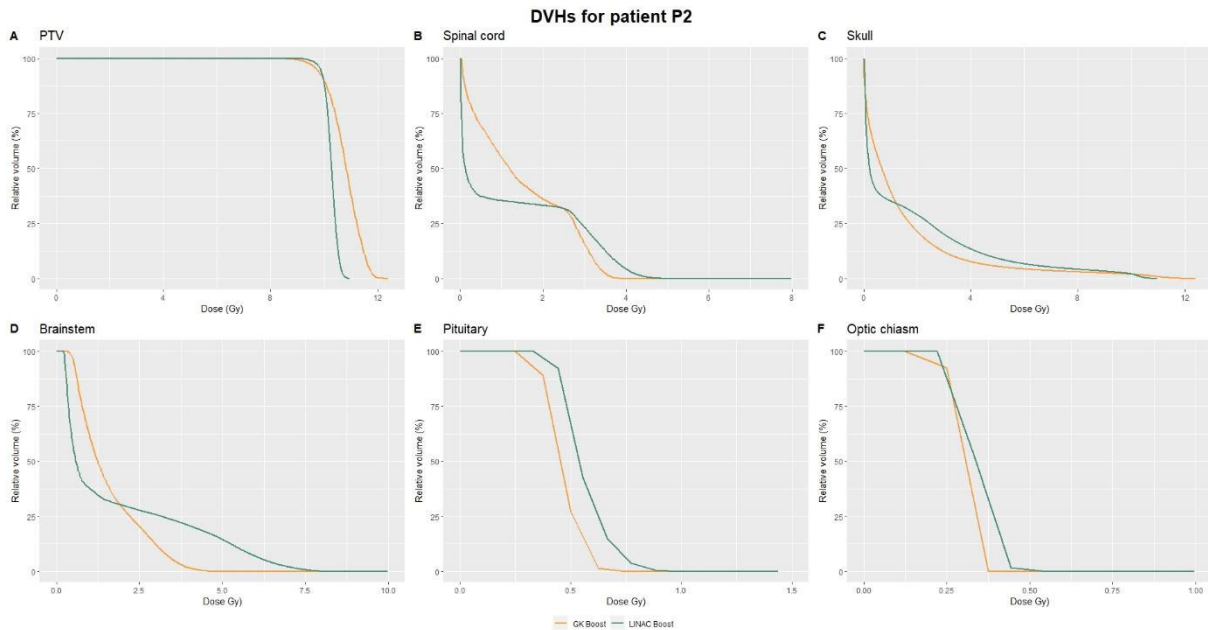


Figure 3.18: DVHs for patient P2, the plans GK Boost (yellow) and LINAC Boost (green) and the structures PTV (A), spinal cord (B), skull (C), brainstem (D), pituitary (E) and optic chiasm (F). DVHs = dose-volume histograms, GK = Gamma Knife, LINAC = linear accelerator, PTV = planning target volume, Gy = Gray.

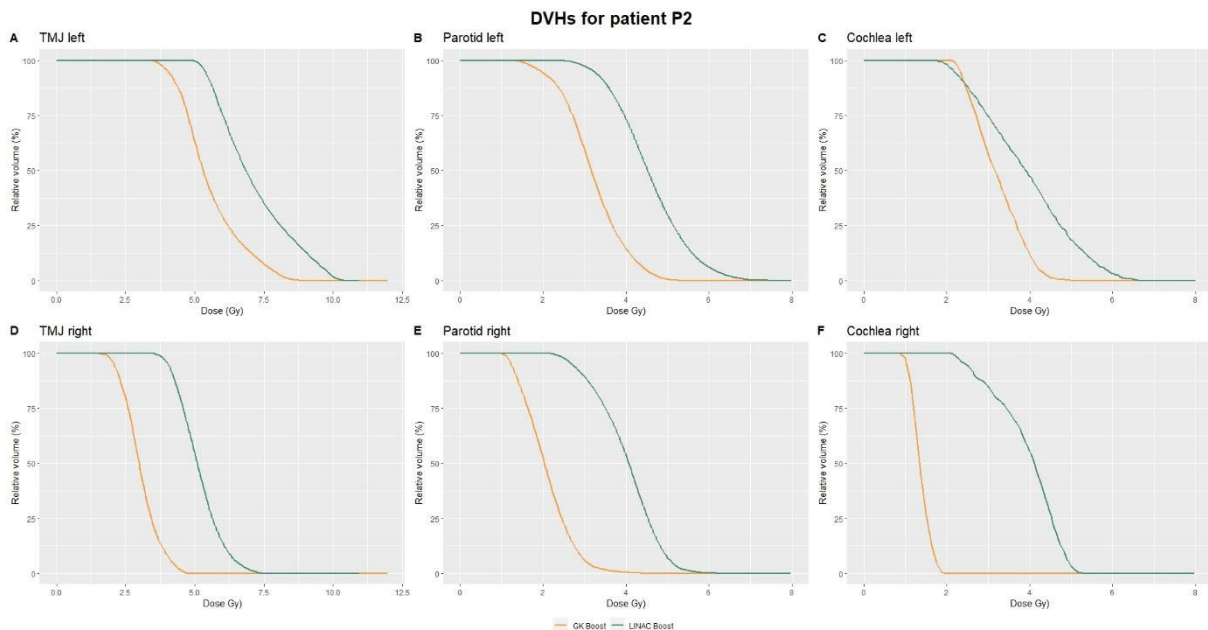


Figure 3.19: DVHs for patient P2, the plans GK Boost (yellow) and LINAC Boost (green) and the structures TMJ left (A), parotid left (B), cochlea left (C), TMJ right (D), parotid right (E) and cochlea right (F). DVHs = dose-volume histograms, GK = Gamma Knife, LINAC = linear accelerator, PTV = planning target volume, TMJ = temporomandibular joint, Gy = Gray.

Table 3.11 gives the boost plan values and the LINAC + boost sum plan values. The sum dose values are extracted from the sum plans. Dose values exceeding the planning constraint in table 2.3 are highlighted in red and OAR intersecting or abutting the PTVs are marked with asterisks * (PTV60 one asterisk, PTV boost two asterisks).

Table 3.11: Dose constraints and metrics (GI, PCI) for patient P2 and the LINAC base, LINAC boost, GK boost and the sum plans LINAC+GK boost and LINAC+LINAC boost. The dose values are in the unit Gray (Gy) and the red shaded areas in the sum plan columns represent dose values exceeding the planning constraints. OAR intersecting or abutting PTV60 (base plan) are marked with one asterisk and OAR intersecting or abutting PTV boost with two asterisks. GI = gradient index, PCI = Paddick conformity index, GK = Gamma Knife, LINAC = linear accelerator, TMJ = temporomandibular joint, OAR = organ at risk.

Patient P2	LINAC base	GK boost	LINAC boost	LINAC+GK boost	LINAC+LINAC boost	Constraints
Brainstem (D _{0.035cc}) [Gy]	35.1	4.4	8.0	37.2	40.2	< 60
Spinal cord (D _{0.035cc}) [Gy]	34.0	3.6	4.8	37.0	37.8	< 52.8
Parotid left* (D _{0.035cc}) [Gy]	62.8	5.2	7.1	68.0	69.7	< 32
Parotid right* (D _{0.035cc}) [Gy]	62.3	4.4	6.2	66.3	68.9	< 32
Parotid left* (D _{mean}) [Gy]	45.5	3.2	4.6	52.3	53.7	< 26
Parotid right* (D _{mean}) [Gy]	23.4	2.1	4.0	25.7	27.6	< 26
Cochlea left (D _{0.035cc}) [Gy]	27.0	4.2	5.7	27.5	28.8	< 40
Cochlea right (D _{0.035cc}) [Gy]	24.7	1.7	4.9	24.8	27.6	< 40
TMJ left (D _{0.035cc}) [Gy]	61.4	8.5	10.2	69.2	71.0	< 65
TMJ right (D _{0.035cc}) [Gy]	49.3	4.6	7.2	50.6	53.2	< 65
Pituitary gland* (D _{0.035cc}) [Gy]	16.4	0.6	0.8	13.7	14.0	< 50
Optic chiasm (D _{0.035cc}) [Gy]	5.3	0.4	0.4	5.2	5.2	< 52
PTV (D _{0.035cc}) [Gy]	65.5	12.2	10.9	76.3	75.2	-
PTV (D _{mean}) [Gy]	60.9	10.4	10.5	71.3	71.4	-
GI PCI	-	2.88 0.84	4.50 0.79	-	-	-

For Patient P2 (table 3.11 and figures 3.18 and 3.19) the OAR TMJ left and both parotids are included in the PTV60 of the base plan resulting in parotid doses already exceeding the planning thresholds D_{0.035 cc} with the LINAC base plan. The mean parotid

dose constraint is exceeded for the left parotid in the base plan. Nevertheless, with GK boost, a $D_{0.035 \text{ cc}}$ dose reduction of 2.4% (left parotid) and 3.8% (right parotid) and a mean dose reduction of 2.6% (left parotid) and 6.9% (right parotid) is reached in the sum plans. Additionally, with GK boost, the mean dose constraint for the right parotid in the sum plan is not exceeded whereas with LINAC boost the constraint is violated. TMJ left is abutting the boost volume resulting in high boost doses which, when summed with the already high base dose, exceed the 65 Gy dose limit for both boost plans. With GK boost, however, the dose for the left TMJ in the sum plan is 2.5% lower and for the right TMJ even 4.9% lower. For the remaining OAR, the pituitary and chiasm doses are similarly low between the two boost plans whereas the OAR in the higher dose regions are better spared with the GK boost plan. The dose reduction between LINAC boost and GK Boost plans is especially expressed for the right cochlea resulting in a dose reduction of about 10% when comparing the sum plans. The dose reduction achieved for the brainstem (sum 7.5%) is also noteworthy. As for the PTV, the maximum dose difference between GK and LINAC boost plan is found to be 1.3 Gy. Additionally, the DVH for PTV shows a slight underdosage as already observed in figure 3.17. This underdosage can partially be explained by the dose restriction for the left parotid which is crossing the boost volume. The mean PTV dose of 10 Gy is achieved by both boost plans and the mean doses are similar. For this patient, the dose conformity for the GK boost plan is higher (PCI: 0.84 vs. 0.79) which was already seen in figure 3.17. Additionally, the GI for the GK boost plan is 36% lower than the LINAC boost GI.

Patient P3

The dose distributions for the boost plans in three axial slices is shown in figure 3.20. Figures 3.21 and 3.22 show the DVHs per structure for LINAC and GK boost plans of patient P3 and table 3.12 gives the dose values for the considered OAR.

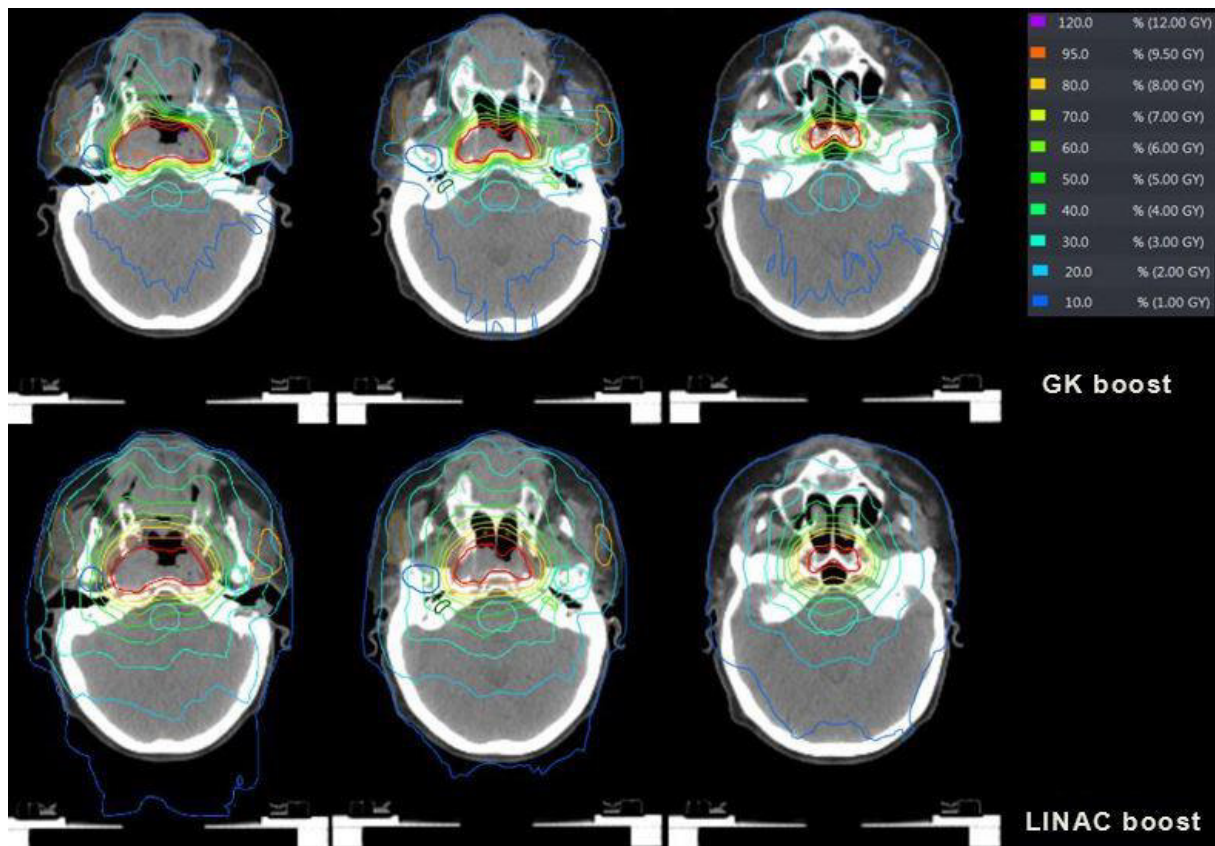


Figure 3.20: Dose distribution for patient P3 and the GK and LINAC boost plans. Planning target volume (red), left parotid (light orange), right parotid (dark orange), left temporomandibular joint (light blue), right temporomandibular joint (dark blue), brainstem (blue). The isodose lines are represented on the right side of the figure. GK = Gamma Knife, LINAC = linear accelerator.

The above figure 3.20 shows the dose distributions in three slices for the GK and LINAC boost plans and patient P3 (central NPC). The dose distribution in the GK plan appears more conformal which also results in lower OAR exposure in the represented slices. While the dose reduction for the OAR brainstem, both TMJs and the right parotid is clearly visible, the dose sparing for the left parotid appears less expressed. The PTV, however, shows hotspots and underdosed regions with the GK boost. Especially in the third axial slice where the PTV is surrounded by air filled cavities and bones, the convolution dose algorithm fails at depositing 95% of the PD in the integrity of the PTV. With the LINAC plan, however, no underdosage is observed which can be explained

by the superiority of the Monte Carlo dose algorithm compared to the convolution dose algorithm⁷³⁻⁷⁶ especially at tissue junctions with lower density.

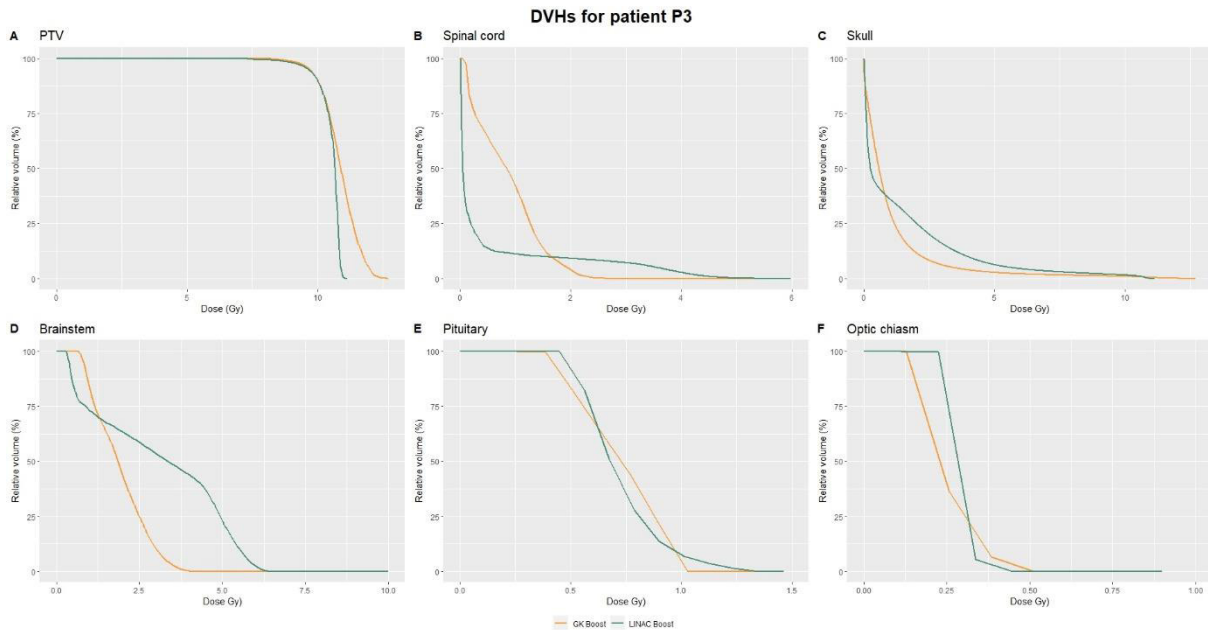


Figure 3.21: DVHs for patient P3, the plans GK Boost (yellow) and LINAC Boost (green) and the structures PTV (A), spinal cord (B), skull (C), brainstem (D), pituitary (E) and optic chiasm (F). DVHs = dose-volume histograms, GK = Gamma Knife, LINAC = linear accelerator, PTV = planning target volume, Gy = Gray.

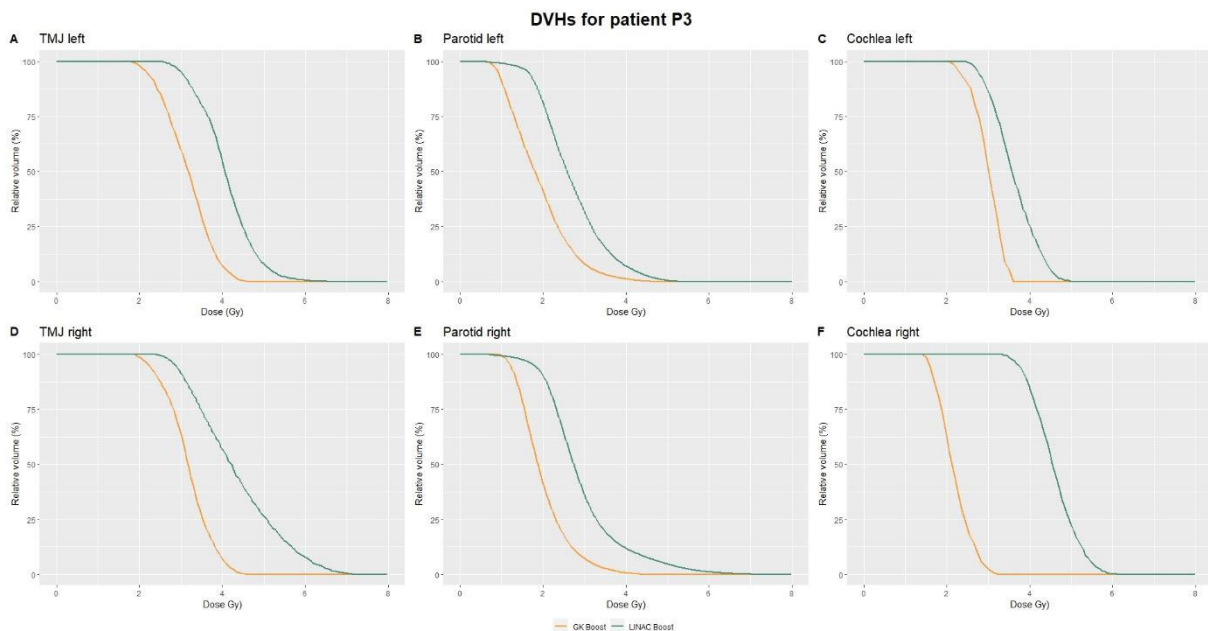


Figure 3.22: DVHs for patient P3, the plans GK Boost (yellow) and LINAC Boost (green) and the structures TMJ left (A), parotid left (B), cochlea left (C), TMJ right (D), parotid right (E) and cochlea right (F). DVHs = dose-volume histograms, GK = Gamma Knife, LINAC = linear accelerator, PTV = planning target volume, TMJ = temporomandibular joint, Gy = Gray.

Table 3.12 gives the boost plan values and the LINAC + boost sum plan values. The sum dose values are extracted from the sum plans. Dose values exceeding the planning constraint in table 2.3 are highlighted in red and OAR intersecting or abutting the PTVs are marked with asterisks * (PTV60 one asterisk, PTV boost two asterisks).

Table 3.12: Dose constraints and metrics (GI, PCI) for patient P3 and the LINAC base, LINAC boost, GK boost and the sum plans LINAC+GK boost and LINAC+LINAC boost. The dose values are in the unit Gray (Gy) and the red shaded areas in the sum plan columns represent dose values exceeding the planning constraints. OAR intersecting or abutting PTV60 (base plan) are marked with one asterisk and OAR intersecting or abutting PTV boost with two asterisks. GI = gradient index, PCI = Paddick conformity index, GK = Gamma Knife, LINAC = linear accelerator, TMJ = temporomandibular joint, OAR = organ at risk.

Patient P3	LINAC base	GK boost	LINAC boost	LINAC+GK boost	LINAC+LINAC boost	Constraints
Brainstem (D _{0.035cc}) [Gy]	33.3	4.0	6.4	36.1	38.8	< 60
Spinal cord (D _{0.035cc}) [Gy]	35.2	2.4	5.1	35.4	36.3	< 52.8
Parotid left* (D _{0.035cc}) [Gy]	63.8	4.5	5.2	65.8	66.9	< 32
Parotid right* (D _{0.035cc}) [Gy]	63.5	4.4	7.1	65.6	67.6	< 32
Parotid left* (D _{mean}) [Gy]	27.1	1.9	2.8	28.9	29.7	< 26
Parotid right* (D _{mean}) [Gy]	26.8	2.0	3.1	28.7	29.7	< 26
Cochlea left (D _{0.035cc}) [Gy]	40.6	3.4	4.3	43.4	44.1	< 40
Cochlea right (D _{0.035cc}) [Gy]	39.4	2.7	5.3	42.3	44.9	< 40
TMJ left (D _{0.035cc}) [Gy]	53.8	4.4	5.7	57.3	59.0	< 65
TMJ right (D _{0.035cc}) [Gy]	53.9	4.3	6.8	58.6	61.2	< 65
Pituitary gland* (D _{0.035cc}) [Gy]	42.4	1.0	1.0	42.5	42.5	< 50
Optic chiasm (D _{0.035cc}) [Gy]	4.1	0.4	0.3	4.1	4.2	< 52
PTV (D _{0.035cc}) [Gy]	64.2	12.4	10.5	75.7	74.6	-
PTV (D _{mean}) [Gy]	60.2	10.5	10.0	70.7	70.1	-
GI PCI	-	2.84 0.85	5.68 0.82	-	-	-

For Patient P3 (table 3.12 and figure 3.21 and 3.22) both parotids and TMJ are intersecting with PTV60. The pituitary gland and cochleae are in close proximity to PTV60. For both parotids and the left cochlea, the dose constraints are already

exceeded in the base plan. The dose value for the right cochlea was already very close to the 40 Gy limit so that the constraint is exceeded with either boost plan. Despite the excessive cochlea dose, the dose sparing reached with the GK boost plan is in the order of almost 6% in the sum plans. Similarly, the $D_{0.035\text{ cc}}$ dose for both parotids is 1.6% (left) and 3.0% (right) lower in the GK sum plan compared to the LINAC sum plan. The mean parotid dose is also 2.7% (left) and 3.4% (right) lower.

The GK boost dose sparing for the brainstem shows the most benefit with a dose reduction of about 7% in the sum plans. The PTV dose for LINAC + GK boost plan, however, is 1.5% higher than for the LINAC + LINAC boost plan. Additionally, the DVH for PTV shows a slight underdosage which was already visible in figure 3.19. The mean PTV dose for the GK boost plan is 0.5 Gy higher than in the LINAC boost and mean PTV doses above 70 Gy are reached for both plans. For this patient, as already seen in figure 3.20, the dose distribution with the GK boost is more conformal than with the LINAC boost (PCI: 0.85 vs. 0.82) and the GI is halved (2.84 vs. 5.68).

Patient P4

The dose distributions for the boost plans in three axial slices is shown in figure 3.23. Figures 3.24 and 3.25 show the DVHs per structure for LINAC and GK boost plans of patient P4 and table 3.13 gives the dose values for the considered OAR.

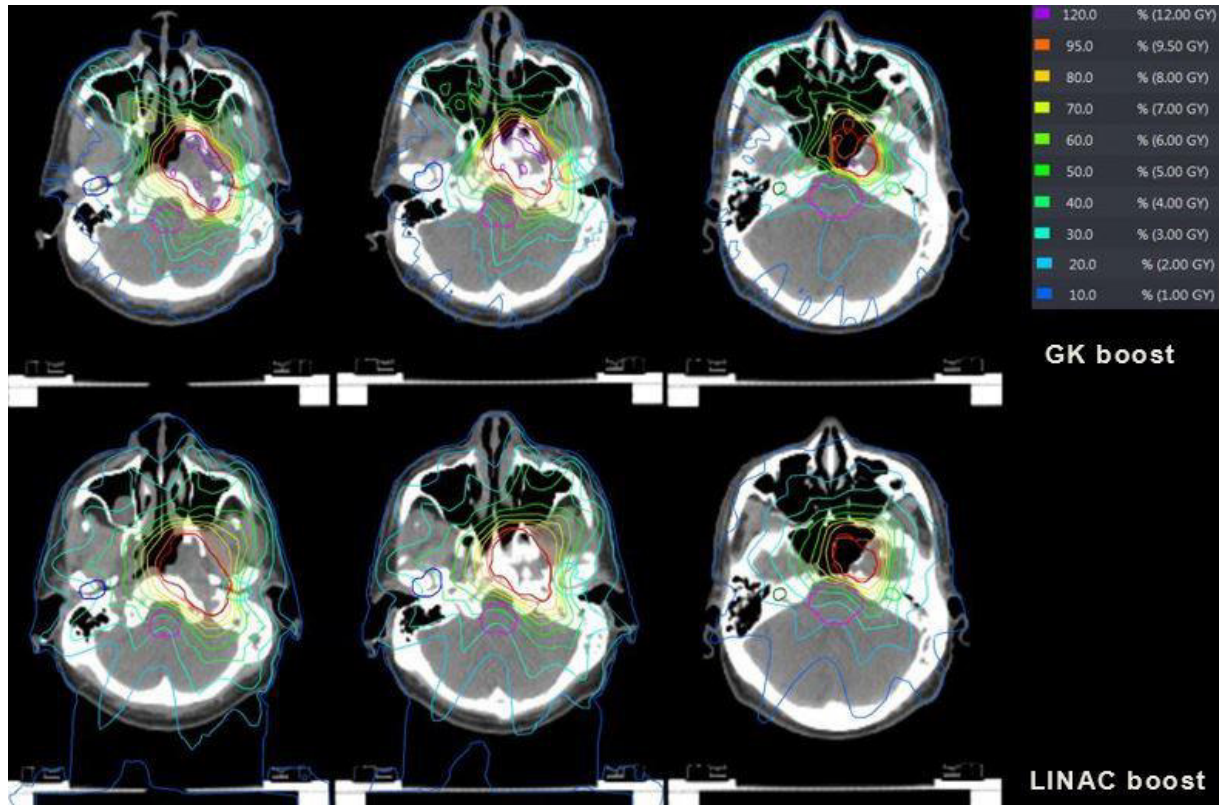


Figure 3.23: Dose distribution for patient P4 and the GK and LINAC boost plans. Planning target volume (red), left temporomandibular joint (light blue), right temporomandibular joint (dark blue), brainstem (pink), left cochlea (light green), right cochlea (dark green). The isodose lines are represented on the right side of the figure. GK = Gamma Knife, LINAC = linear accelerator.

The dose distribution for GK and LINAC boost plans and patient P4 are represented in figure 3.23. This patient has a more left-sided NPC compared to the other patients of the cohort. As for the previous patients, the dose distribution with the GK boost plan appears more conformal than for the LINAC plan. The OAR parotid right and both cochleae seem to benefit from the GK boost plan. Additionally, the left parotid is crossing the PTV and seems to be better spared with the LINAC boost plan. As for the PTV, an underdosage in the third slice is visible for the GK plan. In this slice, half of the PTV is located in the air cavity so that the Monte Carlo dose algorithm shows its superiority compared to the convolution dose algorithm. For this patient, the number and extent of hotspots with the GK plan are more expressed than for the previous patients.

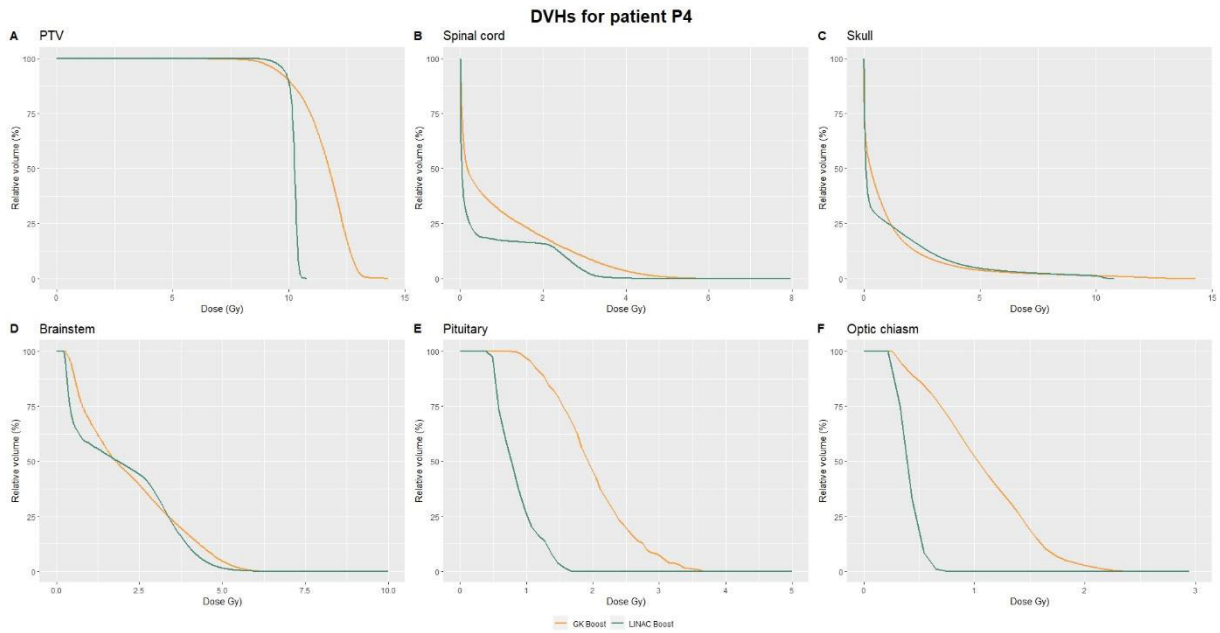


Figure 3.24: DVHs for patient P4, the plans GK Boost (yellow) and LINAC Boost (green) and the structures PTV (A), spinal cord (B), skull (C), brainstem (D), pituitary (E) and optic chiasm (F). DVHs = dose-volume histograms, GK = Gamma Knife, LINAC = linear accelerator, PTV = planning target volume, Gy = Gray.

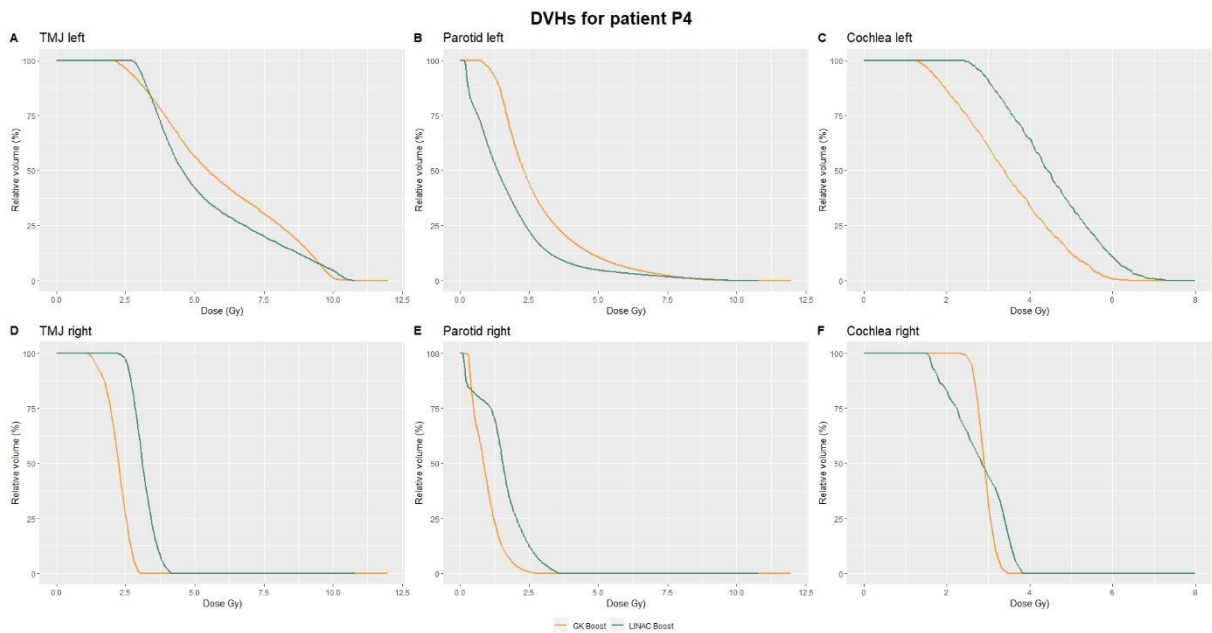


Figure 3.25: DVHs for patient P4, the plans GK Boost (yellow) and LINAC Boost (green) and the structures TMJ left (A), parotid left (B), cochlea left (C), TMJ right (D), parotid right (E) and cochlea right (F). DVHs = dose-volume histograms, GK = Gamma Knife, LINAC = linear accelerator, PTV = planning target volume, TMJ = temporomandibular joint, Gy = Gray.

Table 3.13 gives the boost plan values and the LINAC + boost sum plan values. The sum dose values are extracted from the sum plans. Dose values exceeding the planning constraint in table 2.3 are highlighted in red and OAR intersecting or abutting the PTVs are marked with asterisks * (PTV60 one asterisk, PTV boost two asterisks).

Table 3.13: Dose constraints and metrics (GI, PCI) for patient P4 and the LINAC base, LINAC boost, GK boost and the sum plans LINAC+GK boost and LINAC+LINAC boost. The dose values are in the unit Gray (Gy) and the red shaded areas in the sum plan columns represent dose values exceeding the planning constraints. OAR intersecting or abutting PTV60 (base plan) are marked with one asterisk and OAR intersecting or abutting PTV boost with two asterisks. GI = gradient index, PCI = Paddick conformity index, GK = Gamma Knife, LINAC = linear accelerator, TMJ = temporomandibular joint, OAR = organ at risk.

Patient P4	LINAC base	GK boost	LINAC boost	LINAC+GK boost	LINAC+LINAC boost	Constraints
Brainstem (D _{0.035cc}) [Gy]	30.7	6.1	5.9	34.5	35.3	< 60
Spinal cord (D _{0.035cc}) [Gy]	30.1	5.4	3.9	32.5	32.2	< 52.8
Parotid left* (D _{0.035cc}) [Gy]	63.1	9.3	9.5	72.7	71.5	< 32
Parotid right* (D _{0.035cc}) [Gy]	64.5	2.8	3.6	65.4	66.4	< 32
Parotid left* (D _{mean}) [Gy]	41.9	2.8	1.8	44.9	43.7	< 26
Parotid right* (D _{mean}) [Gy]	28.0	0.9	1.5	28.9	29.5	< 26
Cochlea left (D _{0.035cc}) [Gy]	39.2	5.4	6.2	42.7	43.5	< 40
Cochlea right (D _{0.035cc}) [Gy]	32.7	3.2	3.6	34.8	35.3	< 40
TMJ left (D _{0.035cc}) [Gy]	63.1	10.0	10.5	74.1	73.1	< 65
TMJ right (D _{0.035cc}) [Gy]	54.0	3.0	4.1	57.1	58.2	< 65
Pituitary gland* (D _{0.035cc}) [Gy]	27.0	3.0	1.4	27.9	24.3	< 50
Optic chiasm (D _{0.035cc}) [Gy]	8.6	1.9	0.6	8.3	7.6	< 52
PTV (D _{0.035cc}) [Gy]	65.8	14.0	10.7	78.4	76.5	-
PTV (D _{mean}) [Gy]	60.6	10.3	10.0	71.0	70.6	-
GI PCI	-	3.17 0.77	4.40 0.84	-	-	-

Patient P4 (table 3.13 and figure 3.24 and 3.25) has several OAR intersecting with PTV60 namely the left cochlea, both TMJ and both parotids. Additionally, TMJ left and

parotid left are intersecting with the boost volume resulting in higher GK boost doses. In the base plan, the parotid doses are already exceeded and the dose limit for the left cochlea is almost reached. Similarly, TMJ left already reaches 63.1 Gy in the base plan so that the dosimetric constraints (65 Gy) is exceeded with either boost plan. The distance between the boost PTV and the pituitary gland and the chiasma is ≥ 1 cm. With this distance these two organs can be blocked out of the treatment field while the LINAC gantry is rotating around the patient head. With GK, however, the radiation originates from 192 directions but the sources cannot be individually blocked out. The smallest unit that can be shielded is one out of the eight sectors each containing 24 sources. Even by blocking one sector, incident radiation through these OAR remains explaining why the LINAC boost doses are lower than the GK boost doses.

The highest benefit of GK boost can be found for the dose sparing of the right parotid (sum 2.0%) and TMJ (sum 1.9%). This percentual advantage, however, is low compared to the disadvantage that can be observed for the high dose in the PTV (+3.3 Gy) and the OAR pituitary gland and optic chiasm. Additionally, the DVH for PTV shows a slight underdosage, which was already visible in one of the axial slices of figure 3.23. In both plans, a mean dose of at least 10 Gy is delivered to the PTV and the GK boost mean dose is 0.2 Gy higher than the LINAC boost mean dose. The dose conformity is lower with the GK boost compared to the LINAC boost (PCI: 0.77 vs. 0.84). The GI, however is reduced by almost 30% with the GK boost plan (3.17 vs. 4.40).

Patient P5

The dose distributions for the boost plans in three axial slices is shown in figure 3.26. Figures 3.27 and 3.28 show the DVHs per structure for LINAC and GK boost plans of patient P5 and table 3.14 gives the dose values for the considered OAR.

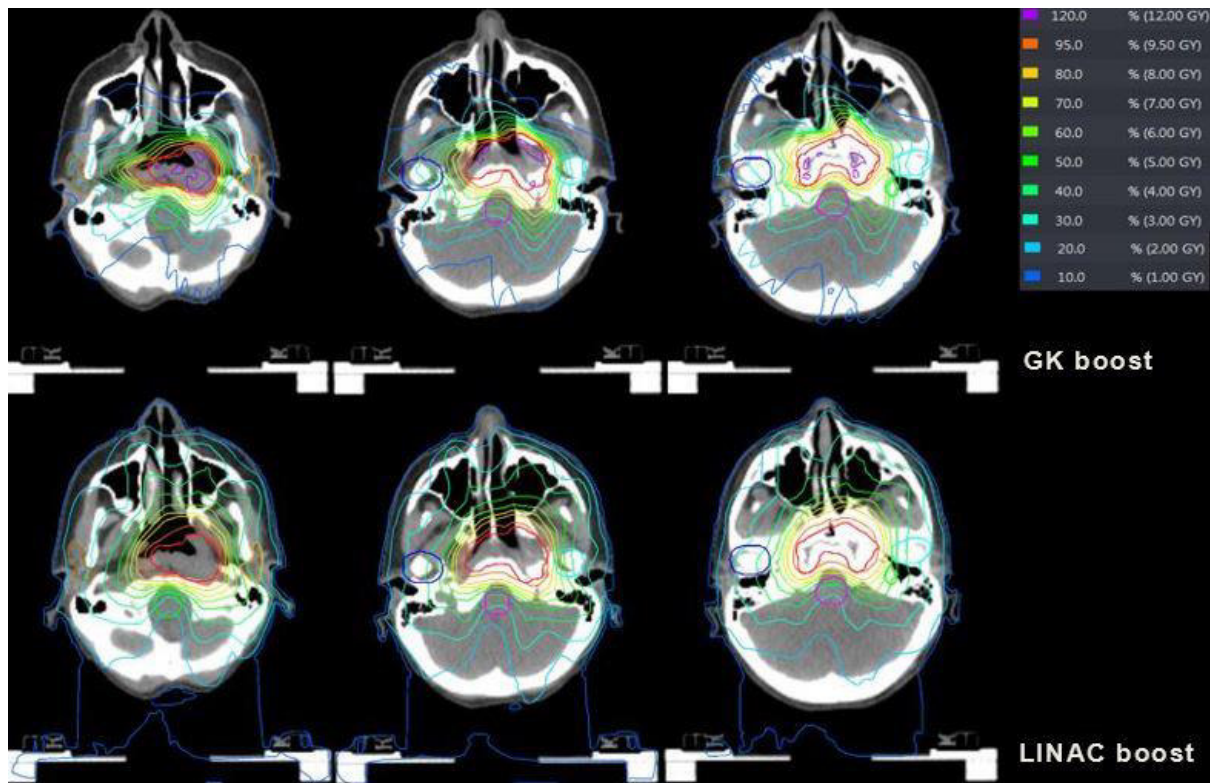


Figure 3.26: Dose distribution for patient P5 and the GK and LINAC boost plans. Planning target volume (red), left parotid (light orange), right parotid (dark orange), left temporomandibular joint (light blue), right temporomandibular joint (dark blue), spinal cord (neon green), brainstem (pink), left cochlea (light green), right cochlea (dark green). The isodose lines are represented on the right side of the figure. GK = Gamma Knife, LINAC = linear accelerator.

The dose distributions in three slices for patient P5 and the plans GK and LINAC boost are represented in figure 3.26. This patient has a central NPC and the extent and number of the GK hotspots compared to patients P1–P3 are increased but their location is outside of critical areas. Additionally, in the first of the three slices, a slight PTV underdosage can be seen in the air cavity region for the GK boost (convolution) compared to the LINAC boost (Monte Carlo). As for the OAR, the dose sparing with GK appears less expressed than for the other patients. The spinal cord, TMJ left and both parotids seem to benefit the most from the GK boost plan.

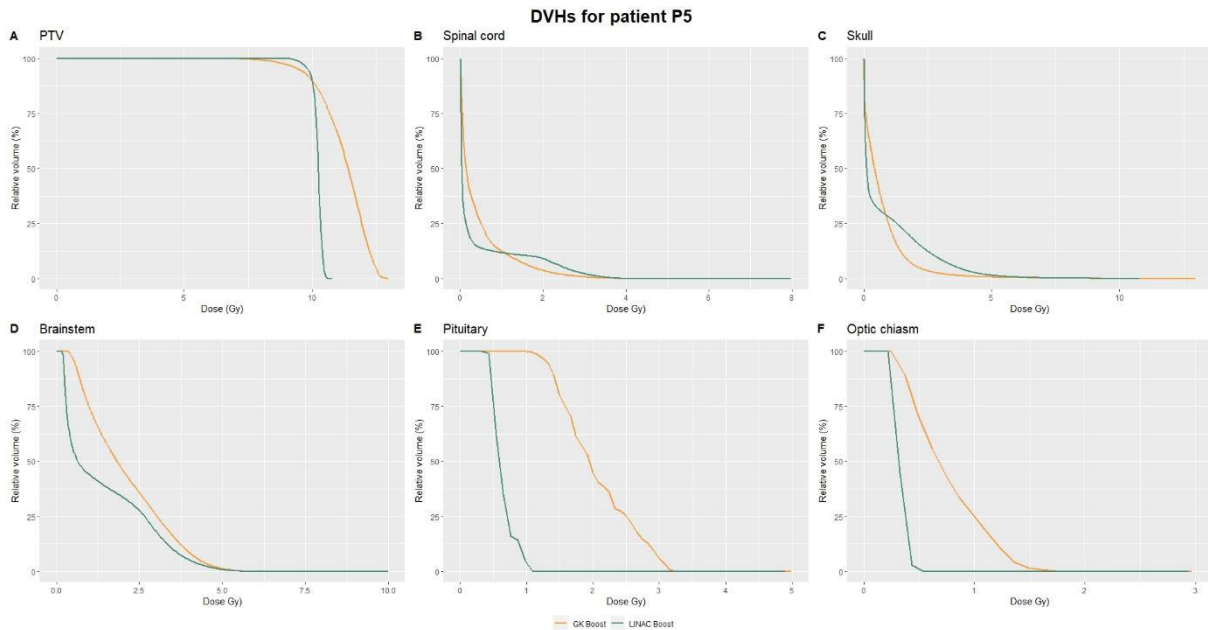


Figure 3.27: DVHs for patient P5, the plans GK Boost (yellow) and LINAC Boost (green) and the structures PTV (A), spinal cord (B), skull (C), brainstem (D), pituitary (E) and optic chiasm (F). DVHs = dose-volume histograms, GK = Gamma Knife, LINAC = linear accelerator, PTV = planning target volume, Gy = Gray.

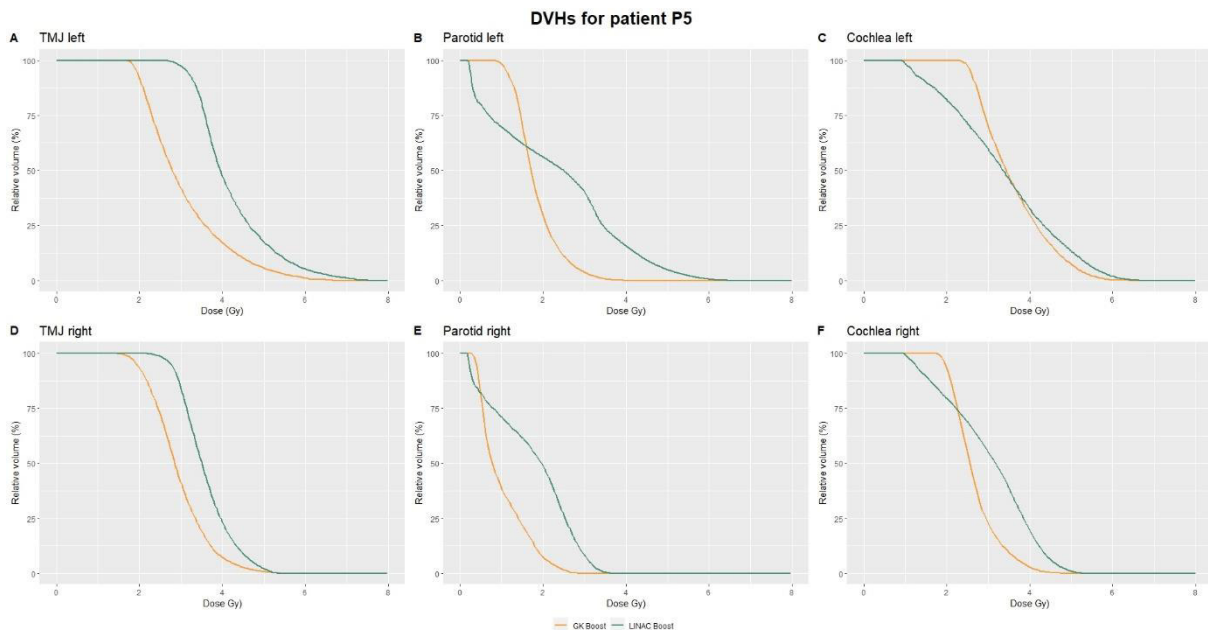


Figure 3.28: DVHs for patient P5, the plans GK Boost (yellow) and LINAC Boost (green) and the structures TMJ left (A), parotid left (B), cochlea left (C), TMJ right (D), parotid right (E) and cochlea right (F). DVHs = dose-volume histograms, GK = Gamma Knife, LINAC = linear accelerator, PTV = planning target volume, TMJ = temporomandibular joint, Gy = Gray.

Table 3.14 gives the boost plan values and the LINAC + boost sum plan values. The sum dose values are extracted from the sum plans. Dose values exceeding the planning constraint in table 2.3 are highlighted in red and OAR intersecting or abutting the PTVs are marked with asterisks * (PTV60 one asterisk, PTV boost two asterisks).

Table 3.14: Dose constraints and metrics (GI, PCI) for patient P5 and the LINAC base, LINAC boost, GK boost and the sum plans LINAC+GK boost and LINAC+LINAC boost. The dose values are in the unit Gray (Gy) and the red shaded areas in the sum plan columns represent dose values exceeding the planning constraints. OAR intersecting or abutting PTV60 (base plan) are marked with one asterisk and OAR intersecting or abutting PTV boost with two asterisks. GI = gradient index, PCI = Paddick conformity index, GK = Gamma Knife, LINAC = linear accelerator, TMJ = temporomandibular joint, OAR = organ at risk.

Patient P5	LINAC base	GK boost	LINAC boost	LINAC+GK boost	LINAC+LINAC boost	Constraints
Brainstem (D _{0.035cc}) [Gy]	54.8	5.6	5.5	60.2	60.2	< 60
Spinal cord (D _{0.035cc}) [Gy]	47.2	3.3	3.7	50.4	50.7	< 52.8
Parotid left* (D _{0.035cc}) [Gy]	63.1	3.6	6.1	66.9	68.5	< 32
Parotid right* (D _{0.035cc}) [Gy]	64.5	2.7	3.5	67.0	67.8	< 32
Parotid left* (D _{mean}) [Gy]	44.8	2.3	1.9	46.7	46.5	< 26
Parotid right* (D _{mean}) [Gy]	41.0	1.0	1.7	41.9	42.5	< 26
Cochlea left (D _{0.035cc}) [Gy]	43.2	5.4	6.0	48.1	49.4	< 40
Cochlea right (D _{0.035cc}) [Gy]	45.7	4.1	4.8	49.7	50.1	< 40
TMJ left (D _{0.035cc}) [Gy]	56.5	6.1	7.1	62.4	63.0	< 65
TMJ right (D _{0.035cc}) [Gy]	60.0	4.8	5.2	64.7	65.2	< 65
Pituitary gland* (D _{0.035cc}) [Gy]	42.3	3.0	1.0	44.9	43.0	< 50
Optic chiasm (D _{0.035cc}) [Gy]	5.5	1.4	0.4	6.3	5.9	< 52
PTV (D _{0.035cc}) [Gy]	66.3	12.8	10.6	78.1	75.1	-
PTV (D _{mean}) [Gy]	60.6	10.0	10.0	70.6	70.4	-
GI PCI	-	3.24 0.78	5.15 0.81	-	-	-

Patient P5 (table 3.14 and figure 3.27 and 3.28) has both parotids and both TMJ intersecting with PTV60 of the base plan. Nevertheless, dose sparing is achieved with

the GK boost plan. Additionally, PTV60 is very close to the brainstem, spinal cord and cochleae in some slices. Consequently, the dose constraint for both parotids and cochleae is already exceeded with the base plan and the brainstem dose limit is slightly violated with both boost plans. As for the TMJ, the dose constraint for the right side is slightly exceeded with LINAC + LINAC boost and dose sparing is reached for both sides with the GK boost. The difference of PTV high dose is 2.2 Gy. Additionally, the DVH for PTV and GK boost shows a slight underdosage, which was already visible in one of the axial slices in figure 3.26. The mean dose of 10 Gy in the boost PTV is reached for both plans and a mean dose difference of 0.2 Gy is visible in the sum plans. The conformity of the GK boost plan is slightly reduced compared to the LINAC boost plan (PCI: 0.78 vs. 0.81) and the GK boost GI is improved by 37% compared to the LINAC boost GI.

3.3.3 Mean dose volume histograms and dose values

Figures 3.29 and 3.30 give the mean DVHs over all patients for the different structures and boost plans and table 3.15 features the dose values ($D_{0.035cc}$ and D_{mean}) and plan quality metrics (PCI, GI) over all patients.

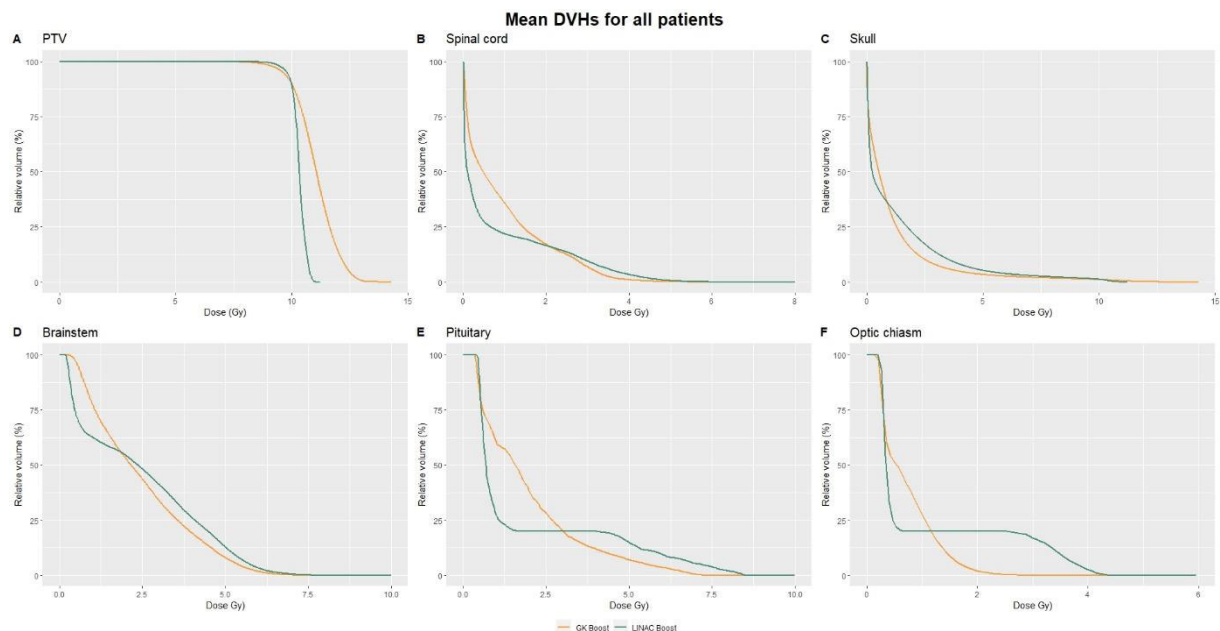


Figure 3.29: Mean DVHs for all patients, the plans GK Boost (yellow) and LINAC Boost (green) and the structures PTV (A), spinal cord (B), skull (C), brainstem (D), pituitary (E) and optic chiasm (F). DVHs = dose-volume histograms, GK = Gamma Knife, LINAC = linear accelerator, PTV = planning target volume, Gy = Gray.

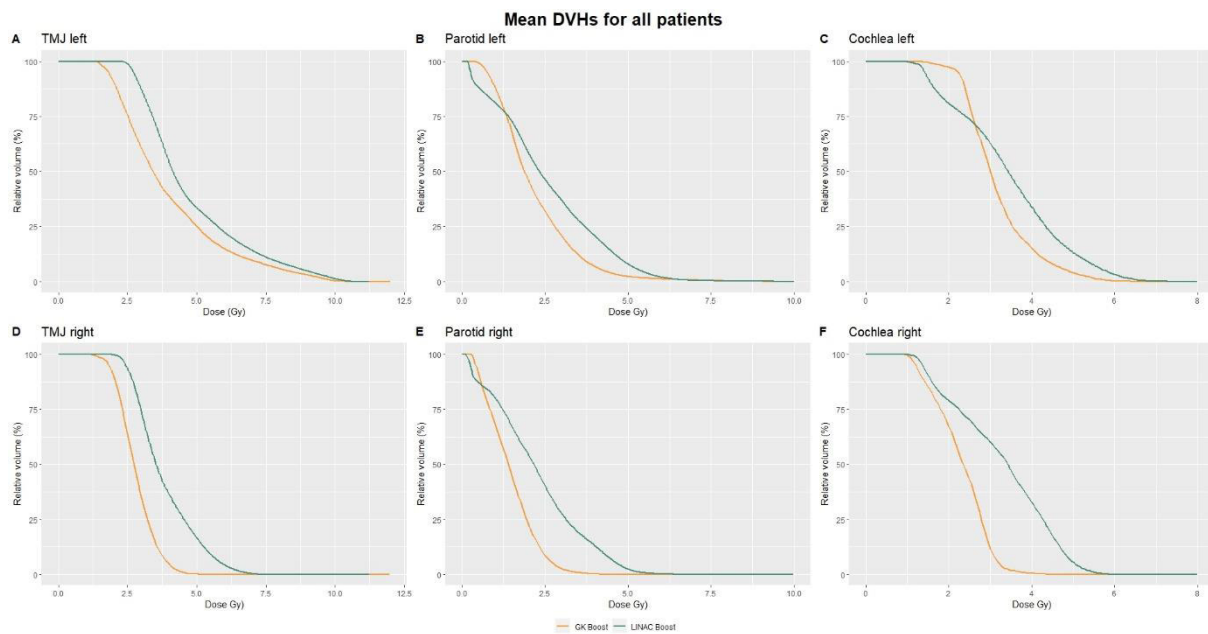


Figure 3.30: Mean DVHs for all patients, the plans GK Boost (yellow) and LINAC Boost (green) and the structures TMJ left (A), parotid left (B), cochlea left (C), TMJ right (D), parotid right (E) and cochlea right (F). DVHs = dose-volume histograms, GK = Gamma Knife, LINAC = linear accelerator, PTV = planning target volume, TMJ = temporomandibular joint, Gy = Gray.

Table 3.15: Mean dose constraints and metrics (GI, PCI) for all patients and the LINAC base, LINAC boost, GK boost and the sum plans LINAC+GK boost and LINAC+LINAC boost. The dose values are in the unit Gray (Gy) and the red shaded areas in the sum plan columns represent dose values exceeding the planning constraints. OAR intersecting or abutting PTV60 (base plan) are marked with one asterisk and OAR intersecting or abutting PTV boost with two asterisks. GI = gradient index, PCI = Paddick conformity index, GK = Gamma Knife, LINAC = linear accelerator, TMJ = temporomandibular joint, OAR = organ at risk.

All patients	LINAC base	GK boost	LINAC boost	LINAC+GK boost	LINAC+LINAC boost	Constraints
Brainstem (D _{0.035cc}) [Gy]	38.4	5.5	6.6	42.6	43.9	< 60
Spinal cord (D _{0.035cc}) [Gy]	35.1	3.9	4.7	37.5	38.1	< 52.8
Parotid left* (D _{0.035cc}) [Gy]	62.6	5.0	6.2	67.0	67.8	< 32
Parotid right* (D _{0.035cc}) [Gy]	63.3	3.4	4.6	65.7	66.9	< 32
Parotid left* (D _{mean}) [Gy]	39.8	2.3	2.5	42.8	43.0	< 26
Parotid right* (D _{mean}) [Gy]	29.9	1.4	2.3	31.3	32.1	< 26
Cochlea left (D _{0.035cc}) [Gy]	36.6	4.3	5.0	39.6	40.4	< 40
Cochlea right (D _{0.035cc}) [Gy]	36.0	3.0	4.6	38.3	39.8	< 40
TMJ left (D _{0.035cc}) [Gy]	55.5	6.5	7.6	61.5	62.3	< 65
TMJ right (D _{0.035cc}) [Gy]	51.0	4.1	5.6	54.4	55.9	< 65
Pituitary gland* (D _{0.035cc}) [Gy]	35.6	2.9	2.5	35.9	35.2	< 50
Optic chiasm (D _{0.035cc}) [Gy]	9.0	1.3	1.2	9.5	9.5	< 52
PTV (D _{0.035cc}) [Gy]	65.2	12.9	10.7	76.7	75.3	-
PTV (D _{mean}) [Gy]	60.3	10.3	10.1	70.6	70.4	-
GI PCI	-	3.07 0.80	4.65 0.81	-	-	-

Over all patients, the GK boost PTV D_{0.035cc} is about 2.2 Gy higher than the LINAC dose and the PTV appears slightly underdosed in the DVH. As mentioned previously,

when OAR are abutting or intersecting with the boost PTV GK coverage is often reduced. Similarly, hotspots are avoided in the aforementioned critical structures (bones, mucous membranes, nerves) so that the coverage is often compromised. Here it has to be emphasized, that the first homogenous prototype version of Lightning was used and that future versions might enable even higher homogeneity so that the target coverage will not necessarily be compromised. Additionally, as it is shown in the dose distributions for some patients, the convolution algorithm has difficulties with dose deposition in air cavities and osseous structures. These structures have Hounsfield units outside the CT calibration range so that values below (air) and above (bone) are truncated to the lowest and highest electron density value of the calibration curve. Although Monaco TPs employs the same procedure, underdosage is only observed using the GK TPS, so that the differences can be explained by the higher accuracy of Monte Carlo compared to convolution especially at interfaces of tissues with different densities ⁷³⁻⁷⁶.

Across all patients, the conformity of the LINAC and GK boost plans is very similar (PCI GK: 0.80; PCI LINAC: 0.81) but the GI is improved by a mean percentage of 34%. As shown previously, the GI with the GK boost plans is improved for all patients while the PCI is increased for patients P2 and P3 only.

In general, since the studied patients mostly presented with central NPC, both parotids are inside the PTV60 structure and are irradiated with a LINAC base plan dose of at least 60 Gy. Hence, the parotid dose constraints are already violated with the base plans. Despite the excessive doses, it is noteworthy that over all patient the GK achieves a $D_{0.035 \text{ cc}}$ /mean dose reduction of 19.1%/10.3% (parotid left) and 25.9%/36.8% (parotid right) in the boost plans and 1.1 %/0.6% (parotids left) and 1.8 %/2.4% (parotid right) in the sum plan.

Similarly, for most patients, one or both cochleae are overlapping or in close proximity to the PTV60 structure resulting in high doses close to the threshold with the base plan. By adding the boost plans, the constraints are exceeded for the LINAC plan and the left cochlea. The right cochlea dose for LINAC is very close to the threshold. With GK, no cochlea doses are exceeded and the dose is reduced by 14.6% (cochlea left) and 35.8% (cochlea right) on average in the boost plans and 2.0% (cochlea left) and 3.8% (cochlea right) in the sum plans.

Across all patients, the TMJ left doses are close to the constraint of 65 Gy but the limit is not exceeded. Here, the GK boost plan results in a dose sparing of 14.3% (left) and 26.1% (right) which corresponds to 1.3% (left) and 2.7% (right) in the sum plans.

The brainstem and spinal cord doses are overall more than 10 Gy below the constraints. With GK, boost doses are reduced by 17.6% (sum 3.0%) and 18.0% (sum 1.7%), respectively.

As for the skull doses, they appear slightly reduced with the GK boost compared to the LINAC boost plan. The extent of the difference, however, is small compared to the differences that are observed with other structures.

Finally, the pituitary gland and optic chiasm doses are far below the considered constraint. However, the GK boost plan results in higher doses of 15.8% (sum 1.9%) and 9.8% (sum 0.1%), respectively, in the boost plans. This is due to the previously mentioned fact that the GK radiation strikes from 192 different directions so that these two structures—usually located in cranial direction above the PTV—cannot be shielded from the treatment field, as it is the case with LINAC treatment. The doses, although being higher with GK boost, are still far below the threshold and the assessment of the clinical importance of the difference is outside the scope of this work.

4 DISCUSSION

In this work the feasibility of combining LINAC and GK treatment for NPC was investigated. For this purpose, newly developed inverse planning for GK treatment was analyzed for malignant and benign brain tumors and the benefit compared to forward planning was assessed. While the advantages compared to forward planning were numerous and significant, the loss of direct control over the planning IDL and hence the degree of inhomogeneity represents one disadvantage especially for healthy structures in proximity of or crossing the target volume. As the optimizer does not allow for input of the maximum dose to the target below 133% of the prescription dose, a more homogenous version of the TPS which would reduce in-tumor hotspots was needed and provided for research purposes by the manufacturer. The degree of homogeneity and OAR sparing that can be achieved with the prototype version compared to the current clinical version and LINAC plans was assessed for brain tumors with OAR involvement. Finally, with improved homogeneity, boost plans for NPC were calculated for LINAC and GK, summed with the base plan and the dosimetric benefit of combining LINAC with GK treatment for NPC was assessed. To conclude, since the presented work is a feasibility study, advantages and challenges for clinical implementation are discussed.

4.1 Inverse planning with Leksell GK Lightning: Advantages and limitations

The conducted analysis showed that inverse planning with the new optimizer is advantageous compared to forward planning and the extent of the benefits depends on the studied medical condition. In general, the optimizer enabled the creation of treatment plans with improved coverage (up to 3.6%) and GI (reduction of up to 18.1%), especially for the irregular shaped benign lesions with OAR involvement. When using the full coverage setting, the target coverage was the highest but at the cost of reduced selectivity. Without this setting, the inverse plans showed equal or increased selectivity (AN: 1.8%, MEN: 1%, MET: 2.9%) while tumor coverage was increased in the benign groups. For all medical conditions, the optimizer chose a higher planning IDL for inverse and full coverage plans than the clinician's prescription for forward planning and the number of shots is increased^{77, 78}.

4.1.1 Plan quality: metastases

As metastases commonly have distinct margins and are known to grow by displacing healthy brain tissue, their radiosurgical treatment can be done with low harm to the healthy brain ⁷⁹. Additionally, because of the typically regular and round shape of METs, manual forward planning already provides satisfying results for the plan quality and efficiency. While coverage of ≥ 0.99 was already achieved in the forward plans and maintained in the inverse plans, full coverage plans managed to increase the coverage even more but at the cost of selectivity. GI was reduced for both Lightning plans and $V_{12\text{Gy}}$ skull decreased for the inverse plans. While manual forward plans were generated according to clinician's prescription using the 50% IDL, the optimizer chose slightly higher IDL for the Lightning plans. Although using the 50% IDL for treatment of METs is a common clinical practice depending on the target volume as it is assumed to provide the steepest dose fall-off ²⁸, Ma et al. showed that an increased IDL above 50% resulted in a reduction of normal brain integral dose as well as NTCP ⁸⁰. This is in accordance with the decrease in GI and $V_{12\text{Gy}}$ skull that was found for inverse plans despite the higher planning IDL compared to forward planning. When limiting D_{max} target, significant differences were found in planning IDL, number of shots and GI for full coverage plans. Here, the importance of limiting the maximum dose to the target, which in turn affects the planning IDL, has to be discussed by experienced clinicians and is outside the scope of this work. Similarly, the clinical importance of the improvements reached with the inverse plans (cov, sel, GI, $V_{12\text{Gy}}$ skull) as well as the deterioration when using the full coverage setting (sel, $V_{12\text{Gy}}$ skull) have to be assessed by experienced clinicians. With the full coverage setting the selectivity of the plans was still very high and satisfying and the rise in skull dose doesn't exceed clinical thresholds and is not it statistically significant.

Consequently, the analysis showed that inverse planning with Lightning does not provide a tremendous advantage in plan quality for METs.

4.1.2 Plan quality: acoustic neuromas and meningiomas

The coverage was enhanced for both Lightning plans while, as already observed with METs, the selectivity was compromised in the full coverage plans but maintained in the inverse plans. GI was similar (MEN) or reduced (AN) and $V_{12\text{Gy}}$ skull was slightly reduced. Both Lightning plans showed a decrease in maximum doses to the OAR of

up to 4.5% (AN) and 17.5% (MEN) but only the change in the inverse plans was significant. When using the fc coverage setting, the dose reduction for OAR is more important for MEN than for AN. This can be explained by the distance between OAR and target which is typically greater for MEN. Hence, the distance between OAR and target should be considered when deciding whether to use the full coverage setting for optimization.

The aforementioned results correlate with the findings of Pokhrel et al. stating that GI, brain and OAR doses can be considerably reduced for studied benign cases (arteriovenous malformations, pituitary adenomas)⁷⁷. Similarly, Wieczorek et al. analyzed benign and metastatic lesions and found GI to be significantly improved in the former cases. As for the OAR dose reduction, even though not significant in the full coverage plans, it is in general a promising and very powerful tool, which can be a great asset in the management of side effects for a number of targets with nearby OAR^{81, 82}. Minniti et al., for instance, studied the risk of developing clinically significant radiation induced neuropathy for patients with skull base meningiomas and found no risk for maximum doses below 10 Gy to the optic pathways⁸². Peak et al. looked at prognostic factors for hearing deterioration in patients with acoustic neuromas and found the maximum dose to the cochlear nucleus to be the only significant factor⁸³. As previously mentioned, the optimizer chose higher IDL than prescribed for forward planning resulting in lower maximum target doses. The clinical version of Lightning does not allow D_{\max} target input $\leq 133\%$ of the PD. However, this is sometimes necessary in clinical practice in order to protect critical, healthy structures crossing or abutting the target volume (e. g. cranial nerves⁸⁴⁻⁸⁶) and will be addressed further in the discussion.

The analysis shows that for the benign groups the optimizer generates plans with increased coverage and reduced OAR doses. The use of the full coverage settings, however, should be avoided for close critical structures.

4.1.3 Plan efficiency, inter-operator-variability and additional findings

The BOT was reduced for all medical conditions and both Lightning plans. While the BOT shortening was substantial for the benign groups with a mean BOT reduction of up to 49.5%, it was only slightly pronounced for METs. Additionally, in the benign groups the IQR was small, which shows the influence the operator has on the BOT. Similarly, for a meningioma case and a plan promoting BOT shortening, which was calculated with Lightning, Sjölund et al. reported a BOT shortened by more than 50%

⁶¹. BOT shortening has been one of the main objectives researchers have been working on in the development of inverse planning approaches. Tian et al. reduced the BOT by 8–52% compared to forward planning for five meningiomas using their multiresolution-level inverse planning approach ⁸⁷. Levivier et al. used their inverse planning approach for GK and reduced the BOT of two out of five forward planned clinical cases by up to 35%. Together with BOT shortening, the authors found, similar to the analysis in this work, improved target coverage, selectivity, GI and D_{\max} OAR but increased D_{\max} target. In general, the BOT shortening and improved control over it is a real asset in treatment efficiency as the treatment plan can be even more individualized with regards to the patient's tolerated treatment time and treatment time slot allocation can be designed in a more efficient way.

With Lightning, very similar plans can be obtained even by unexperienced operators. The highest differences were found in the plan efficiency (BOT: difference 1–3.3 min), which can directly be influenced and adapted by the operator according to the patient's physical and mental resilience, and in the metrics IDL and number of shots, which do not affect the plan quality. The forward plans showed less variations overall and the highest differences were found in GI and $V_{12\text{Gy}}$ skull. The forward plans represent one of the weaknesses of this analysis as all operators had prior LGP forward planning experience. Another weakness is the number of operators with different experiences which requires further investigations. Cui et al., for instance, analyzed the plan variations using Lightning for 40 patients and three users (two experienced, one novice) and, similar to this work, only found small variations in plan metrics ⁸⁸.

As Lightning does not maintain the operator's input of the planning IDL during optimization, clinicians need to familiarize with a new way of prescribing. The prescription should include the PD and maximum dose to the target or an allowed IDL range rather than a fixed IDL. Finally, an important decrease in the time needed for plan optimization was noticed. Even for large targets, a treatment plan can be generated in less than one minute and only a few optimizations are needed to achieve a clinically acceptable plan. Indeed, several groups recorded the planning time and reported a mean optimization time of ≤ 5 min compared to estimated forward planning times of 30–90 minutes for benign targets ^{77, 78}.

4.2 Homogenous Leksell GK Lightning: OAR dose sparing and homogeneity

4.2.1 Target dose homogeneity

When comparing Lightning and LINAC plans, the inhomogeneity of the dose distribution inside the target was significantly increased (LGK Hom: 9.2%; LGK OAR: 14.8%; LGK: 25%) and highest for PA and the plans LGK Hom and OAR (LGK Hom: 11.2%; LGK OAR: 16.8%). With a variety of formulas available in literature, the use of HI as an objective measure for target dose homogeneity is challenging. Kataria et al., for instance, used various formulas for HI from literature and associated their results with the PD, location and size of the target ⁸⁹. The authors found improved homogeneity with decreasing target size and reported the highest values for brain lesions. This is in opposition to the results of this work, but the impact of the target shape has not been analyzed and needs consideration. Additionally, in order to increase the significance of HI, the authors emphasized that the formula should include biological information to use it as a predictor for outcome. Indeed, the work of others showed that increased TCP can result in higher dose inhomogeneity inside the target while at the same time sparing the nearby OAR thanks to steep dose gradients ⁹⁰⁻⁹². Tomé et al. analyzed TCP for different boost doses, radio-resistant tumor cells and tumor sub-volumes and, even for the most resistant cells, predicted important increases when the boost to PD ratio was 1.2–1.5 to $\geq 60\%$ of the target volume. Today's improvements in imaging and image processing methods allow for the extraction of valuable information about the tumor and its sub-volumes, which can then be used as biomarkers to assist in the determination of the best suited treatment planning strategies. Radiomics, for instance, can help with identifying radio-resistant areas in the tumor volume that could be targeted for dose intensification to enhance outcomes ^{93, 94}. Thus, dose escalation in advantageous tumor locations while sparing OAR can be accomplished with Gamma Knife's superior dose gradients by combining imaging data information with the benefits of improved control over inhomogeneity given by the prototype version. The enhanced homogeneity of this version can also reduce the need for LINAC treatments in situations where OAR are located within the tumor volume, such as in AN ⁹⁵ and skull base MEN ⁹⁶. This is in accordance with the findings of this work for the studied AN and PA cases, where LGK Hom showed improved GI and comparable OAR doses despite showing more inhomogeneity.

4.2.2 Plan quality and efficiency

In this analysis, the Lightning plans outperformed LINAC plans in terms of GI, which is in accordance with the classical advantage of steeper dose gradients outside the target volume ^{24, 26, 27}. The median GI was found to be improved by 42% (LGK Hom), 48% (LGK OAR) and 52% (LGK) but was the least expressed in the MEN group (LGK Hom: 0.33%, LGK OAR: 0.38% and LGK: 0.43%). For larger targets (median target size: 3.31 cc), the optimizer tends to use larger shot collimations to ensure adequate target coverage compared to AN and PA (AN: 1.2 cc; PA: 1.77 cc). Vergalasova et al. used commercially available SRS systems for the treatment of brain metastases. Their analysis revealed that GK only showed an advantage over the other devices for small lesions. For larger targets, the GI of GK was similar to VMAT ⁹⁷. Additionally, the authors reported improved target conformity for smaller lesions, which is not in accordance with the results of this work but can be explained by more complex target geometries compared to metastases. Indeed, Wu et al. analyzed the conformity of different lesions and observed that targets of more ellipsoid shapes (e. g. PA, MEN) resulted in different conformities compared to targets with sharper corners (AN) ⁹⁸.

While all LINAC and Lightning plans met the institutional dose constraints, the Lightning plans achieved an OAR dose reduction of at least 6.5% (AN), 15.8% (PA) and 8.5% (MEN). For LGK OAR and LGK plans, significant dose reductions were reached and especially expressed for the larger targets (MEN). At this point it should be noted that treatment planning with both TPSs was based on the LINAC PTV. With GK, however, even for fractionated treatments PTV margins can be reduced due to enhanced system accuracy which in turn enlarges the distance between PTV and OAR ^{29, 30}. Hence, applying the clinical GK target delineation would result in further reduced OAR doses and, because of the diminished target size, BOT would be shortened. Regarding the skull doses lower and similar values were found for the Lightning plans compared to LINAC, which is also known to be one of the main advantages of GK treatment ²⁵.

The great amount of shots with high degrees of modulation especially for large and complex targets resulted in plans with up to five times longer median BOTs (MEN: LGK Hom and LGK OAR) compared to LINAC BOTs. Liu et al. reported similar results when analyzing the BOT for metastases between 0.1 cc and 10.5 cc. They found the GK BOTs to be three to five times longer than VMAT BOTs ²⁵. The authors suggested that the use of larger collimator sizes and fewer amounts of shots could improve treatment

efficiency, which, however, would deteriorate the conformity of the target and worsen the low-dose spread in the healthy brain. It should be emphasized that although GK BOTs are longer, the average BOT in this study were still clinically acceptable with 8.5 min per fraction. Additionally, the time needed for couch rotation in the LINAC plans should not be neglected. While the rotation is used to increase the GI and reduce OAR doses, it also adds a theoretical insecurity regarding patient positioning and prolongs the total treatment time⁹⁹. The impact of couch rotation on the aforementioned factors, however, was not within the scope of this analysis.

This homogeneity and OAR sparing analysis did not aim at establishing a general plan comparison between GK and LINAC since both plan qualities could have been optimized further by, for instance, allowing longer BOT for GK or increasing the number of non-coplanar beam for LINAC²⁵. The aim of this investigation was to explore the dosimetric potential when stretching the commonly assumed limits of GK treatment. This way, the range of GK applications could be expanded to treat tumors requiring a higher degree of homogeneity than what's possible in the current clinical version. With further investigations and cooperation with the manufacturer, even more homogenous plans could be generated, as the current prototype version does not seem to leverage the full potential of more homogenous and inverse GK treatment planning.

4.3 Homogenous Leksell GK Lightning for treatment planning of NPC

This feasibility analysis was based on the previous work analyzing (i) the benefit of inverse planning with Leksell Gamma Knife Lightning (chapter 4.1) and (ii) the potential of its homogenous prototype version that was provided for research purposes (chapter 4.2). Even though the retrospective patient population—due to the low incidence of NPC in Germany and the limitations imposed by GKs geometry—was small, the feasibility of GK boost treatment of NPC was shown.

4.3.1 Anatomical changes and dose distribution

In this work, the gross tumor with an extension margin of 3 mm was boosted with 10 Gy normofractionation. Due to previous irradiation of PTV60 comprising the boost volume, an average gross tumor $D_{0.035cc}$ dose of about 77Gy (LINAC + GK boost) and 75 Gy (LINAC + LINAC boost) was reached. For four out of five patients, however, the boost

volume treated with GK appeared slightly underdosed, which can be due to several reasons. One reason is the higher accuracy of Monte Carlo algorithm used in LINAC TPS compared to the convolution algorithm used in GK TPS⁷³⁻⁷⁶. Studies showed that inhomogeneities due to air cavities result in reduced dose at the air-tissue boundary and that the magnitude of the reduction is larger with e. g. smaller field size (GK) and larger cavity volume¹⁰⁰⁻¹⁰². Especially in regions with lateral scatter disequilibrium, which can be due to the treatment of low-density tissue with small fields, Monte Carlo provides more accurate dose distribution than other commercially available dose algorithms⁷³. Lee et al. compared collapsed cone convolution and Monte Carlo algorithms in treatment planning of canine sinonasal tumors and found significant dosimetric differences⁷⁴. Convolution underestimated the dose in air (1.1%) and overestimated the dose in bone (3%) compared to Monte Carlo. With this knowledge and the fact that NPC treatment generally involves the nasal cavity, it is apparent that in this work the dose distribution with Monte Carlo in regions involving air cavities and bones (hotspots) was improved compared to convolution. Two more reasons for the underdosage are linked to the homogenous planning attempt. First, in some of the cases OAR were crossing or abutting the boost volume and the dose limitation counteracted with the currently achievable homogeneity of the prototype version, resulting in underdosed regions. Second, analogously to the first reason, the pursued avoidance of hotspots in critical areas not delineated as OAR (osseous and mucous structures, nerves) again undermined the homogeneity level that can be reached. By performing intermediate diagnostic imaging and replanning, the first concern can be addressed. As it was shown for one of the patients, gross tumor shrinkage to about 20% of the initial volume occurred within less than one week after initial imaging and start of irradiation after inductive chemotherapy. In fact, the anatomy of the head and neck region is known to be changing during radiotherapy. Tumor and OAR shrinkage, weight loss, local inflammations and changes in muscle density, fat and fluid distributions affect the rigidity of the head and neck anatomical structure¹⁰³⁻¹⁰⁵. With OAR commonly located in close proximity to the target volumes, even the slightest changes in anatomy can have an impact on target coverage and OAR doses in these sharp dose gradient regions¹⁰⁴. Barker et al. performed three weekly CTs on HNC patients treated with radiotherapy with or without concurrent chemotherapy (no inductive chemotherapy) and a prescription of 72 Gy (42 fractions), 70 Gy (35 fractions) or 60 Gy (30 fractions). They reported a median GTV reduction rate of 1.8 % of the initial volume per fraction, which resulted

in a median relative volume loss of about 70% of the initial GTV at the end of the treatment. They also reported a final median center of mass displacement of about 3.3 mm and correlated the rate of volume loss with the initial GTV size determined with CT imaging. For the OAR, they noted a decrease in parotid gland volume with a median loss of 0.6% per fraction (others reported 4.9% per week on average ¹⁰⁵). Additionally, they showed a median center of mass shift of about 3.1 mm, which correlated with weight loss. Limitations of their study, however, included variations in contouring especially for small tumors ¹⁰⁶. Bhide et al. reported most significant OAR and target volume changes already by week two of radiotherapy with inductive and concurrent chemotherapy ¹⁰⁴. Wang et al. analyzed the benefit of IMRT replanning for 28 NPC patients after variations in OAR and target dose distribution. Replanning was done based on intermediate CT imaging before the 25th treatment fraction and resulted in a significant increase of the prescription dose delivered to the gross tumor and significant decrease in OAR doses (spinal cord, parotid glands). Among the replanned plans, none violated the dose constraints for normal structures while half of the not replanned plans were out of limit ¹⁰⁷. Chen et al. analyzed the clinical outcome for HNC patients treated with or without adaptive radiotherapy under IMRT technique ¹⁰³. Out of 317 patients treated with a median dose of 66 Gy (range: 60—74 Gy), 51 had adaptive radiotherapy with IMRT plan modification based on new imaging after a median dose of 40 Gy. They reported a local-regional control advantage for the patients treated with adaptive radiotherapy (ART) (88% vs. 79%) but no difference in OS and distant metastasis-free survival. Late grade 3+ toxicity was reduced with ART (14% vs. 19%). Even though it is unclear whether changes in anatomy and dose distribution result in improved clinical outcome, patients' quality of life (QoL) can significantly be improved ¹⁰⁸. Yang et al. analyzed the benefit replanning has on the QoL of patients treated for NPC with IMRT. In their study, 86 out of 129 patients received IMRT replanning before the 15th fraction and/or 25th fraction. With replanning, the authors showed an improvement in local-regional control after 2 years (97.2% vs. 92.4%, $p=0.040$) but not in OS rate (89.9% vs. 82.2%, $p=0.475$). The QoL was significantly improved and patients without replanning reported more difficulties with speech, teeth, dry mouth, sticky saliva and social contact ¹⁰⁹. Although the OS rate was not significantly improved with replanning, there is increasing evidence that an improved QoL may have a prognostic impact on cancer patients' survival ^{46, 110}. With the results of the aforementioned studies, intermediate imaging and replanning accounting for anatomical changes especially in

the first half of the treatment (with chemotherapy even earlier) can result in improved target coverage and decreased OAR doses. Similarly, with decreased gross tumor compared to initial imaging, calculation and BOTs for GK planning can be reduced. This way, the restriction of BOT during optimization would be unnecessary and the optimizer could use its full potential to generate homogenous plans with focus on OAR and maximum dose restrictions only.

4.3.2 Benefit of OAR sparing

The studied patients mostly presented with central NPC which compromised the possibility of unilateral OAR sparing. Even though dose constraints were exceeded for some OAR, the doses were lower with the GK boosts which showed an average GI improvement of 34% compared to the LINAC boosts for plans with equal conformality. Especially for the parotids, excessive doses violating the defined planning constraints were already reached with the LINAC base plans due to their partial location inside the PTV60 structure. With xerostomia strongly compromising patients' QoL and being closely related to the irradiation of the parotid glands, most ART studies analyzed the changes of this structure. Beetz et al. developed predictive models for HNC patients treated with IMRT predicting the risk of xerostomia and sticky saliva six months after treatment. They found the mean ipsi- and contralateral parotid gland dose to be associated with xerostomia after treatment and concluded that the mean contralateral parotid gland dose was the strongest predictor for xerostomia ¹¹¹. Deasy et al. reviewed publications associating parotid gland dose-volume characteristics with salivary toxicity after radiotherapy. The consensus was that late salivary dysfunction was correlated with mean parotid gland dose and they recommended to keep the parotid mean dose as low as possible to increase the chances of better organ function ¹¹². The results of this work showed, that parotid mean doses can be reduced by up to 36.8% on average for a 10 Gy boost plan resulting in a reduction of 2.4% for a sum plan with a total dose prescription of 70 Gy.

As the cochlea is often located in the area of radiation, hearing impairment is an observed adverse event of radiotherapy in the upper head and neck region ¹¹³⁻¹¹⁶. Honoré et al. analyzed the pre- and post-therapeutic hearing levels of 20 patients (36 ears) receiving radiotherapy for NPC with inner ear doses below 2.44 Gy per fraction ¹¹⁷.

They found the incidence of the sensori-neural hearing loss (SNHL) to increase significantly with higher cochlea doses and found a dose-response relationship for sensory hearing loss at 4000 Hz. Even though the frequency range of human speech is between 1000 and 3000 Hz, the authors emphasized, that a hearing loss at 4000 Hz still has an influence on patient's general hearing. Their analysis, however, included different fractionation regimens and prescription doses and the results were not corrected for general hearing deterioration occurring with age. Hwang et al. analyzed the long-term hearing loss after radiotherapy (early stage) or chemoradiotherapy (advanced stage) for NPC patients and corrected the hearing thresholds for age-related deteriorations¹¹⁸. They treated 92 patients (182 ears) with either 2D CRT, 3D CRT or IMRT and with a total radiation dose of 59.4-79.2 Gy (mean dose 70.86 Gy). They found hearing deterioration to be progressive for all frequencies and the radiation technique (2D CRT, 3D CRT, IMRT) and dose (< 72 Gy or > 72 Gy) appeared to be significant factors of hearing deterioration via bone and air conduction. Five years after RT completion, deterioration of bone and air conduction thresholds was inferior in IMRT compared to 2D and 3D CRT. Additionally, when the primary tumor was irradiated with a prescription dose > 72 Gy, the deterioration in hearing threshold was higher. Yip et al. investigated the role of IMRT doses and cisplatin use on SNHL for 156 ears¹¹⁹. They found that every 10 Gy increase in cochlea/inner ear mean dose translated into 6 dB/5 dB ($p=0.014/p=0.031$) hearing threshold changes. They observed severe (≥ 30 dB) late high-frequency SNHL in the chemoradiotherapy group for cochlear doses of 40 Gy (14%) and 44 Gy (25%) and concluded that the cochlear dose should be kept as low as possible, especially with administration of cisplatin. In the presented feasibility analysis, the use of a 10 Gy GK boost enabled an average cochlea sparing of 3.8% in the sum plan which, according the aforementioned studies, could already account for some dB.

Similar to the parotids and cochleae, the TMJs are often included in the irradiation field. A side-effect of excessive radiation exposure which can be found in 5–17% of the patient is trismus¹²⁰. It restricts jaw motion and mouth opening and can deteriorate nutritional intake and oral hygiene in severe cases. The radiation field and dose were linked to the severity of radiation-induced trismus^{121, 122}. Wu et al. assessed the TMJs characteristics of 114 NPC patients four years after completion of radiotherapy and found that the mean TMJ dose for patients with trismus was significantly higher than for patients without trismus ($p=0.017$). For the patients in this feasibility analysis, the TMJ

dose constraint was exceeded for one side and two patients. In one case, one TMJ was abutting the boost volume and the GK boost plan enabled a dose sparing in the sum plan of 2.5% compared to the LINAC sum plan. For the other patient, however, the TMJ was intersecting with the boost volume so that the higher degree of inhomogeneity with the GK resulted in 1.4% higher dose compared to the LINAC sum plan. Nevertheless, across all patients GK boost plans enabled total dose reductions of almost 3% in the sum plans.

The remaining analyzed OAR—namely pituitary gland, optic chiasm, brainstem and spinal cord—were not included in radiation fields, but located in close proximity to the PTV60 and/or boost field for some patients. The pituitary gland and optic chiasm are located in cranial direction above the treatment field. When comparing the boost plans, it was apparent that for some patients with low dose exposure to these OAR, LINAC plans resulted in a better sparing compared to GK. This can be due to the fact that if the distance between the target volume and pituitary/chiasm is large enough, LINAC plans can make use of the LINAC MLC to appropriately bar these structures from the treatment field. With GK, however, the radiation strikes from 192 directions to enable such sharp gradients, making it technically impossible to shield organs from the treatment field. The resulting GK boost doses, however, are still very low and resulted in neglectable differences in the sum plans (optic chiasm 0%, 0 Gy; pituitary gland 1.9%, 0.7 Gy) across all patients. Despite these two organs often being further away from the treatment field, the dose to the pituitary gland should be kept reasonably low to avoid dose-dependent complications such as radiation-induced hypopituitarism ¹²³. As for the optic chiasm, the reached $D_{0.035\text{ cc}}$ were far from the critical threshold resulting in complications as radiation-induced optic neuropathy (RION). Zhang et al. even tried loosening the constraints of neuro-optic structures for patients with T4 NPC treated with IMRT to improve tumor control ¹²⁴. In the two groups ($D_{2\%} > 55\text{ Gy}$ and $D_{2\%} < 55\text{ Gy}$) they found no significant difference in five-year OS nor in the incidence of RION up to a cut-off dose of 70.77 Gy. Additionally, no patient developed severe RION. Consequently, the chiasm doses should still be watched but dose restrictions could be carefully loosened to increase target coverage. In this analysis, brainstem dose constraints were marginally exceeded once and dose reduction with GK boost was in the order of 3.0%. Radiation-induced brainstem injury and brainstem necrosis are rare conditions occurring after radiotherapy of NPC ¹²⁵. Huang et al. assessed the

evolution of radiation-induced brainstem injury after IMRT for NPC with the aim of identifying dosimetric predictors for this side effect ¹²⁶. They found brainstem injury in 24 out of 6288 patients and concluded, that those whose brainstem maximum dose was > 67.4 Gy were more likely to develop the condition. Finally, for one patient, the spinal cord dose was close to the constraint. Considering all patients it was 1.7% (sum) lower with GK boost.

4.3.3 SRT for NPC

The points discussed in 4.3.1 and 4.3.2 show that intermediate imaging and adaptation of treatment plans could benefit the target coverage and OAR sparing for NPC patients. Additionally, in this work the improved GK dose gradients mostly resulted in better sparing of the healthy structures adjacent to and outside of the boost volume, but the extent and location of hotspots inside the target volume need to be evaluated carefully in order to not harm sensitive osseous, nervous or mucous structures. Hence, by combining replanning and GK boost using a more homogenous version of Lightning, gross tumor treatment with better OAR sparing could be performed. The higher degree of inhomogeneity with the prototype version compared to the LINAC version could even be used as dose intensification to increase TCP if the hotspots are adequately positioned.

In the past, the combination of SRT boost following EBRT for NPC has already been investigated and researchers mostly reported excellent LC rates with acceptable late toxicity ¹²⁷⁻¹³⁰. Hara et al. treated 82 NPC patients with SRT after EBRT. The EBRT dose was 66 Gy delivered in 2 Gy/fractions (5 fractions/week) ¹²⁷. SRT boost was delivered with either conventional LINAC with stereotactic head fixation or with CK. The single fraction boost of 7–15 Gy was delivered 2–6 weeks after EBRT. They reported 98% of the patients to be free from local progression but also stated a 12% risk of developing temporal lobe necrosis especially in patients with T4 tumors. The authors emphasized that adequate fractionated boost strategy, homogeneity and target delineation should be determined for both EBRT and the following SRT boost. Because of its good LC rates SRT has also been widely used for the treatment of recurrent NPC after EBRT ^{131, 132}. For these kinds of tumors reirradiation is especially challenging since OAR were already exposed to an amount of radiation dose at the time of initial

radiotherapy treatment, meaning that toxicities are likely to occur. With SRT, the radiation dose to the recurrent gross tumor can be escalated while keeping the dose to the OAR as low as possible. In 2018, Díaz-Martínez et al. published a study on GK boost for sinonasal malignancies (SNMs) and NPCs following chemoradiotherapy¹³³. The authors clinically incorporated a GK boost as an additional modality for selected SNMs and NPCs with the aim of improving LC and ultimately survival. Nine patients (n=5 SNMs, n=4 NPCs) were treated between 2014 and 2017 using the GK boost after IMRT treatment. The mean PTV dose was 64.3 Gy (range: 54–70 Gy) delivered in 2 Gy/fraction with or without SIB and the time between completion of IMRT and start of GK boost was in median 2.2 months (range: 1–4 months). The patients qualifying for GK SRS boost typically presented intracranial tumor extension where IMRT delivery of the full prescription dose would have exceeded optic pathways tolerance doses. Consequently, 54–60 Gy were delivered to the cavernous sinus and, after four weeks (for n=8 patients), the single fraction GK boost was delivered with a median dose of 13 Gy (range: 12–20 Gy) and a median prescription IDL of 50%. For all patients, LC was achieved at the time of last follow-up (median follow-up time: 13.3 months, range: 4–32 months) and three patients experienced failure outside of the PTV (n=1 NPC, n=2 SNM). Across all patients, no acute grade 3–5 toxicity was observed although one patient experienced late grade 4 toxicity, which can be attributed to irradiation. The NPC patients (maximum target volume: 5.55 cc) experienced grade 1 (n=3) and grade 2 (n=1) toxicities. Since GK model Perfexion was used, FSRT—which might have decreased the toxicity—was not possible. Other limitations of their study included the short follow-up period not accounting for late complications (e. g. temporal lobe necrosis) or recurrence and the heterogeneous and restricted number of patients.

4.3.4 Limitations and future challenges

Besides the restricted patient cohort, the presented work had other limitations. First, because of the retrospective nature of the analysis, patient positioning using the GK setup had to be estimated with the available LINAC imaging. Even though this was performed by an experienced MTRA, real-time positioning with the adequate GK positioning aids would have been more accurate and would potentially have resulted in the inclusion of more patients. In fact, as opposed to LINAC setup, the cushions used for GK are customized and the shoulder position can be adjusted in a caudal direction

according to patients' comfort, so that patient positioning can be tailored to the GK geometry. Second, four out of the five patients had only the initial dataset as base for boost treatment planning. With intermediate imaging, volume reduction and displacements in tumor and OAR could have been identified. Consequently, with reduced target volume, the BOT restriction would impact the optimization less and more distance between target and critical structures would be favorable for OAR doses. Another limitation of the study is the comparison of treatment plans generated by two algorithms with different accuracies. As mentioned previously, convolution tends to overestimate the dose deposition in bones and underestimate the dose deposition in air compared to Monte Carlo ⁷⁴. Even though convolution is fast enough for clinical use and shows a clinically acceptable precision in heterogeneous medium, the superiority of Monte Carlo must be considered in this comparison.

Adequate patient selection for replanning is one of the future challenges for using the GK as boost treatment after IMRT. Identifying patients that would benefit from replanning, however, is a common challenge in ART and calls for further research for NPC ^{104, 109}. Another important step is the determination of the adequate time for replanning. Although difficult, this setting is of crucial importance as repeated replanning might create additional work and cost but add no real value in terms of outcome or QoL. Similarly, defining a time frame between last IMRT and first GK fraction requires further research, as time periods strongly differ in literature. Next, the thermoplastic masks for patient fixation need to be reviewed for stability, as the boost volumes might extend in a more caudal direction than the brain lesions typically treated with the GK. With a number of OAR close to the boost volume, ensuring patient immobilization is crucial in order to leverage the full SRT potential. Finally, the question about the GK total dose and fractionation regimen arises. The patients of this analysis were replanned with 10 Gy in 2 Gy/fraction. Higher prescription doses to increase LC and hypofractionation as commonly used in SRT could be an option. Eventually, the potential of GK as up-front, single fraction boost instead of surgery before IMRT could be studied to reduce the primary GTV size.

Regardless of the limitations and the future challenges, this study—involving preliminary analysis of the clinically used treatment optimizer and its more homogeneous research version—showed that a combination of LINAC IMRT followed by GK boost for NPC is feasible and in most cases beneficial from a dosimetric point of view. In the future, the aforementioned challenges need to be addressed and more homogeneous

plans have to be created (new Lightning prototype version), which, combined with the favorable GK GI and the advantage of FSRT (GK Icon), can contribute to increased LC of NPC by adding treatment fractions as long as the biological OAR tolerances are not exceeded.

5 SUMMARY

Despite the globally low incidence of nasopharyngeal carcinoma (NPC), the treatment of this disease is challenging and radiotherapy often represents the most promising option. Although advances in imaging and radiation delivery techniques have significantly improved clinical outcomes, recurrences especially in high dose regions and acute and late toxicities remain one of the major concerns. In order to improve local control and reduce the dose to the surrounding healthy tissues, stereotactic radiotherapy (SRT) to the gross tumor in addition to the primary irradiation has been used with promising results. In the past, the most common SRT devices that have been used for this purpose were linear accelerators (LINACs) which, especially with the advent of intensity modulated radiotherapy (IMRT), deliver dose to the tumor with a rapid dose fall-off at its edges. The Leksell Gamma Knife (GK), however, is characterized by an even sharper dose gradient resulting in improved sparing of organs at risk (OAR). The aim of this work was to retrospectively evaluate the feasibility and dosimetric advantage of a fractionated, inversely planned GK boost to the gross tumor after previous LINAC IMRT treatment of the extended tumor volume. Only one related article could be found in the available literature and (unlike this work) the corresponding study used single fraction stereotactic GK treatment several weeks after primary irradiation on four NPC, without using inverse planning or dosimetric comparison of devices.

The first part of this work aimed at assessing the benefit of the newly available inverse treatment planning optimizer for GK compared to manual forward planning. For this purpose, a pre-release version was provided by the manufacturer and the plan quality and efficiency of forward and inverse treatment plans for different medical conditions were compared. Additionally, an inter-operator-variability analysis was conducted to assess the effect different operators have on the optimization. The results showed that the use of inverse planning with GK improves the plan quality especially for the studied benign medical conditions (acoustic neuromas, meningiomas) with OAR involvement. For the aforementioned tumors with nearby critical structures, using inverse planning resulted in increased target coverage (up to 3.6%) due to the possibility of limiting OAR doses, and dose gradients were improved (up to 18.1%). Additionally, for all studied medical conditions the optimizer drastically reduced the time needed for treatment

planning, and low variability between the user dependent plans even for novice users was observed.

The second part of the presented work dealt with the degree of homogeneity and OAR sparing that can be achieved with a more homogenous prototype version of the clinical treatment planning system, featuring the inverse treatment optimizer from the first analysis. A higher degree of homogeneity was shown to be necessary for target volumes involving or abutting radiosensitive structures such as cranial/ facial nerves, cochleae or optical pathways. The degree of homogeneity and OAR sparing for different medical conditions (acoustic neuromas, pituitary adenomas, meningiomas) that can be achieved with LINAC and three GK plans was compared. One GK plan was calculated using the limitations of the current clinical version, while the others aimed at either improving the OAR sparing or the homogeneity. In general, all GK plans showed inferior homogeneity (prototype: 14.8%; clinical: 25%) but improved dose fall-off (prototype: 48%; clinical: 52%) and OAR doses ($\geq 6.5\%$) compared to LINAC plans. In cases with OAR crossing the target volume, the homogenous GK plans, despite being characterized by higher inhomogeneity compared to the LINAC plans, resulted in similar OAR doses and improved dose gradients. Consequently, this more homogenous prototype version can be used for enhanced sparing of radiosensitive structures inside or abutting the target volumes, which was crucial for the third and last part of this work.

As NPC are known to be abutting or involving critical tissues such as cranial nerves, osseous and mucous structures, hotspots within the boost volume need to be controlled. LINAC and GK boost plans using the more homogenous prototype version were calculated, and the target homogeneity and OAR sparing were assessed on a restricted patient cohort, which was linked to the low incidence of NPC and anatomical reasons. In many cases, the volume targeted during primary LINAC irradiation comprised a number of OAR whose planning constraints were already exceeded. For the delineated critical structures, the GK boost showed a dosimetric benefit over LINAC boost for the parotids (up to 36% reduction), cochleae (up to 35.8% reduction), temporomandibular joints (up to 26.1% reduction), brainstem (up to 17.6% reduction) and spinal cord (up to 18% reduction). The dose inhomogeneity with the GK boost plan, however, was shown to be higher (boost: 19.7%; base + boost: 1.9%), but the location and extent of the hotspots were judged uncritical.

Overall, the initial question about the feasibility and dosimetric advantage of GK boost treatment for NPC following primary radiotherapy with LINACs was demonstrated. With

intermediate imaging and plan adaptation, a combination of primary radiotherapy and fractionated, homogenous GK boost could be clinically used for dose intensification considering biological OAR constraints in order to yield better outcomes.

6 BIBLIOGRAPHY

1. Krebsinformationsdienst: Krebsstatistiken: So häufig ist Krebs in Deutschland. <https://www.krebsinformationsdienst.de/tumorarten/grundlagen/krebsstatistiken.php>. Retrieved February 17th.
2. W.H.O.: Cancer, 2022. <https://www.who.int/news-room/fact-sheets/detail/cancer>. Retrieved March 3rd.
3. ASCO: Head and Neck Cancer: Statistics, 2022. <https://www.cancer.net/cancer-types/head-and-neck-cancer/statistics>. Retrieved March 3rd.
4. Alfouzan, AF: Radiation therapy in head and neck cancer. *Saudi Med J*, 42: 247-254, 2021. <https://doi.org/10.15537/smj.2021.42.3.20210660>
5. Perri, F, Della Vittoria Scarpati, G, Caponigro, F, Ionna, F, Longo, F, Buonopane, S, Muto, P, Di Marzo, M, Pisconti, S, Solla, R: Management of recurrent nasopharyngeal carcinoma: current perspectives. *Onco Targets Ther*, 12: 1583-1591, 2019. <https://doi.org/10.2147/OTT.S188148>
6. Tsao, SW, Yip, YL, Tsang, CM, Pang, PS, Lau, VM, Zhang, G, Lo, KW: Etiological factors of nasopharyngeal carcinoma. *Oral Oncol*, 50: 330-338, 2014. <https://doi.org/10.1016/j.oraloncology.2014.02.006>
7. Chua, MLK, Wee, JTS, Hui, EP, Chan, ATC: Nasopharyngeal carcinoma. *Lancet*, 387: 1012-1024, 2016. [https://doi.org/10.1016/S0140-6736\(15\)00055-0](https://doi.org/10.1016/S0140-6736(15)00055-0)
8. Tseng, M, Ho, F, Leong, YH, Wong, LC, Tham, IW, Cheo, T, Lee, AW: Emerging radiotherapy technologies and trends in nasopharyngeal cancer. *Cancer Commun (Lond)*, 40: 395-405, 2020. <https://doi.org/10.1002/cac2.12082>
9. ASCO: Head and Neck Cancer: Types of Treatment, 2022. <https://www.cancer.net/cancer-types/head-and-neck-cancer/types-treatment>. Retrieved March 5th.
10. Rosen, RD, Sapra, A: TNM Classification. In: *StatPearls*. Treasure Island (FL), 2023.
11. Niu, X, Xue, F, Liu, P, Hu, C, He, X: Long-term outcomes of nasopharyngeal carcinoma patients with T1-2 stage in intensity-modulated radiotherapy era. *Int J Med Sci*, 19: 267-273, 2022. <https://doi.org/10.7150/ijms.68394>
12. Kong, F, Zhou, J, Du, C, He, X, Kong, L, Hu, C, Ying, H: Long-term survival and late complications of intensity-modulated radiotherapy for recurrent nasopharyngeal carcinoma. *BMC Cancer*, 18: 1139, 2018. <https://doi.org/10.1186/s12885-018-5055-5>
13. Chen, YP, Chan, ATC, Le, QT, Blanchard, P, Sun, Y, Ma, J: Nasopharyngeal carcinoma. *Lancet*, 394: 64-80, 2019. [https://doi.org/10.1016/S0140-6736\(19\)30956-0](https://doi.org/10.1016/S0140-6736(19)30956-0)
14. Kirthi Koushik, AS, Harish, K, Avinash, HU: Principles of radiation oncology: a beams eye view for a surgeon. *Indian J Surg Oncol*, 4: 255-262, 2013. <https://doi.org/10.1007/s13193-013-0231-1>
15. Nourollahi, S, Ghate, A, Kim, M: Optimal modality selection in external beam radiotherapy. *Math Med Biol*, 36: 361-380, 2019. <https://doi.org/10.1093/imammb/dqy013>
16. Longobardi, B, De Martin, E, Fiorino, C, Dell'oca, I, Broggi, S, Cattaneo, GM, Calandrino, R: Comparing 3DCRT and inversely optimized IMRT planning for head and neck cancer: equivalence between step-and-shoot and sliding window

- techniques. *Radiother Oncol*, 77: 148-156, 2005. <https://doi.org/10.1016/j.radonc.2005.09.011>
17. Ding, M, Newman, F, Chen, C, Stuhr, K, Gaspar, LE: Dosimetric comparison between 3DCRT and IMRT using different multileaf collimators in the treatment of brain tumors. *Med Dosim*, 34: 1-8, 2009. <https://doi.org/10.1016/j.meddos.2007.04.001>
 18. Osborn, J: Is VMAT beneficial for patients undergoing radiotherapy to the head and neck? *Radiography (Lond)*, 23: 73-76, 2017. <https://doi.org/10.1016/j.radi.2016.08.008>
 19. Ghemis, DM, Marcu, LG: Progress and prospects of flattening filter free beam technology in radiosurgery and stereotactic body radiotherapy. *Crit Rev Oncol Hematol*, 163: 103396, 2021. <https://doi.org/10.1016/j.critrevonc.2021.103396>
 20. Dang, TM, Peters, MJ, Hickey, B, Semciw, A: Efficacy of flattening-filter-free beam in stereotactic body radiation therapy planning and treatment: A systematic review with meta-analysis. *J Med Imaging Radiat Oncol*, 61: 379-387, 2017. <https://doi.org/10.1111/1754-9485.12583>
 21. Yao, CH, Chang, TH, Lin, CC, Lai, YC, Chen, CH, Chang, YJ: Three-dimensional dose comparison of flattening filter (FF) and flattening filter-free (FFF) radiation therapy by using NIPAM gel dosimetry. *PLoS One*, 14: e0212546, 2019. <https://doi.org/10.1371/journal.pone.0212546>
 22. Leksell, L: Stereotactic radiosurgery. *J Neurol Neurosurg Psychiatry*, 46: 797-803, 1983. <https://doi.org/10.1136/jnnp.46.9.797>
 23. Fallows, P, Wright, G, Harrold, N, Bownes, P: A comparison of the convolution and TMR10 treatment planning algorithms for Gamma Knife((R)) radiosurgery. *J Radiosurg SBRT*, 5: 157-167, 2018.
 24. Han, EY, Wang, H, Luo, D, Li, J, Wang, X: Dosimetric comparison of fractionated radiosurgery plans using frameless Gamma Knife ICON and CyberKnife systems with linear accelerator-based radiosurgery plans for multiple large brain metastases. *J Neurosurg*, 132: 1473-1479, 2019. <https://doi.org/10.3171/2019.1.JNS182769>
 25. Liu, H, Andrews, DW, Evans, JJ, Werner-Wasik, M, Yu, Y, Dicker, AP, Shi, W: Plan Quality and Treatment Efficiency for Radiosurgery to Multiple Brain Metastases: Non-Coplanar RapidArc vs. Gamma Knife. *Front Oncol*, 6: 26, 2016. <https://doi.org/10.3389/fonc.2016.00026>
 26. Schelin, ME, Liu, H, Ali, A, Shi, W, Yu, Y, Mooney, KE: Dosimetric comparison of Gamma Knife(R) Icon(TM) and linear accelerator-based fractionated stereotactic radiotherapy (FSRT) plans for the re-irradiation of large (>14 cm(3)) recurrent glioblastomas. *J Radiosurg SBRT*, 7: 233-243, 2021.
 27. Braunstein, S, Ma, L: Stereotactic radiosurgery for vestibular schwannomas. *Cancer Manag Res*, 10: 3733-3740, 2018. <https://doi.org/10.2147/CMAR.S140764>
 28. Johnson, PB, Monterroso, MI, Yang, F, Mellon, E: Optimization of the prescription isodose line for Gamma Knife radiosurgery using the shot within shot technique. *Radiat Oncol*, 12: 187, 2017. <https://doi.org/10.1186/s13014-017-0919-4>
 29. Chung, HT, Park, WY, Kim, TH, Kim, YK, Chun, KJ: Assessment of the accuracy and stability of frameless gamma knife radiosurgery. *J Appl Clin Med Phys*, 19: 148-154, 2018. <https://doi.org/10.1002/acm2.12365>
 30. Mack, A, Czempiel, H, Kreiner, HJ, Durr, G, Wowra, B: Quality assurance in stereotactic space. A system test for verifying the accuracy of aim in radiosurgery. *Med Phys*, 29: 561-568, 2002. <https://doi.org/10.1118/1.1463062>

31. Kutuk, T, Kotecha, R, Tolakanahalli, R, Wieczorek, DJJ, Lee, YC, Ahluwalia, MS, Hall, MD, McDermott, MW, Appel, H, Gutierrez, AN, Mehta, MP, Tom, MC: Zero Setup Margin Mask versus Frame Immobilization during Gamma Knife((R)) Icon Stereotactic Radiosurgery for Brain Metastases. *Cancers (Basel)*, 14, 2022. <https://doi.org/10.3390/cancers14143392>
32. Desai, R, Rich, KM: Therapeutic Role of Gamma Knife Stereotactic Radiosurgery in Neuro-Oncology. *Mo Med*, 117: 33-38, 2020.
33. Rojas-Villabona, A, Kitchen, N, Paddick, I: Investigation of dosimetric differences between the TMR 10 and convolution algorithm for Gamma Knife stereotactic radiosurgery. *J Appl Clin Med Phys*, 17: 217-229, 2016. <https://doi.org/10.1120/jacmp.v17i6.6347>
34. Logothetis, A, Pantelis, E, Zoros, E, Pappas, EP, Dimitriadis, A, Paddick, I, Garding, J, Johansson, J, Kollias, G, Karaiskos, P: Dosimetric evaluation of the Leksell GammaPlan() Convolution dose calculation algorithm. *Phys Med Biol*, 65: 045011, 2020. <https://doi.org/10.1088/1361-6560/ab64b7>
35. Nakazawa, H, Komori, M, Shibamoto, Y, Tsugawa, T, Mori, Y, Kobayashi, T: Dosimetric comparison of absolute and relative dose distributions between tissue maximum ratio and convolution algorithms for acoustic neurinoma plans in Gamma Knife radiosurgery. *Acta Neurochir (Wien)*, 156: 1483-1489; discussion 1489, 2014. <https://doi.org/10.1007/s00701-014-2143-4>
36. Pantelis, E, Logothetis, A, Zoros, E, Pappas, EP, Papagiannis, P, Paddick, I, Nordstrom, H, Kollias, G, Karaiskos, P: Dosimetric accuracy of the Convolution algorithm for Leksell Gamma Plan radiosurgery treatment planning: Evaluation in the presence of clinically relevant inhomogeneities. *J Appl Clin Med Phys*: e13903, 2023. <https://doi.org/10.1002/acm2.13903>
37. Petti, PL, Rivard, MJ, Alvarez, PE, Bednarz, G, Daniel Bourland, J, DeWerd, LA, Drzymala, RE, Johansson, J, Kunugi, K, Ma, L, Meltsner, SG, Neyman, G, Seuntjens, JP, Shiu, AS, Goetsch, SJ: Recommendations on the practice of calibration, dosimetry, and quality assurance for gamma stereotactic radiosurgery: Report of AAPM Task Group 178. *Med Phys*, 48: e733-e770, 2021. <https://doi.org/10.1002/mp.14831>
38. Elekta Instrument, A: *Leksell GammaPlan Online Reference Manual*, 2015.
39. Schlegel, W, Kneschaurek, P: [Inverse radiotherapy planning]. *Strahlenther Onkol*, 175: 197-207, 1999. <https://doi.org/10.1007/BF02742396>
40. Ng, WT, Chow, JCH, Beitler, JJ, Corry, J, Mendenhall, W, Lee, AWM, Robbins, KT, Nuyts, S, Saba, NF, Smee, R, Stokes, WA, Stojan, P, Ferlito, A: Current Radiotherapy Considerations for Nasopharyngeal Carcinoma. *Cancers (Basel)*, 14, 2022. <https://doi.org/10.3390/cancers14235773>
41. Ho, FC, Tham, IW, Earnest, A, Lee, KM, Lu, JJ: Patterns of regional lymph node metastasis of nasopharyngeal carcinoma: a meta-analysis of clinical evidence. *BMC Cancer*, 12: 98, 2012. <https://doi.org/10.1186/1471-2407-12-98>
42. Lee, AW, Ng, WT, Pan, JJ, Poh, SS, Ahn, YC, AlHussain, H, Corry, J, Grau, C, Gregoire, V, Harrington, KJ, Hu, CS, Kwong, DL, Langendijk, JA, Le, QT, Lee, NY, Lin, JC, Lu, TX, Mendenhall, WM, O'Sullivan, B, Ozyar, E, Peters, LJ, Rosenthal, DI, Soong, YL, Tao, Y, Yom, SS, Wee, JT: International guideline for the delineation of the clinical target volumes (CTV) for nasopharyngeal carcinoma. *Radiother Oncol*, 126: 25-36, 2018. <https://doi.org/10.1016/j.radonc.2017.10.032>

43. Gregoire, V, Ng, WT: Special section on intensity-modulated radiation therapy for head and neck cancer (IMRT). *Oral Oncol*, 88: 49-50, 2019. <https://doi.org/10.1016/j.oraloncology.2018.11.018>
44. Tham, IW, Hee, SW, Yeo, RM, Salleh, PB, Lee, J, Tan, TW, Fong, KW, Chua, ET, Wee, JT: Treatment of nasopharyngeal carcinoma using intensity-modulated radiotherapy-the national cancer centre singapore experience. *Int J Radiat Oncol Biol Phys*, 75: 1481-1486, 2009. <https://doi.org/10.1016/j.ijrobp.2009.01.018>
45. Au, KH, Ngan, RKC, Ng, AWY, Poon, DMC, Ng, WT, Yuen, KT, Lee, VHF, Tung, SY, Chan, ATC, Sze, HCK, Cheng, ACK, Lee, AWM, Kwong, DLW, Tam, AHP: Treatment outcomes of nasopharyngeal carcinoma in modern era after intensity modulated radiotherapy (IMRT) in Hong Kong: A report of 3328 patients (HKNPCSG 1301 study). *Oral Oncol*, 77: 16-21, 2018. <https://doi.org/10.1016/j.oraloncology.2017.12.004>
46. Fang, FM, Chien, CY, Tsai, WL, Chen, HC, Hsu, HC, Lui, CC, Huang, TL, Huang, HY: Quality of life and survival outcome for patients with nasopharyngeal carcinoma receiving three-dimensional conformal radiotherapy vs. intensity-modulated radiotherapy-a longitudinal study. *Int J Radiat Oncol Biol Phys*, 72: 356-364, 2008. <https://doi.org/10.1016/j.ijrobp.2007.12.054>
47. Luo, MS, Huang, GJ, Liu, HB: Oncologic outcomes of IMRT versus CRT for nasopharyngeal carcinoma: A meta-analysis. *Medicine (Baltimore)*, 98: e15951, 2019. <https://doi.org/10.1097/MD.00000000000015951>
48. Leong, YH, Soon, YY, Lee, KM, Wong, LC, Tham, IWK, Ho, FCH: Long-term outcomes after reirradiation in nasopharyngeal carcinoma with intensity-modulated radiotherapy: A meta-analysis. *Head Neck*, 40: 622-631, 2018. <https://doi.org/10.1002/hed.24993>
49. Huang, TL, Chien, CY, Tsai, WL, Liao, KC, Chou, SY, Lin, HC, Dean Luo, S, Lee, TF, Lee, CH, Fang, FM: Long-term late toxicities and quality of life for survivors of nasopharyngeal carcinoma treated with intensity-modulated radiotherapy versus non-intensity-modulated radiotherapy. *Head Neck*, 38 Suppl 1: E1026-1032, 2016. <https://doi.org/10.1002/hed.24150>
50. Ng, WT, Lee, MC, Hung, WM, Choi, CW, Lee, KC, Chan, OS, Lee, AW: Clinical outcomes and patterns of failure after intensity-modulated radiotherapy for nasopharyngeal carcinoma. *Int J Radiat Oncol Biol Phys*, 79: 420-428, 2011. <https://doi.org/10.1016/j.ijrobp.2009.11.024>
51. Li, JX, Huang, SM, Jiang, XH, Ouyang, B, Han, F, Liu, S, Wen, BX, Lu, TX: Local failure patterns for patients with nasopharyngeal carcinoma after intensity-modulated radiotherapy. *Radiat Oncol*, 9: 87, 2014. <https://doi.org/10.1186/1748-717X-9-87>
52. Kong, L, Wang, L, Shen, C, Hu, C, Wang, L, Lu, JJ: Salvage Intensity-Modulated Radiation Therapy (IMRT) for Locally Recurrent Nasopharyngeal Cancer after Definitive IMRT: A Novel Scenario of the Modern Era. *Sci Rep*, 6: 32883, 2016. <https://doi.org/10.1038/srep32883>
53. Bakst, RL, Lee, N, Pfister, DG, Zelefsky, MJ, Hunt, MA, Kraus, DH, Wolden, SL: Hypofractionated dose-painting intensity modulated radiation therapy with chemotherapy for nasopharyngeal carcinoma: a prospective trial. *Int J Radiat Oncol Biol Phys*, 80: 148-153, 2011. <https://doi.org/10.1016/j.ijrobp.2010.01.026>
54. Kwong, DL, Sham, JS, Leung, LH, Cheng, AC, Ng, WM, Kwong, PW, Lui, WM, Yau, CC, Wu, PM, Wei, W, Au, G: Preliminary results of radiation dose

- escalation for locally advanced nasopharyngeal carcinoma. *Int J Radiat Oncol Biol Phys*, 64: 374-381, 2006. <https://doi.org/10.1016/j.ijrobp.2005.07.968>
55. Woods, K, Lee, P, Kaprealian, T, Yang, I, Sheng, K: Cochlea-sparing acoustic neuroma treatment with 4pi radiation therapy. *Adv Radiat Oncol*, 3: 100-107, 2018. <https://doi.org/10.1016/j.adro.2018.01.004>
 56. Yang, I, Sughrue, ME, Han, SJ, Fang, S, Aranda, D, Cheung, SW, Pitts, LH, Parsa, AT: Facial nerve preservation after vestibular schwannoma Gamma Knife radiosurgery. *J Neurooncol*, 93: 41-48, 2009. <https://doi.org/10.1007/s11060-009-9842-3>
 57. Fang, C, Zhong, Y, Chen, T, Li, D, Li, C, Qi, X, Zhu, J, Wang, R, Zhu, J, Wang, S, Ruan, Y, Zhou, M: Impairment mechanism of nasal mucosa after radiotherapy for nasopharyngeal carcinoma. *Front Oncol*, 12: 1010131, 2022. <https://doi.org/10.3389/fonc.2022.1010131>
 58. Bar, W, Schwarz, M, Alber, M, Bos, LJ, Mijnheer, BJ, Rasch, C, Schneider, C, Nusslin, F, Damen, EM: A comparison of forward and inverse treatment planning for intensity-modulated radiotherapy of head and neck cancer. *Radiother Oncol*, 69: 251-258, 2003. <https://doi.org/10.1016/j.radonc.2003.08.002>
 59. Nasr, A, Habash, A: Dosimetric analytic comparison of inverse and forward planned IMRT techniques in the treatment of head and neck cancer. *J Egypt Natl Canc Inst*, 26: 119-125, 2014. <https://doi.org/10.1016/j.jnci.2014.03.004>
 60. Levivier, M, Carrillo, RE, Charrier, R, Martin, A, Thiran, JP: A real-time optimal inverse planning for Gamma Knife radiosurgery by convex optimization: description of the system and first dosimetry data. *J Neurosurg*, 129: 111-117, 2018. <https://doi.org/10.3171/2018.7.GKS181572>
 61. Sjolund, J, Riad, S, Hennix, M, Nordstrom, H: A linear programming approach to inverse planning in Gamma Knife radiosurgery. *Med Phys*, 46: 1533-1544, 2019. <https://doi.org/10.1002/mp.13440>
 62. Shepard, DM, Chin, LS, DiBiase, SJ, Naqvi, SA, Lim, J, Ferris, MC: Clinical implementation of an automated planning system for gamma knife radiosurgery. *Int J Radiat Oncol Biol Phys*, 56: 1488-1494, 2003. [https://doi.org/10.1016/s0360-3016\(03\)00440-1](https://doi.org/10.1016/s0360-3016(03)00440-1)
 63. Ghobadi, K, Ghaffari, HR, Aleman, DM, Jaffray, DA, Ruschin, M: Automated treatment planning for a dedicated multi-source intracranial radiosurgery treatment unit using projected gradient and grassfire algorithms. *Med Phys*, 39: 3134-3141, 2012. <https://doi.org/10.1118/1.4709603>
 64. Minniti, G, Osti, MF, Niyazi, M: Target delineation and optimal radiosurgical dose for pituitary tumors. *Radiat Oncol*, 11: 135, 2016. <https://doi.org/10.1186/s13014-016-0710-y>
 65. Combs, SE, Baumert, BG, Bendszus, M, Bozzao, A, Brada, M, Fariselli, L, Fiorentino, A, Ganswindt, U, Grosu, AL, Lagerwaard, FL, Niyazi, M, Nyholm, T, Paddick, I, Weber, DC, Belka, C, Minniti, G: ESTRO ACROP guideline for target volume delineation of skull base tumors. *Radiother Oncol*, 156: 80-94, 2021. <https://doi.org/10.1016/j.radonc.2020.11.014>
 66. Grimm, MA, Koppen, U, Stieler, F, Welzel, G, Ruder, AM, Polednik, M, Wenz, F, Mai, SK, Giordano, FA: Prospective assessment of mask versus frame fixation during Gamma Knife treatment for brain metastases. *Radiother Oncol*, 147: 195-199, 2020. <https://doi.org/10.1016/j.radonc.2020.05.011>
 67. Yi, J, Huang, X, Gao, L, Luo, J, Zhang, S, Wang, K, Qu, Y, Xiao, J, Xu, G: Intensity-modulated radiotherapy with simultaneous integrated boost for locoregionally

- advanced nasopharyngeal carcinoma. *Radiat Oncol*, 9: 56, 2014. <https://doi.org/10.1186/1748-717X-9-56>
68. Tripathi, M, Kumar, N, Mukherjee, KK: Pushing the limits of the Leksell stereotactic frame for spinal lesions up to C3: fixation at the maxilla. *Acta Neurochir (Wien)*, 158: 1691-1695, 2016. <https://doi.org/10.1007/s00701-016-2878-1>
 69. Tonetti, D, Bhatnagar, J, Lunsford, LD: Quantitative analysis of movement of a cervical target during stereotactic radiosurgery using the Leksell Gamma Knife Perfexion. *J Neurosurg*, 117 Suppl: 211-216, 2012. <https://doi.org/10.3171/2012.3.GKS1266>
 70. Tuleasca, C, Broome, M, Mosimann, PJ, Schiappacasse, L, Zeverino, M, Dorenlot, A, Champoudry, J, Regis, J, Levivier, M: Jaw Immobilization for Gamma Knife Surgery in Patients with Mandibular Lesions: A Newly, Innovative Approach. *Stereotact Funct Neurosurg*, 94: 342-347, 2016. <https://doi.org/10.1159/000449065>
 71. Moon, HC, Lee, D, Min, BJ, Kim, YG, Dho, YS: Avoiding a Collision in Gamma Knife Radiosurgery : A Modified Mask Fixation Method. *J Korean Neurosurg Soc*, 2022. <https://doi.org/10.3340/jkns.2022.0164>
 72. Timmerman, R: A Story of Hypofractionation and the Table on the Wall. *Int J Radiat Oncol Biol Phys*, 112: 4-21, 2022. <https://doi.org/10.1016/j.ijrobp.2021.09.027>
 73. Sharma, S, Ott, J, Williams, J, Dickow, D: Dose calculation accuracy of the Monte Carlo algorithm for CyberKnife compared with other commercially available dose calculation algorithms. *Med Dosim*, 36: 347-350, 2011. <https://doi.org/10.1016/j.meddos.2010.09.001>
 74. Lee, BI, Boss, MK, LaRue, SM, Martin, T, Leary, D: Comparative study of the collapsed cone convolution and Monte Carlo algorithms for radiation therapy planning of canine sinonasal tumors reveals significant dosimetric differences. *Vet Radiol Ultrasound*, 63: 91-101, 2022. <https://doi.org/10.1111/vru.13039>
 75. Fotina, I, Winkler, P, Kunzler, T, Reiterer, J, Simmat, I, Georg, D: Advanced kernel methods vs. Monte Carlo-based dose calculation for high energy photon beams. *Radiother Oncol*, 93: 645-653, 2009. <https://doi.org/10.1016/j.radonc.2009.10.013>
 76. Krieger, T, Sauer, OA: Monte Carlo- versus pencil-beam-/collapsed-cone-dose calculation in a heterogeneous multi-layer phantom. *Phys Med Biol*, 50: 859-868, 2005. <https://doi.org/10.1088/0031-9155/50/5/010>
 77. Pokhrel, D, Bernard, ME, Knight, J, 2nd, St Clair, W, Fraser, JF: Clinical validation of novel lightning dose optimizer for gamma knife radiosurgery of irregular-shaped arteriovenous malformations and pituitary adenomas. *J Appl Clin Med Phys*, 23: e13669, 2022. <https://doi.org/10.1002/acm2.13669>
 78. Wiczorek, DJ, Kotecha, R, Hall, MD, Tom, MC, Davis, S, Ahluwalia, MS, McDermott, MW, Mehta, MP, Gutierrez, AN, Tolakanahalli, R: Systematic evaluation and plan quality assessment of the Leksell(R) gamma knife(R) lightning dose optimizer. *Med Dosim*, 47: 70-78, 2022. <https://doi.org/10.1016/j.meddos.2021.08.006>
 79. Alexander, E, 3rd, Moriarty, TM, Davis, RB, Wen, PY, Fine, HA, Black, PM, Kooy, HM, Loeffler, JS: Stereotactic radiosurgery for the definitive, noninvasive treatment of brain metastases. *J Natl Cancer Inst*, 87: 34-40, 1995. <https://doi.org/10.1093/jnci/87.1.34>
 80. Ma, L: Dependence of normal brain integral dose and normal tissue complication probability on the prescription isodose values for gamma-knife radiosurgery.

- Phys Med Biol*, 46: 3031-3041, 2001. <https://doi.org/10.1088/0031-9155/46/11/317>
81. Scoccianti, S, Detti, B, Gadda, D, Greto, D, Furfaro, I, Meacci, F, Simontacchi, G, Di Brina, L, Bonomo, P, Giacomelli, I, Meattini, I, Mangoni, M, Cappelli, S, Cassani, S, Talamonti, C, Bordi, L, Livi, L: Organs at risk in the brain and their dose-constraints in adults and in children: a radiation oncologist's guide for delineation in everyday practice. *Radiother Oncol*, 114: 230-238, 2015. <https://doi.org/10.1016/j.radonc.2015.01.016>
 82. Minniti, G, Amichetti, M, Enrici, RM: Radiotherapy and radiosurgery for benign skull base meningiomas. *Radiat Oncol*, 4: 42, 2009. <https://doi.org/10.1186/1748-717X-4-42>
 83. Paek, SH, Chung, HT, Jeong, SS, Park, CK, Kim, CY, Kim, JE, Kim, DG, Jung, HW: Hearing preservation after gamma knife stereotactic radiosurgery of vestibular schwannoma. *Cancer*, 104: 580-590, 2005. <https://doi.org/10.1002/cncr.21190>
 84. Coppa, ND, Raper, DM, Zhang, Y, Collins, BT, Harter, KW, Gagnon, GJ, Collins, SP, Jean, WC: Treatment of malignant tumors of the skull base with multi-session radiosurgery. *J Hematol Oncol*, 2: 16, 2009. <https://doi.org/10.1186/1756-8722-2-16>
 85. Mayo, C, Martel, MK, Marks, LB, Flickinger, J, Nam, J, Kirkpatrick, J: Radiation dose-volume effects of optic nerves and chiasm. *Int J Radiat Oncol Biol Phys*, 76: S28-35, 2010. <https://doi.org/10.1016/j.ijrobp.2009.07.1753>
 86. Plowman, PN, Doughty, D: Stereotactic radiosurgery, X: clinical isodosimetry of gamma knife versus linear accelerator X-knife for pituitary and acoustic tumours. *Clin Oncol (R Coll Radiol)*, 11: 321-329, 1999. <https://doi.org/10.1053/clon.1999.9074>
 87. Tian, Z, Yang, X, Giles, M, Wang, T, Gao, H, Butker, E, Liu, T, Kahn, S: A preliminary study on a multiresolution-level inverse planning approach for Gamma Knife radiosurgery. *Med Phys*, 47: 1523-1532, 2020. <https://doi.org/10.1002/mp.14078>
 88. Cui, T, Nie, K, Zhu, J, Danish, S, Weiner, J, Chundury, A, Ohri, N, Zhang, Y, Vergalasova, I, Yue, N, Wang, X: Clinical Evaluation of the Inverse Planning System Utilized in Gamma Knife Lightning. *Front Oncol*, 12: 832656, 2022. <https://doi.org/10.3389/fonc.2022.832656>
 89. Kataria, T, Sharma, K, Subramani, V, Karrthick, KP, Bisht, SS: Homogeneity Index: An objective tool for assessment of conformal radiation treatments. *J Med Phys*, 37: 207-213, 2012. <https://doi.org/10.4103/0971-6203.103606>
 90. Deasy, JO: Partial tumor boosts: even more attractive than theory predicts? *Int J Radiat Oncol Biol Phys*, 51: 279-280, 2001. [https://doi.org/10.1016/s0360-3016\(01\)01611-x](https://doi.org/10.1016/s0360-3016(01)01611-x)
 91. Tome, WA, Fowler, JF: Selective boosting of tumor subvolumes. *Int J Radiat Oncol Biol Phys*, 48: 593-599, 2000. [https://doi.org/10.1016/s0360-3016\(00\)00666-0](https://doi.org/10.1016/s0360-3016(00)00666-0)
 92. Craft, D, Khan, F, Young, M, Bortfeld, T: The Price of Target Dose Uniformity. *Int J Radiat Oncol Biol Phys*, 96: 913-914, 2016. <https://doi.org/10.1016/j.ijrobp.2016.07.033>
 93. Lambin, P, Leijenaar, RTH, Deist, TM, Peerlings, J, de Jong, EEC, van Timmeren, J, Sanduleanu, S, Larue, R, Even, AJG, Jochems, A, van Wijk, Y, Woodruff, H, van Soest, J, Lustberg, T, Roelofs, E, van Elmpt, W, Dekker, A, Mottaghy, FM, Wildberger, JE, Walsh, S: Radiomics: the bridge between medical imaging and

- personalized medicine. *Nat Rev Clin Oncol*, 14: 749-762, 2017. <https://doi.org/10.1038/nrclinonc.2017.141>
94. Bogowicz, M, Pavic, M, Riesterer, O, Finazzi, T, Garcia Schuler, H, Holz-Sapra, E, Rudofsky, L, Basler, L, Spaniol, M, Ambrusch, A, Hullner, M, Guckenberger, M, Tanadini-Lang, S: Targeting Treatment Resistance in Head and Neck Squamous Cell Carcinoma - Proof of Concept for CT Radiomics-Based Identification of Resistant Sub-Volumes. *Front Oncol*, 11: 664304, 2021. <https://doi.org/10.3389/fonc.2021.664304>
 95. Perks, JR, St George, EJ, El Hamri, K, Blackburn, P, Plowman, PN: Stereotactic radiosurgery XVI: Isodosimetric comparison of photon stereotactic radiosurgery techniques (gamma knife vs. micromultileaf collimator linear accelerator) for acoustic neuroma--and potential clinical importance. *Int J Radiat Oncol Biol Phys*, 57: 1450-1459, 2003. [https://doi.org/10.1016/s0360-3016\(03\)01580-3](https://doi.org/10.1016/s0360-3016(03)01580-3)
 96. Faramand, A, Kano, H, Niranjana, A, Johnson, SA, Hassib, M, Park, KJ, Arai, Y, Flickinger, JC, Lunsford, LD: Cranial nerve outcomes after primary stereotactic radiosurgery for symptomatic skull base meningiomas. *J Neurooncol*, 139: 341-348, 2018. <https://doi.org/10.1007/s11060-018-2866-9>
 97. Vergalasova, I, Liu, H, Alonso-Basanta, M, Dong, L, Li, J, Nie, K, Shi, W, Teo, BK, Yu, Y, Yue, NJ, Zou, W, Li, T: Multi-Institutional Dosimetric Evaluation of Modern Day Stereotactic Radiosurgery (SRS) Treatment Options for Multiple Brain Metastases. *Front Oncol*, 9: 483, 2019. <https://doi.org/10.3389/fonc.2019.00483>
 98. Wu, QR, Wessels, BW, Einstein, DB, Maciunas, RJ, Kim, EY, Kinsella, TJ: Quality of coverage: conformity measures for stereotactic radiosurgery. *J Appl Clin Med Phys*, 4: 374-381, 2003. <https://doi.org/10.1120/jacmp.v4i4.2506>
 99. Thomas, EM, Popple, RA, Wu, X, Clark, GM, Markert, JM, Guthrie, BL, Yuan, Y, Dobeilbower, MC, Spencer, SA, Fiveash, JB: Comparison of plan quality and delivery time between volumetric arc therapy (RapidArc) and Gamma Knife radiosurgery for multiple cranial metastases. *Neurosurgery*, 75: 409-417; discussion 417-408, 2014. <https://doi.org/10.1227/NEU.0000000000000448>
 100. Joshi, CP, Darko, J, Vidyasagar, PB, Schreiner, LJ: Dosimetry of interface region near closed air cavities for Co-60, 6 MV and 15 MV photon beams using Monte Carlo simulations. *J Med Phys*, 35: 73-80, 2010. <https://doi.org/10.4103/0971-6203.62197>
 101. Behrens, CF: Dose build-up behind air cavities for Co-60, 4, 6 and 8 MV. Measurements and Monte Carlo simulations. *Phys Med Biol*, 51: 5937-5950, 2006. <https://doi.org/10.1088/0031-9155/51/22/015>
 102. Li, XA, Yu, C, Holmes, T: A systematic evaluation of air cavity dose perturbation in megavoltage x-ray beams. *Med Phys*, 27: 1011-1017, 2000. <https://doi.org/10.1118/1.598966>
 103. Chen, AM, Daly, ME, Cui, J, Mathai, M, Benedict, S, Purdy, JA: Clinical outcomes among patients with head and neck cancer treated by intensity-modulated radiotherapy with and without adaptive replanning. *Head Neck*, 36: 1541-1546, 2014. <https://doi.org/10.1002/hed.23477>
 104. Bhide, SA, Davies, M, Burke, K, McNair, HA, Hansen, V, Barbachano, Y, El-Hariry, IA, Newbold, K, Harrington, KJ, Nutting, CM: Weekly volume and dosimetric changes during chemoradiotherapy with intensity-modulated radiation therapy for head and neck cancer: a prospective observational study. *Int J Radiat Oncol Biol Phys*, 76: 1360-1368, 2010. <https://doi.org/10.1016/j.ijrobp.2009.04.005>

105. Robar, JL, Day, A, Clancey, J, Kelly, R, Yewondwossen, M, Hollenhorst, H, Rajaraman, M, Wilke, D: Spatial and dosimetric variability of organs at risk in head-and-neck intensity-modulated radiotherapy. *Int J Radiat Oncol Biol Phys*, 68: 1121-1130, 2007. <https://doi.org/10.1016/j.ijrobp.2007.01.030>
106. Barker, JL, Jr., Garden, AS, Ang, KK, O'Daniel, JC, Wang, H, Court, LE, Morrison, WH, Rosenthal, DI, Chao, KS, Tucker, SL, Mohan, R, Dong, L: Quantification of volumetric and geometric changes occurring during fractionated radiotherapy for head-and-neck cancer using an integrated CT/linear accelerator system. *Int J Radiat Oncol Biol Phys*, 59: 960-970, 2004. <https://doi.org/10.1016/j.ijrobp.2003.12.024>
107. Wang, W, Yang, H, Hu, W, Shan, G, Ding, W, Yu, C, Wang, B, Wang, X, Xu, Q: Clinical study of the necessity of replanning before the 25th fraction during the course of intensity-modulated radiotherapy for patients with nasopharyngeal carcinoma. *Int J Radiat Oncol Biol Phys*, 77: 617-621, 2010. <https://doi.org/10.1016/j.ijrobp.2009.08.036>
108. Sun, XS, Li, XY, Chen, QY, Tang, LQ, Mai, HQ: Future of Radiotherapy in Nasopharyngeal Carcinoma. *Br J Radiol*, 92: 20190209, 2019. <https://doi.org/10.1259/bjr.20190209>
109. Yang, H, Hu, W, Wang, W, Chen, P, Ding, W, Luo, W: Replanning during intensity modulated radiation therapy improved quality of life in patients with nasopharyngeal carcinoma. *Int J Radiat Oncol Biol Phys*, 85: e47-54, 2013. <https://doi.org/10.1016/j.ijrobp.2012.09.033>
110. Movsas, B, Moughan, J, Sarna, L, Langer, C, Werner-Wasik, M, Nicolaou, N, Komaki, R, Machtay, M, Wasserman, T, Bruner, DW: Quality of life supersedes the classic prognosticators for long-term survival in locally advanced non-small-cell lung cancer: an analysis of RTOG 9801. *J Clin Oncol*, 27: 5816-5822, 2009. <https://doi.org/10.1200/JCO.2009.23.7420>
111. Beetz, I, Schilstra, C, van der Schaaf, A, van den Heuvel, ER, Doornaert, P, van Luijk, P, Vissink, A, van der Laan, BF, Leemans, CR, Bijl, HP, Christianen, ME, Steenbakkers, RJ, Langendijk, JA: NTCP models for patient-rated xerostomia and sticky saliva after treatment with intensity modulated radiotherapy for head and neck cancer: the role of dosimetric and clinical factors. *Radiother Oncol*, 105: 101-106, 2012. <https://doi.org/10.1016/j.radonc.2012.03.004>
112. Deasy, JO, Moiseenko, V, Marks, L, Chao, KS, Nam, J, Eisbruch, A: Radiotherapy dose-volume effects on salivary gland function. *Int J Radiat Oncol Biol Phys*, 76: S58-63, 2010. <https://doi.org/10.1016/j.ijrobp.2009.06.090>
113. Johannesen, TB, Rasmussen, K, Winther, FO, Halvorsen, U, Lote, K: Late radiation effects on hearing, vestibular function, and taste in brain tumor patients. *Int J Radiat Oncol Biol Phys*, 53: 86-90, 2002. [https://doi.org/10.1016/s0360-3016\(01\)02810-3](https://doi.org/10.1016/s0360-3016(01)02810-3)
114. Talmi, YP, Finkelstein, Y, Zohar, Y: Postirradiation hearing loss. *Audiology*, 28: 121-126, 1989. <https://doi.org/10.3109/00206098909081617>
115. Ondrey, FG, Greig, JR, Herscher, L: Radiation dose to otologic structures during head and neck cancer radiation therapy. *Laryngoscope*, 110: 217-221, 2000. <https://doi.org/10.1097/00005537-200002010-00006>
116. Gibb, AG, Loh, KS: The role of radiation in delayed hearing loss in nasopharyngeal carcinoma. *J Laryngol Otol*, 114: 139-144, 2000. <https://doi.org/10.1258/0022215001904905>
117. Honore, HB, Bentzen, SM, Moller, K, Grau, C: Sensori-neural hearing loss after radiotherapy for nasopharyngeal carcinoma: individualized risk estimation.

- Radiother Oncol*, 65: 9-16, 2002. [https://doi.org/10.1016/s0167-8140\(02\)00173-1](https://doi.org/10.1016/s0167-8140(02)00173-1)
118. Hwang, CF, Fang, FM, Zhuo, MY, Yang, CH, Yang, LN, Hsieh, HS: Hearing Assessment after Treatment of Nasopharyngeal Carcinoma with CRT and IMRT Techniques. *Biomed Res Int*, 2015: 769806, 2015. <https://doi.org/10.1155/2015/769806>
119. Yip, PL, Mok, KCJ, Ho, HS, Lee, WYV, Wong, ACL, Lau, CT, Wong, FCS, Yeung, KW, Lee, SF: Sensorineural Hearing Loss in Nasopharyngeal Carcinoma Survivors in the Modern Treatment Era - The Early and Late Effects of Radiation and Cisplatin. *Clin Oncol (R Coll Radiol)*, 34: e160-e167, 2022. <https://doi.org/10.1016/j.clon.2021.10.013>
120. Wang, CJ, Huang, EY, Hsu, HC, Chen, HC, Fang, FM, Hsiung, CY: The degree and time-course assessment of radiation-induced trismus occurring after radiotherapy for nasopharyngeal cancer. *Laryngoscope*, 115: 1458-1460, 2005. <https://doi.org/10.1097/01.mlg.0000171019.80351.46>
121. Wu, VW, Lam, YN: Radiation-induced temporo-mandibular joint disorder in post-radiotherapy nasopharyngeal carcinoma patients: assessment and treatment. *J Med Radiat Sci*, 63: 124-132, 2016. <https://doi.org/10.1002/jmrs.145>
122. Wu, VW, Ying, MT, Kwong, DL: A study on the post-radiotherapy changes of temporomandibular joint in nasopharyngeal carcinoma patients. *Br J Radiol*, 90: 20170375, 2017. <https://doi.org/10.1259/bjr.20170375>
123. Littley, MD, Shalet, SM, Beardwell, CG, Robinson, EL, Sutton, ML: Radiation-induced hypopituitarism is dose-dependent. *Clin Endocrinol (Oxf)*, 31: 363-373, 1989. <https://doi.org/10.1111/j.1365-2265.1989.tb01260.x>
124. Zhang, T, Xu, M, Mi, J, Yang, H, Liu, Z, Huang, L, Hu, K, Wang, R: Loosening Neuro-Optic Structures Dosimetric Constraints Provides High 5-Year Local Recurrence-Free Survival With Acceptable Toxicity in T4 Nasopharyngeal Carcinoma Patients Treated With Intensity-Modulated Radiotherapy. *Front Oncol*, 11: 598320, 2021. <https://doi.org/10.3389/fonc.2021.598320>
125. Li, YC, Chen, FP, Zhou, GQ, Zhu, JH, Hu, J, Kang, DH, Wu, CF, Lin, L, Wang, XJ, Ma, J, Sun, Y: Incidence and dosimetric parameters for brainstem necrosis following intensity modulated radiation therapy in nasopharyngeal carcinoma. *Oral Oncol*, 73: 97-104, 2017. <https://doi.org/10.1016/j.oraloncology.2017.08.011>
126. Huang, XD, Li, YC, Chen, FP, Zheng, WH, Zhou, GQ, Lin, L, Hu, J, He, WJ, Zhang, LL, Kou, J, Ma, J, Zhang, WD, Qi, ZY, Sun, Y: Evolution and Dosimetric Analysis of Magnetic Resonance Imaging-Detected Brain Stem Injury After Intensity Modulated Radiation Therapy in Nasopharyngeal Carcinoma. *Int J Radiat Oncol Biol Phys*, 105: 124-131, 2019. <https://doi.org/10.1016/j.ijrobp.2019.04.032>
127. Hara, W, Loo, BW, Jr., Goffinet, DR, Chang, SD, Adler, JR, Pinto, HA, Fee, WE, Kaplan, MJ, Fischbein, NJ, Le, QT: Excellent local control with stereotactic radiotherapy boost after external beam radiotherapy in patients with nasopharyngeal carcinoma. *Int J Radiat Oncol Biol Phys*, 71: 393-400, 2008. <https://doi.org/10.1016/j.ijrobp.2007.10.027>
128. Chang, SD, Tate, DJ, Goffinet, DR, Martin, DP, Adler, JR, Jr.: Treatment of nasopharyngeal carcinoma: stereotactic radiosurgical boost following fractionated radiotherapy. *Stereotact Funct Neurosurg*, 73: 64-67, 1999. <https://doi.org/10.1159/000029753>

129. Le, QT, Tate, D, Koong, A, Gibbs, IC, Chang, SD, Adler, JR, Pinto, HA, Terris, DJ, Fee, WE, Goffinet, DR: Improved local control with stereotactic radiosurgical boost in patients with nasopharyngeal carcinoma. *Int J Radiat Oncol Biol Phys*, 56: 1046-1054, 2003. [https://doi.org/10.1016/s0360-3016\(03\)00117-2](https://doi.org/10.1016/s0360-3016(03)00117-2)
130. Tate, DJ, Adler, JR, Jr., Chang, SD, Marquez, S, Eulau, SM, Fee, WE, Pinto, H, Goffinet, DR: Stereotactic radiosurgical boost following radiotherapy in primary nasopharyngeal carcinoma: impact on local control. *Int J Radiat Oncol Biol Phys*, 45: 915-921, 1999. [https://doi.org/10.1016/s0360-3016\(99\)00296-5](https://doi.org/10.1016/s0360-3016(99)00296-5)
131. Xiao, JP, Xu, GZ: Stereotactic radiotherapy--an approach to improve local control of nasopharyngeal carcinoma. *Chin J Cancer*, 29: 123-125, 2010. <https://doi.org/10.5732/cjc.009.10434>
132. Pai, PC, Chuang, CC, Wei, KC, Tsang, NM, Tseng, CK, Chang, CN: Stereotactic radiosurgery for locally recurrent nasopharyngeal carcinoma. *Head Neck*, 24: 748-753, 2002. <https://doi.org/10.1002/hed.10116>
133. Diaz-Martinez, JA, Esquenazi, Y, Martir, M, Citardi, MJ, Karni, RJ, Blanco, AI: Planned Gamma Knife Boost After Chemoradiotherapy for Selected Sinonasal and Nasopharyngeal Cancers. *World Neurosurg*, 119: e467-e474, 2018. <https://doi.org/10.1016/j.wneu.2018.07.183>

7 CURRICULUM VITAE

PERSONAL INFORMATION

Name: Manon Spaniol
Date of birth: 18.08.1995
Place of birth: Saarbrücken, Germany
Marital status: single
Nationality: German

EDUCATION

09/2001 – 07/2006 Elementary school (École primaire Jean Gutenberg, Bettviller, France)
09/2006 – 07/2010 Middle school (Collège Jean Seitlinger, Rohrbach-lès-Bitche, France)
09/2010 – 07/2013 High school (Lycée Louis Casimir Teyssier, Bitche, France)
French university entrance certificate (Baccalauréat général):
04.07.2013 (German grade: 1.2)
10/2013 – 09/2014 Biophysics, Universität des Saarlandes, Germany
10/2014 – 03/2018 Biomedical engineering (Bachelor of Science), Hochschule für Technik und Wirtschaft des Saarlandes, Germany
Thesis title: „Auswirkungen atmungsbedingter Bewegungen auf die Dosisverteilung am Beispiel von Lungentumoren“
30.03.2018 (Grade: 1.9)
04/2018 – 02/2020 Medical physics (Master of Science), Hochschule für Technik und Wirtschaft des Saarlandes, Germany
Thesis title: „Benefit of MR-guided radiotherapy: from motion compensation to radiation induced tissue changes“
18.02.2020 (Grade: 1.2)

10/2020 – present Doctoral student (doctor scientiarum humanarum)

02/2022 – present State-certified medical physicist

8 OWN PUBLICATIONS

Journal Articles:

1. Spaniol, M., Mai, S., Zakrzewski, T., Ehmann, M., Stieler, F.: Inverse Planning in Gamma Knife Radiosurgery: a Comparative Planning Study.
Physica Medica European Journal of Medical Physics 82: 269 – 278, 2021
2. Spaniol, M., Abo-Madyan, Y., Ruder, A., Fleckenstein, J., Giordano, F., Stieler, F.: Homogenous Dose Prescription in Gamma Knife Radiotherapy: Combining the Best of Both Worlds.
Submitted to Physica Medica European Journal of Medical Physics

Posters and talks:

1. Spaniol, M., Mai, S., Zakrzewski, T., Ehmann, M., Stieler, F.: Inverse Planning with Leksell Gamma Knife Lightning: Clinical plan quality and efficiency. IOP Physics world webinar, 18.05.2021
2. Spaniol, M., Mai, S., Zakrzewski, T., Ehmann, M., Stieler, F.: Inverse Planning in Gamma Knife Radiotherapy for Benign Tumors. Poster at the European Society for Radiotherapy and Oncology (ESTRO) annual congress, Madrid, Spain, August 2021
3. Spaniol, M., Abo-Madyan, Y., Mai, S., Ehmann, M., Stieler, F.: Gamma Knife Treatment of Acoustic Neuromas: How Homogenous can it be? Poster at the 16th International Stereotactic Radiosurgery Society (ISRS) Congress, Milan, Italy, June 2022
4. Spaniol, M., Mai, S., Zakrzewski, T., Ehmann, M., Stieler, F.: Inverse Treatment Planning at the Gamma Knife. Talk at the 17th Sino-German Radiation Oncology Symposium, virtual event, March 2023

9 ACKNOWLEDGMENT

The completion of this doctoral thesis would not have been possible without the guidance, contribution and support of several individuals, whom I would like to thank.

First and foremost, I would like to express my gratitude to my thesis supervisor Prof. Dr. Frank Giordano for making this project possible and paving the way to present my work at conferences. Furthermore, I am thankful for the opportunity of completing my medical physicist training at the University Medical Center Mannheim, which helped my understanding of this project.

Sincere thanks also go to my direct supervisor Dr. Florian Stieler for his valuable help, inspiring discussions and proof-reading of the submitted thesis. His expertise and patient teaching were invaluable for my research as well as for my work as a medical physicist.

I would like to extend my sincere gratitude to Dr. Yasser Abo-Madyan for his kind explanations and for supporting this project with his medical knowledge. Moreover, I would like to thank Giannoulla Sourmeli, Sarah Fremgen, Dr. Lena Thewes, Dr. Miriam Eckl and all my colleagues of the medical physics staff for their fruitful discussions and help inside and outside work.

Special thanks also go to Björn Somell from Elekta AB for providing the research software which was vital for this work.

Many thanks also go to all my friends for their emotional support and making my time in Mannheim feel like home.

Finally, I would like to thank my parents and my sister Alena for their love and support every step of the way.

I could not have undertaken this journey without all of you.